

AN OFFSHORE WIND RESOURCE ASSESSMENT AND A LOOK  
INTO MODEL ERRORS IN WIND FORECASTS

MATTHEW B. CORKUM

A DISSERTATION SUBMITTED TO THE FACULTY OF GRADUATE  
STUDIES  
IN PARTIAL FULFILMENT OF THE REQUIREMENTS  
FOR THE DEGREE OF

DOCTOR OF PHILOSOPHY

GRADUATE PROGRAM IN EARTH AND SPACE SCIENCE  
YORK UNIVERSITY  
TORONTO, ONTARIO  
SEPTEMBER 2013

© Matthew Corkum, 2013

## **Abstract**

This dissertation will look at 3 related, but different topics. The first, is a VHF wind profiler network in Southern Ontario and Quebec, the OQnet that provides real time wind measurements from 500m - 12000m. This study will look at ways of validating the data from these profilers and comparing them to forecast models such as the Canadian GEM model in Chapter 2.

The second part of this thesis will look at offshore wind resource assessment. Wind energy is a clean and viable alternative to burning fossil fuels for energy and is being expanded all over the world. Europe is a global leader when it comes to wind energy and they have expanded this industry to include many offshore wind farms. As Canada looks to accelerate their wind energy production, companies have begun to study the offshore wind resource in the Great Lakes. In 2010, Toronto Hydro started a 2 year wind resource campaign. The lidar installed by Toronto Hydro measured wind speed and direction up to hub height over a 2 year period but there were many gaps in the record. Other instruments, installed by the York

University team measured platform level winds and other weather variables. Using a combination of lidar extrapolation and platform level winds a continuous series of hub height winds has been generated which is discussed in Chapter 3.

Chapter 4 looks at using these data to look at Measure, Correlate, Predict (MCP) estimations of long term wind speed. Chapter 5 looks at Annual Energy Production (AEP) estimates for two potential wind farm designs for the Toronto Hydro site.

Finally in Chapter 6, this dissertation looks at issues related to wind forecasting for these wind farms and what kind of errors are associated with wind energy forecasts.

## **Dedication**

I would like to dedicate this thesis to my grandfather, Robert Hebb. As a life long farmer, he taught me how important the weather is to farming and got me interested in weather forecasting. It is his interest, knowledge and love of weather that has inspired me to complete a PhD in Atmospheric Science. Thank You Gampy for all your love and support you continue to provide.

## Acknowledgements

I would like to thank my supervisor Dr. Peter Taylor for his support, guidance of and countless hours during my entire PhD. My PhD committee and entire examining committee deserve thanks for their helpful insight, comments and time. I would to acknowledge Dr. Wayne Hocking for his help with the wind profiler work and Jack Simpson for his insight into the Toronto Hydro lidar work.

Also I would like to thank NSERC, CFCAS, and Toronto Hydro for their funding support. In addition, thank you to Zephr North Canada Limited and Dynasty Power for the use of computing resources and commercial software use.

Finally, I'd like to thank my friends and family for their support and encouragement through my entire degree.

# Table of Contents

<b>Abstract</b>	<b>i</b>
<b>Acknowledgements</b>	<b>iv</b>
<b>Table of Contents</b>	<b>v</b>
<b>List of Tables</b>	<b>viii</b>
<b>List of Figures</b>	<b>x</b>
<b>1 Introduction</b>	<b>1</b>
1.1 Upper Air Wind Measurements . . . . .	2
1.2 Offshore Wind Energy and Wind Resource Assessment . . . . .	4
1.3 Wind Forecasting . . . . .	13
<b>2 Analysis of Differences Between GEM Model Predictions and Measured Wind Data from the OQ-Network</b>	<b>16</b>

2.1	The Network . . . . .	16
2.2	Quality Control . . . . .	24
2.3	Comparing with Models . . . . .	32
2.4	Results . . . . .	35
2.5	Comparing Data to Radiosonde . . . . .	46
2.6	OQ-net Summary . . . . .	52
<b>3</b>	<b>Investigating a Possible Wind Energy Site in Lake Ontario</b>	<b>55</b>
3.1	The Site . . . . .	55
3.2	Filling in Missing Data . . . . .	70
3.3	Monthly Averages . . . . .	76
<b>4</b>	<b>Estimating Energy at the Toronto Hydro Site</b>	<b>79</b>
4.1	MCP Statistics for Toronto Hydro Platform based on 1989-2011 . . . . .	79
4.2	Wind Characteristics . . . . .	97
<b>5</b>	<b>Wind farm design</b>	<b>104</b>
<b>6</b>	<b>Wind Forecasting with Wind Energy Applications</b>	<b>117</b>
6.1	Accuracy of Current Weather Models . . . . .	119
6.1.1	Wind Speed and Direction Comparisons with GEM . . . . .	120
6.1.2	Wind Speed and Direction Comparisons with WRF . . . . .	127

6.1.3	Time Series . . . . .	133
6.2	Energy Forecasting Errors . . . . .	136
<b>7</b>	<b>Conclusions</b>	<b>140</b>

## List of Tables

3.1	Percentage of raw measured data at 120 m as well as data after the filtering process described has been executed . . . . .	62
3.2	Methods of filling in data is defined . . . . .	76
3.3	Monthly wind speed averages in m/s at the Toronto Hydro platform at 7 m and 90 m . . . . .	77
4.1	The location of the reference site and changes in the Toronto Island location since 1987. . . . .	81
4.2	Regression constants for the linear regression MCP method . . . . .	83
4.3	Statistics for the VRM MCP method . . . . .	87
4.4	Statistics for the all direction MCP method . . . . .	88
4.5	Short term monthly wind speed averages (m/s) using the five MCP methods outlined in this study . . . . .	89
4.6	Long Term monthly wind speed averages (m/s) using the 5 MCP methods outlined in this study . . . . .	92

4.7	10 m monthly average wind speed (m/s) at Toronto Island from 1989 through 2012. . . . .	93
4.8	Regression constants for the linear regression MCP method using VORTEX as the reference site . . . . .	95
4.9	Statistics for the all direction MCP method at 120 m for the Toronto Hydro platform (target site) and VORTEX data at 100 m. . . . .	96
4.10	The annual wind speed averages (m/s) using the VORTEX MCP analysis . . . . .	96
5.1	The annual energy for the single array and double array wind farm design in GWH . . . . .	115
6.1	The approximate percentages of total wind turbine output that a Siemens 3.5 MW machine would be producing at each wind speed.	137

## List of Figures

1.1	Annual and cumulative growth in offshore wind energy in the EU . . . . .	5
1.2	Wind energy capacity in Canada . . . . .	11
1.3	Approximate wind energy penetration . . . . .	14
2.1	Names and locations of the entire OQnet. . . . .	17
2.2	Schematic of radio waves transmitted and received in the OQnet . . . . .	18
2.3	A picture of the Egbert wind profiler . . . . .	20
2.4	Vectors of wind for a 3 day period at Egbert . . . . .	22
2.5	Transmitter antenna (blue) as a single antenna and the three receiving antennas (black) in spaced antenna method . . . . .	23
2.6	A probability distribution of wind speeds at the Harrow profiler. . . . .	26
2.7	A probability distribution of wind directions at the Harrow profiler . . . . .	27
2.8	A picture of the Harrow profiler from Google Earth . . . . .	28
2.9	Directional distribution of Doppler data at Harrow . . . . .	29
2.10	Wind speed distribution of spaced antenna data at Harrow. . . . .	30

2.11	Wind direction distribution of spaced antenna data at Harrow. . . . .	31
2.12	A schematic of a model grid cell . . . . .	33
2.13	The return rates for five profilers for the 12 month period . . . . .	36
2.14	The mean absolute error (MAE) in wind speed between the profiler data and GEM model data . . . . .	38
2.15	The mean absolute error (MAE) between the profiler data and GEM model data as a percentage of wind speed . . . . .	40
2.16	The wind speed bias in the GEM model compared to each of the wind profilers . . . . .	42
2.17	The MAE in wind direction for each of the five profilers compared with GEM model . . . . .	44
2.18	The bias in wind direction for each of the five profilers compared with GEM model . . . . .	45
2.19	Vertical profiles of wind speed for the Harrow wind profiler, GEM 00Z analysis and the Detroit Radiosonde . . . . .	47
2.20	Vertical profiles of wind direction for the Harrow wind profiler, GEM 00Z analysis and the Detroit Radiosonde . . . . .	49
2.21	Vertical profilers of wind speed for the Aumond wind profiler, GEM 00Z analysis and the Maniwaki Radiosonde . . . . .	50

2.22	Vertical profilers of wind speed for the Aumond wind profiler, GEM 00Z analysis and the Maniwaki Radiosonde . . . . .	51
2.23	Summary statistics of differences between winds measured at the Aumond wind profiler and radiosonde profiles from Maniwaki. May 2012- April 2013. This Figure is from work by Zheng Qi Wang et al. in [25] . . . . .	53
3.1	A map of the 50 m mean wind speed for all of Canada . . . . .	56
3.2	Location of the study area for a potential wind farm proposed by Toronto Hydro . . . . .	57
3.3	The Toronto Hydro platform in location denoted in Figure 3.2 . . . .	59
3.4	A time series of the 10 minute wind speed for December 27, 2010 at 120 m lidar level. . . . .	61
3.5	The ratio's of the 90 m wind speed to the 7 m met. station wind speed by 22.5 degree wind direction sectors including all wind speeds	65
3.6	The ratio's of the 90 m wind speed to the 7 m met. station wind speed by 22.5 degree wind direction sectors for 7 m wind speeds greater than 1 m/s . . . . .	66

3.7	This figure shows the ratio's of the 90 m wind speed to the 7 m met. station wind speed by wind speed sectors for 14 months of data from June 2010 to July 2011. The error bars show 1 standard deviation above and below the mean ratio. . . . .	68
3.8	The ratio's of the 90 m wind speed to the 7 m platform level wind speed by wind speed and wind direction sectors . . . . .	69
3.9	A case when all the wind speed levels have been measured (in blue) and the boundary layer is neutrally stratified . . . . .	71
3.10	A case when all the wind speed levels have been measured (in blue) and the boundary layer is unstable . . . . .	72
3.11	A case when all the wind speed levels are missing except the 7 m and 17 m levels . . . . .	74
3.12	A case when the lower 5 levels are present with 90 m and 120 m missing . . . . .	75
4.1	The 90 m lidar and 10 m Toronto Island (YTZ) monthly wind speed averages . . . . .	90
4.2	Location of the Toronto Hydro platform with onshore and offshore wind directions shown . . . . .	98

4.3	Wind rose showing frequency of wind direction and wind speed for June 2010 - May 2011. The colour coded legend shows wind speed ranges in m/s. . . . .	99
4.4	Average wind profile at the Toronto Hydro platform for a long over water fetch and short over water fetch . . . . .	100
4.5	Average wind profile at the Toronto Hydro platform for a long over water fetch and short over water fetch with a log scale . . . . .	102
5.1	The power curve for a 3 MW Siemens wind turbine. . . . .	105
5.2	A potential single array wind farm design created in the program Wind Farm. . . . .	106
5.3	A potential double array wind farm design created in the program Wind Farm. . . . .	108
5.4	4 panel figure comparing energy estimations for the single array design and double array design . . . . .	109
5.5	3 panel figure comparing energy estimations for individual wind turbines within the wind farm design . . . . .	112
6.1	The fuel types and percentages used to feed Ontario energy demand in 2012 [15]. . . . .	118

6.2	The MAE in wind speed between the Toronto Hydro 6 lidar levels compared with the GEM analysis and forecasts for one year. . . . .	121
6.3	The errors in wind direction between the Toronto Hydro 6 lidar levels compared with the GEM analysis and 3 - 48 hours forecasts for one year. . . . .	123
6.4	The errors in wind speed between the Toronto Hydro 6 lidar levels compared with the GEM analysis and 3 - 48 hours forecasts for one month. . . . .	125
6.5	The errors in wind direction between the Toronto Hydro 6 lidar levels compared with the GEM analysis and 3 - 48 hours forecasts for one month. . . . .	126
6.6	The non-nested WRF domain in blue and the Toronto Hydro platform location is marked with the pink dot and number 1. . . . .	129
6.7	The errors (observation - model) in wind speed between the Toronto Hydro highest 5 lidar levels and the the WRF 24 hours forecasts. . . . .	131
6.8	The errors in wind direction between the Toronto Hydro highest 5 lidar levels and the the WRF 24 hours forecasts . . . . .	132
6.9	A 24 hour time series of wind speed on July 6, 2010 for the 90m lidar measurements, the WRF model and the GEM model . . . . .	134

6.10	A 24 hour time series of wind direction on July 6, 2010 for the 90m lidar measurements, the WRF model and the GEM model. . . . .	135
6.11	A power curve for one of the most popular wind turbines in use today; the Siemens 3.5 MW machine curves. [22] . . . . .	136
6.12	A 24 hour time series of energy output using a Siemens 3.5 MW on July 6, 2010 for the 90m lidar measurements, the WRF model and the GEM model. . . . .	139

# 1 Introduction

This dissertation addresses three somewhat separate but related topics. The first relates to improved monitoring of tropospheric and lower stratospheric winds using VHF windprofilers and differences between windprofiler measurements and numerical weather prediction (NWP) model analyses and forecasts. The main section describes an analysis of lidar windprofiler measurements of winds in the lowest 120 m of the atmosphere from a platform in Lake Ontario plus the use of those measurements to estimate potential Annual Energy Production from a hypothetical wind farm 5km offshore from the Scarborough Bluffs near Toronto. With the assimilation of additional upper level wind measurements from the VHF profilers into NWP models there is a potential to improve the performance of the models in forecasting winds at this and other wind farm locations which is the third topic of wind forecasting relating to wind energy.

## 1.1 Upper Air Wind Measurements

In atmospheric science and meteorology, upper air observations are often hard to find with good temporal and spatial (both vertical and horizontal) resolutions. This type of data can be obtained from the release of radiosondes which collect wind measurements along with temperature and other weather variables, but current radiosonde programs only release every 12 hours and spatial resolution is often too coarse to grasp the overall weather picture. Another source of wind measurements through the atmosphere is AMDAR data that are collected by air planes mostly as they are taking off and landing. This data is again useful, but mostly limited to the area around airports or at cruising altitudes.

As models improve, they can often be used to help fill in gaps in observations to gain knowledge of what is going on at both a meso scale and synoptic scale in the atmosphere. In an effort to improve the resolution of observations both temporally and spatially, a Very High Frequency (VHF) wind profiler network has been constructed in southern Ontario and Quebec. This wind profiler network can measure wind speed and direction from about 400 up to 12000 m or more at very high temporal resolution. Chapter 2 will look at ways of quality controlling the data as well as comparing the data to GEM model forecasts. One issue with a wind profiler network such as the OQ-Net is quality control of the data with so few

existing upper air measurements to compare to. This study will look at ways of using selected data and climatology to quality control and validate the data.

The data are already being used for data assimilation into some of the worlds best weather models (ECMWF and UKMET) and tested in others with the ultimate goal of improving model forecasts.

The operational GEM 15 km regional NWP model uses 80 vertical levels which allows the introduction of a sponge layer to prevent unwanted wave energy reflection from the rigid top of the model [2]. Of these 80 levels, only about 10 levels are located in the lowest 1000 m and about 34 levels below 12 km which is the top height of the profilers that will be investigated in this study. This model uses a two time step implicit semi Lagrangian grid point method and uses a staggered C-grid in the horizontal and un-staggered grid in the vertical. This model uses the MoisTKE Boundary Layer Cloud parameterization while Kuo Transient shallow convection scheme and Kain-Fritsch scheme are used for deep convection[2].

The quality control of the OQ-net data in this study will improve overall the data and data return of the profiles through looking at probability distributions and comparing with radiosonde data from nearby launch sites. As well through comparing wind profiler measurements to the GEM model, considerable differences will be noted between the two which will help motivate more work of data assimilation into models to improve forecasts.

## 1.2 Offshore Wind Energy and Wind Resource Assessment

The amount of wind energy is growing very quickly as onshore wind farms continue to multiply. With regulations in place to have wind turbines set back from residences and power grid limitations, many of the possible and profitable onshore locations have already been developed, at least in Ontario and Europe. Developers are now looking at offshore wind energy projects as an alternative to further expand the wind energy industry. The idea of putting wind turbines offshore was first considered in 1937 when it was suggested placing turbines offshore on pylons. The idea never got off the ground but led to an MIT professor, Dr. William E. Heronemus proposing the idea of floating wind turbine platforms about 40 years later [1]. It wasn't until 1990, a company actually constructed floating wind turbines in the Baltic Sea, off northern Sweden. Offshore wind projects slowly began to be constructed after this first offshore wind project in the European Union but really began to take off around the year 2001 in the EU [1]. In 2002, the largest offshore wind farm for many years, Horns Rev was built to produce 160 MW of power.

Figure 1.1 shows that the cumulative growth in offshore wind energy has grown from under 1000 MW in 2006 to nearly 4000 MW in 2011.

The offshore design of wind turbines is similar to the onshore turbines with some

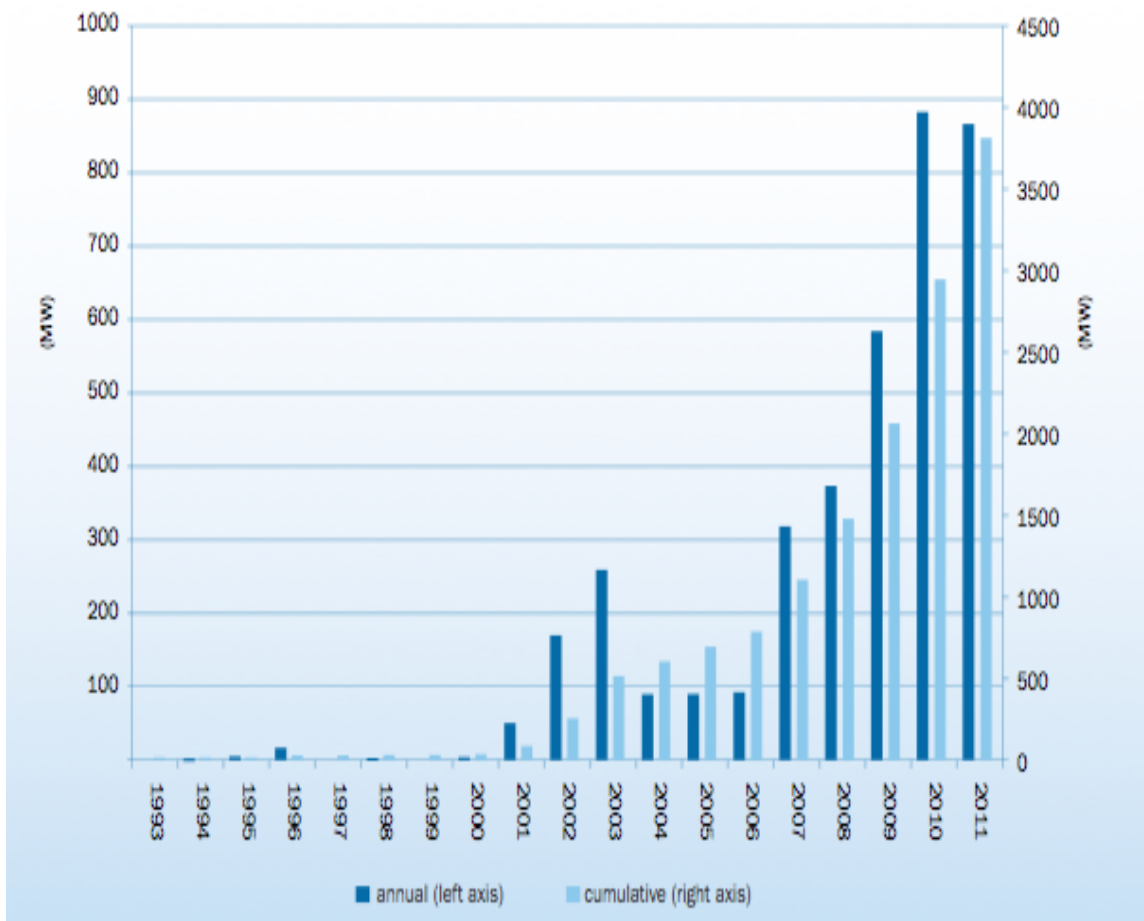


Figure 1.1: Annual (left axis) and cumulative(right axis) growth in offshore wind energy in the EU [6].

notable differences. Marine turbines often have access to the nacelle for helicopters to perform maintenance and small cranes are attached to them to aid the replacement of parts. Helicopter access is referring to having personal lowered from above without actually having a helipad. Wind turbines sometimes are chosen to be designed without a gearbox to make the machine simpler and avoid costly repair or maintenance. In these cases, the generators are run directly at the speed of the rotor hub. Although offshore wind turbines are designed to withstand harsh weather conditions, in terms of the wind characteristics, the wind offshore is generally much smoother with much less turbulence. This can significantly decrease the wear and tear on the turbine itself making for a longer life and cheaper maintenance costs [13].

Most offshore wind turbines use tubular steel monopile foundations that are usually 4 - 6 metres in diameter and are put 22 - 24 metres beneath the sea bed. These foundations only work in conditions with water depths up to about 30 m beyond which the foundations need to be significantly strengthened which increases costs substantially. The steel tower itself usually comes in 20 - 30 m sections and are connected to the transition piece (a section that is connected to the foundation extending to the water surface) of the foundation with concrete grout or bolts. A small platform is usually built on the transition piece to allow for the docking of boats. In many colder locations ice protection may be included in the form of a

sloped collar at the base of the water line to encourage ice to break apart. Ladders or elevators extend inside the tower to access the nacelle from the base [13]. Power and communication is run from the foundation through an under water trench to a transformer station for the wind farm where the voltage is increased and moves to land via an underwater cable which is then connected to a high voltage transmission grid. Internet communication flows along the same underwater cables and often each turbine is assigned its own internet address which allows for monitoring from onshore. On top of all these considerations, engineers have given a lot of thought to ways to limit ongoing maintenance which can be very costly given the offshore locations. Steel components are triple coated with paint while the tower and nacelle are sealed to avoid intrusion of salt (in oceans) and moisture. Different from air cooled machines on land, offshore turbines use heaters to maintain the difference between inside and outside environments while dehumidifiers maintain a relative humidity below the level where corrosion will take place. The electrical components like the generator and control system sometimes have stand-by heating systems to prevent condensation when the temperature fluctuates quickly [13].

Offshore wind farms are just now beginning to be assessed and built in North America and other parts of the world. The first planned in North America seems to be a 130 turbine wind farm on Horseshoe Shoal in Nantucket Sound, off shore of New York. This project has been in the works for many years and has been greatly

slowed by public opposition. It now appears to have past most of the approvals and is well on its way to being constructed [13]. In Ontario, there have been a couple of wind monitoring campaigns happening offshore in the Great Lakes in hopes of future wind farm developments in the lakes. This process has been slowed by a moratorium imposed on all offshore wind farms in the Great Lakes by the government of Ontario [7]. The moratorium on the Great Lakes is unfortunate for the Canadian offshore wind energy industry, particularly since the Great Lakes have a similar wind resource to the near shore wind resource on the Atlantic coast but are far less vulnerable to extreme weather events. The eastern seaboard of North America, while having a good to excellent wind resource is very susceptible to large winter storms and hurricanes. Wind turbines placed in these regions of near shore Atlantic Ocean must be built to withstand such harsh wind conditions and wave heights of several tens of metres which are not uncommon in hurricanes and tropical storms. In the Great Lakes, conditions are not as harsh on a regular basis and synoptic scale storms tend to be less intensive due to the lack of moisture feed from the ocean.

Offshore wind projects, despite being more expensive, have many advantages over onshore wind farms. Wind speed is often stronger and more stable over large bodies of water resulting in higher production per unit installed. As well, many large power customers are often close to large bodies of water, so electricity from large offshore

wind farms can be transported easily and over relatively short distances. If wind farms are far enough offshore the issues of noise and being a visual eye sore to some are nearly eliminated [1]. There are also advantages to the actual installation of offshore wind turbines. As wind turbine size increases, transportation of multi-megawatt projects is becoming more of a problem as onshore wind farms move to small rural communities where the only road in may be a gravel two lane road. These roads not only have weight restrictions on during certain months of the year, they are narrow with low hanging electrical wires. Offshore transportation allows for the transportation to be done by large ships with weight and size restrictions only put in place by the size of the ship itself. This allows for larger wind turbines to be placed offshore for the maximum amount of power extraction [1]. Offshore wind farms do have their disadvantages which are mostly related to cost of installation and maintenance of the wind turbines as well as transmission lines to shore.

Cost of building and operation of offshore wind farms is not the focus of this study, but few costs from Wind Energy The Facts [5] will be quoted as a reference. Installed cost of offshore wind projects was \$2.9 million CAD/MW in 2006 and that was expected to rise to \$3.4 million CAD/MW in 2011 but decrease to 2.5 million CAD/MW by 2015 as technology and installation methods advance. In contrast, onshore wind energy projects installation cost is about \$1.3 - 1.7 million CAD/MW [5]. On the other hand, production costs for offshore wind projects are

given as variable but about \$93 CAD/MWh while onshore production costs are about \$67 - 80 CAD /MWh. These production costs are averaged over a 20 year life time of the wind farm and include all costs, including financing, and is in 2006 Euros (converted using 2013 CAD exchange rates, 1 Euro = \$1.38) [5]. In this case production costs refer the cost of everyday operation of the wind farm once it goes into operation. In these costs, the installation of offshore projects is roughly twice that of onshore while production costs are similar, meaning once a wind turbine is installed, it can produce energy at similar costs whether it is installed onshore or offshore.

In Canada, CanWEA developed wind vision 2025 which argues the wind energy can satisfy 20 percent of Canadas electricity demand by 2025[3]. Figure 1.2 shows the installed wind energy capacity in Canada by province as of June 2013.

The installed 6578 MW in Canada shown in Figure 1.2 represents about 3 % of the total installed energy capacity; a 17 % deficit of the 2025 wind vision goal. It's worth noting here that installed capacity is the capacity if all wind turbines are running at 100 %, but in practice the capacity factor(the actual energy output over a period of time compared to its potential output) of a wind farm is much less than 100 %. As wind energy grows in Canada, one problem that is arising is that many of the favourable onshore wind farms are already developed and those that aren't yet developed face a lot of public opposition for various reasons. For this reason,

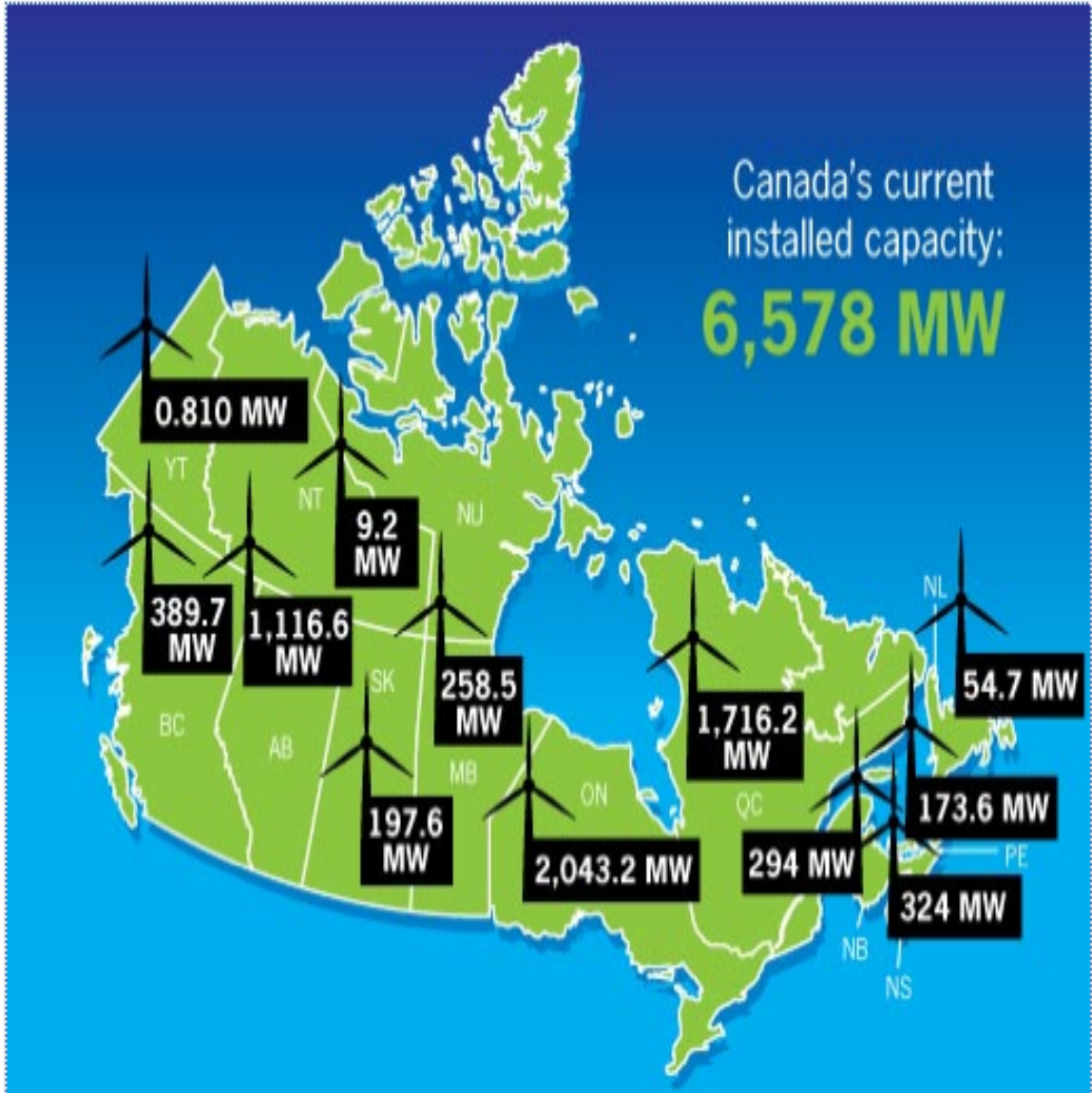


Figure 1.2: The current installed wind energy capacity in Canada as of June 2013 by province [3].

the wind energy sector has started to explore offshore wind energy opportunities. Toronto Hydro launched an offshore wind resource assessment in June 2010 that lasted for just over 2 years. Although the project had some equipment issues, valuable data have been obtained to help decide whether an offshore wind farm in the area makes sense. Missing data is an issue in all types of wind resource assessment, but offshore assessments often have more missing data due to more difficult access for maintenance. Chapter 3 will look at the details of the project, discussing the data and looking at ways to estimate missing data during times when equipment was out of service with the goal of provided a full data set for the length of the wind resource assessment.

Chapter 4 uses the measured data and estimated data (from Chapter 3) to do longterm estimates of wind speed using a nearby station with longterm data for correlation. These methods are used in many onshore projects but not often used in offshore projects. This study uses the same methods employed for onshore wind resource assessment to see if they produce reasonable results for Toronto Hydro's offshore project.

Chapter 5 will look at possible designs for an offshore wind farm in the area of this resource assessment by Toronto Hydro. It will also look at annual energy estimations and capacity factors these designs will produce.

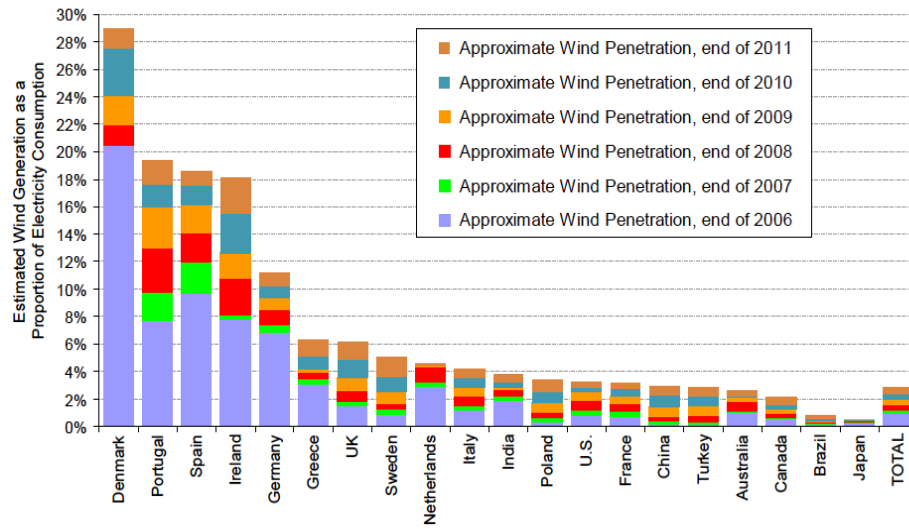
Ultimately, the work in this section of the thesis will take measured data from

the lidar and platform level anemometers to estimate missing data to create a full data set. Using a nearby reference site at Toronto Island, MCP methods will be used to determine if the wind measurements made over the two year wind resource campaign are representative of the long term wind regime in the area. These MCP methods are often used for onshore wind resource assessment, but this is one of the first times the methods have been applied to offshore in North America. Finally, using the full data set, two wind farm designs will be presented using the program WindFarm and annual energy estimations will be done for each wind farm design.

### **1.3 Wind Forecasting**

An important issue once a wind farm is built is wind forecasting. As wind energy projects continue to increase, so do wind penetration rates. The wind penetration rate is the percentage of energy produced by wind energy compared to the total energy amount of energy produced by all sources. As this wind penetration rate grows, system operators face the challenge to manage a non-dispatchable power source; non-dispatchable meaning it can not be turned on and off as needed. Figure 1.3 shows the top 20 countries by their wind penetration rates or total installed capacity and how the rate has grown from 2006 through 2011[24].

In Figure 1.3, the top country by penetration rate is Denmark with nearly 30 % of its energy comes from wind energy. Also notable in Figure 1.3 is USA with about



Source: Berkeley Lab estimates based on data from BTM Consult, EIA, and elsewhere

Figure 1.3: Approximate wind energy penetration or production in the twenty countries with the greatest installed wind energy capacity[24].

3 % and Canada with nearly 2 %. Even the countries with relatively low wind penetration rates can have problems with high penetration rates within areas of the country.

For example within the USA, a country with about 3 % wind penetration, Texas provided about 6.9 % of it electricity from wind energy with a capacity of 10,394 MW by the end of 2011[24]. Although other states provide larger percentages of total electricity from wind power, Texas provided by far the most megawatts of wind energy. The Texas grid is run by Electric Reliability Council of Texas (ERCOT) and has to manage all this wind power while running a cost effective and efficient power grid. In order manage a grid properly, wind forecasts are issued so that

ERCOT can properly plan to have enough energy, but not too much so that they can run a efficient grid. Although Texas is being used as an example, this type of scenario occurs to some extent in every power pool that has wind energy as a part of its available energy sources. Chapter 6 will look at what type of errors in wind speeds are seen in typical model forecasts at the wind energy level. These errors in wind speed will then converted to approximate errors in wind power using a popular wind turbine curve.

By comparing wind energy model forecasts to what actual wind turbines would output, significant differences will be shown between the two. Increasing model resolution does not always increase accuracy which will help motivate the industry to look at other methods of wind forecasting to improve wind energy forecasts so that system operators can better manage large amounts of wind energy.

## **2 Analysis of Differences Between GEM Model Predictions and Measured Wind Data from the OQ-Network**

### **2.1 The Network**

The Ontario-Quebec VHF wind profiler radar network (OQnet) consists of 10 wind profilers in Ontario and Quebec as shown in Figure 2.1. The first profiler to be constructed was at Harrow in 2008 and the others have been gradually constructed ever since with the last one at Fraserdale in 2012. These units use frequencies in the range 40 to 55 MHz corresponding to wave lengths of 7.50 to 5.45 m. These profilers use two different techniques to measure wind speeds and other related parameters in the range of 400 m through to about 15 km [9]. The profilers are set up to make wind measurements at 500 m vertical resolution and this resolution is limited by bandwidth allocation of 250 kHz. The Doppler method is most reliable above 1000 m and works on the theory of the Doppler effect.. This is mostly thought of with

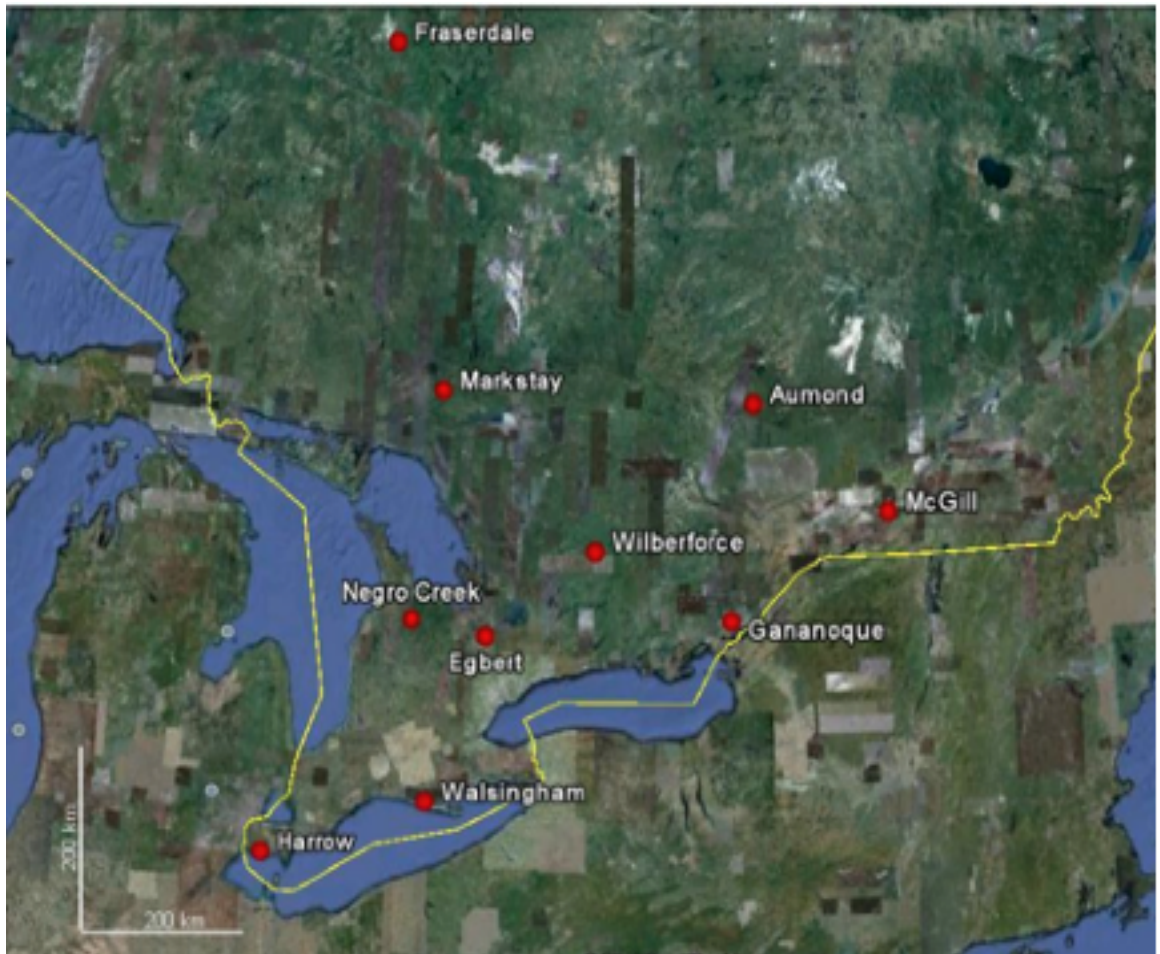


Figure 2.1: Names and locations of all 10 wind profilers in the OQnet. ( Credit to Nimalan Swarnalingam, Western University .)

sound waves but also works on radio waves. Radio waves are transmitted by a radar and when they strike a target( or encounter variations in atmospheric properties caused by turbulence) with a moving component radially towards or away from the radar. The reflected or backscattered radio waves will have a slightly different frequency to the transmitted waves. This difference in frequency can be quite small, as small as 0.1 Hz or less. Despite the small shift, however, many radars (especially windprofiler radars) can not only detect this small shift, but also measure it quite accurately. The Doppler method works best when the radar beam is quite narrow in the polar diagram in Figure 2.2.

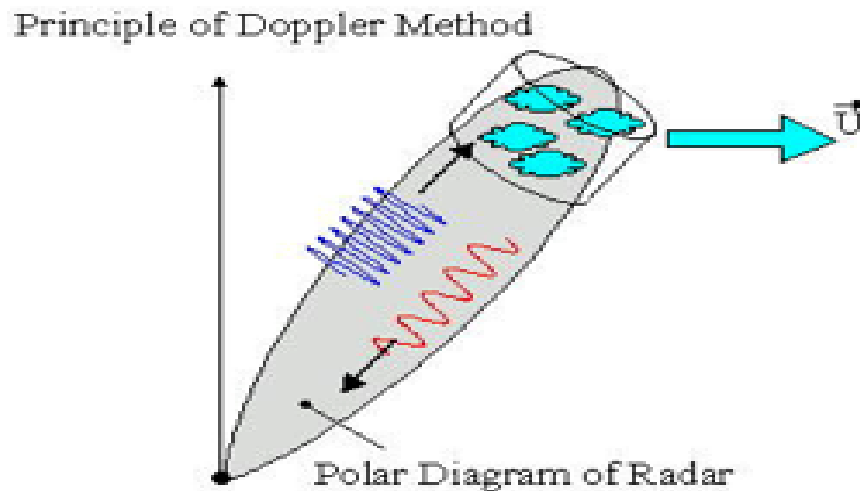


Figure 2.2: A schematic of how radio waves are transmitted and received in the Doppler method used by the radars in the OQnet[9]. The 4 blue patches are areas of turbulence or other scatters that the radio waves will reflect off of.

In Figure 2.2, the radar beam is assumed to be pointing up and to the right, illuminating a small region indicated by the cylinder. Turbulence may exist everywhere in the atmosphere, but only that portion which falls in the path of the radar "beam" will receive significant radiation. This schematic shows the incident waves with more oscillations per unit length that reflect off of while in reality the change in frequency would be much less. The change in frequency of the radar signal is directly related to the speed of the scatterers away from the radar. The speed of these scatterers approximate the speed of the wind since the radar cannot measure the total wind vector with a single measurement like this. The wind profilers in the OQ-net are arrays of radio antenna covering about 100 m by 100 m area as shown in Figure 2.3.

The large array of antenna in Figure 2.3 are the antenna used in the doppler method and the all antenna act as transmitting and receiving antenna. They generate 5 beams, one pointing about 15 degrees east, west, north and south of vertical while the final one points to the vertical, but these could be shifted due to land constraints. As an example, if the radar first measures the radial component of the wind using a beam pointing towards the east, then measures the radial component of the wind with a radar beam pointing to the north and finally measures the vertical wind speed of the wind with a radar beam pointing vertically, an algorithm can combine all this information to determine the horizontal wind speed of the air around the



Figure 2.3: A picture of the Egbert wind profiler and the area taken up by the antenna.

radar. With 5 beams there is some redundancy. Using this method, wind speed can be calculated at a range height which the radar can measure to help build a detailed picture of the profile of the wind through the lower atmosphere. If the radar operates for an extended period of time (many hours or days), a time series of these profiles can be combined to see how the winds evolve with time. These vectors can then be displayed in a form like in Figure 2.4.

A second method to measure wind speeds with these radars is the spaced antenna method (also known as correlation analysis method) which works best at the lower levels from about 400 m to 2000 m. This method can be thought of as measuring the speed of a cloud by watching its shadow as it moves across the ground. The correlation analysis method is based on a similar principle that tends to be applied more often when using broad, vertically directed radar beams. When radio waves encounter a scattering phenomena such as variations in temperature or humidity, the radio waves scatter off in all directions and form a diffraction pattern of the cloud on the ground. As the turbulent eddies in this patch move and are blown by the wind, the diffraction pattern changes and moves along. Since the transmitter and receiver antenna are at similar distances from the cloud, the "shadow" moves at twice the speed of the scatterers because of the distance from the ground and both can be thought of as "point objects" shown in Figure 2.5.

The spaced antenna method name comes from the fact that the receiving antenna

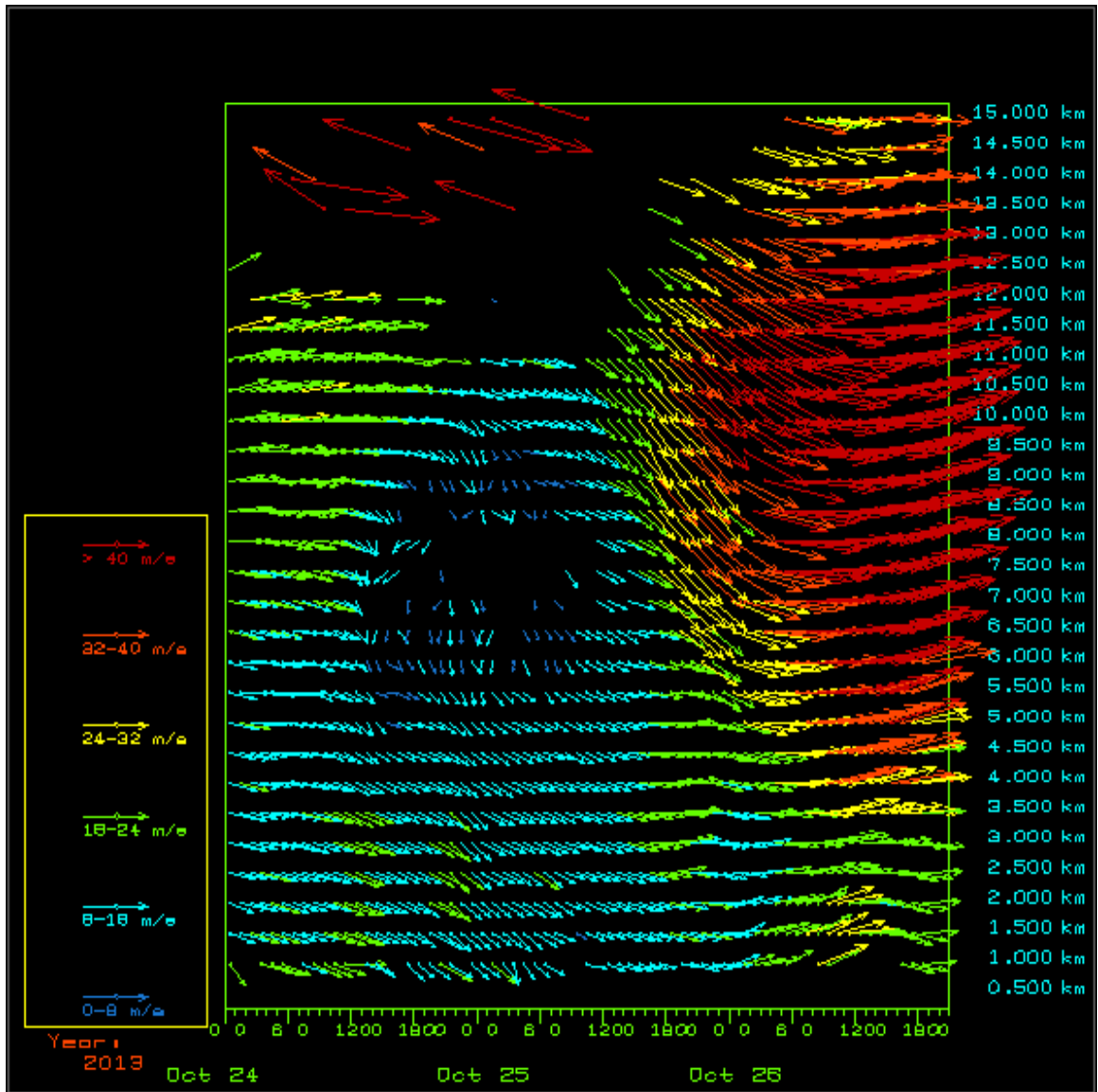


Figure 2.4: Vectors of wind for a 3 day period at Egbert. The orientation shows the horizontal wind direction and the color code shows the magnitude of the wind. These figures are available continuously for all profilers at <http://www.yorku.ca/oqnet/>.

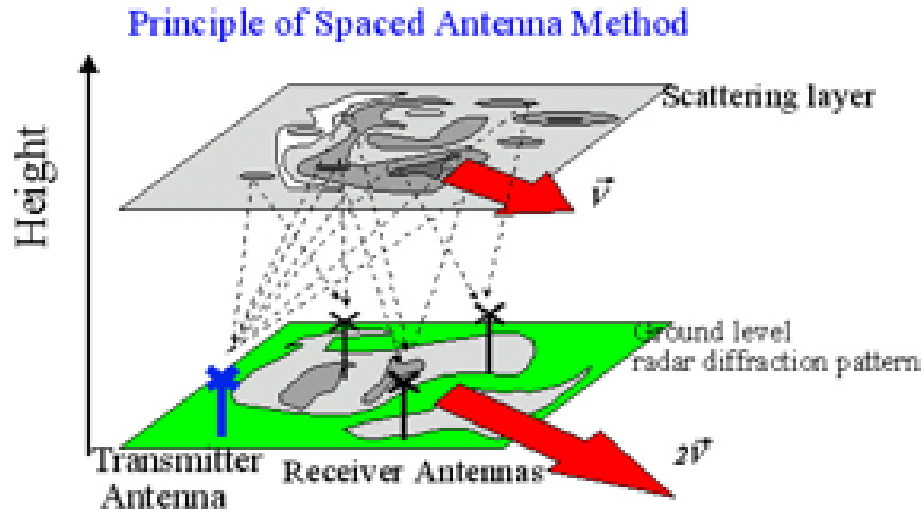


Figure 2.5: The transmitter antenna (blue) as a single antenna and the three receiving antennas (black) are also highlighted. These three receiving antennas are spaced at different points on the ground [9].

are spread out over a certain area. The various broken lines indicate just a few of the many ray paths which transmitted radio waves may take. Each radio wave may scatter in any direction with different strengths and these different ray paths return to different points on the ground. At the ground interface, they interfere with each other to produce electric and magnetic fields which vary as a function of position and time. It is this time and space-varying field which creates the diffraction pattern. These diffraction patterns differ for each height at which we obtain radar scatter and the radar can use range-determination processes to separate out these different "shadows" and decide which one corresponds to which height. Each of the

three receiving antennae a record the electric and magnetic field strengths at its own location. When the diffraction pattern is drifting along as shown in Figure 2.5, the signal that is received by the receiver antenna shown to the left in Figure 2.5 is received by the receiver shown at the front figure a short time later. Comparing these signals on all three receivers and seeking the maximum correlation, it is possible to calculate the time delays between periods when similar signals move over each antenna. Using this information, the wind speed and direction at the height of scatter can be calculated at all heights from which a signal is received, allowing a wind profile to be developed, similar to the Figure 2.4 but over a lower range.

By mid 2013, the entire network is expected to be fully operational which will make it a valuable tool for forecasters predicting severe weather. The data are also being assimilated into a research model at CMC, and by the operational ECMWF and UK meteorological office. They are also being sent to NOAA for evaluation and potential use in the US forecast models.

## **2.2 Quality Control**

For quality control purposes, a starting point was a study of the probability distributions generated for both wind speed and direction for both Doppler data and spaced antenna data. Figure 2.6 shows a speed distribution for the Doppler data

of wind speed data from Harrow for the 11 months of 2010, rather than the entire year due to the availability of data at the time of the study.

Figure 2.6 shows the distribution of wind speed is similar to classic Weibull distribution which is typical of wind speed distributions of this region suggesting that there are no major problems in the wind speed measurements and the algorithm which processes those data. Next we look at the distribution for wind direction of Doppler data at the Harrow site at the same period.

In Figure 2.7, immediately something seems odd with the 4 minima highlighted with red asterisks. In southern Ontario, the high frequency of wind directions between 250 and 300 degrees is expected, but the gaps centred at 49, 139, 229 and 319 degrees are not expected. These correspond exactly to the orientations of the antenna at Harrow as seen in Figure 2.8.

After working with the manufacturer it was discovered that these minima were caused by the sensitivity of the program that filters out interference. The problem is that if the wind is perpendicular to one of the beams, the Doppler shift due to the wind is zero, so the wind signal could be misinterpreted as ground echoes (which should have near zero Doppler shift by definition). When these signals get mixed together, they cannot be separated and therefore do not have 2 components of the wind. As long as the wind is not perpendicular to either beam, we can make a wind direction measurement easily. Through experimentation with the filtering software,

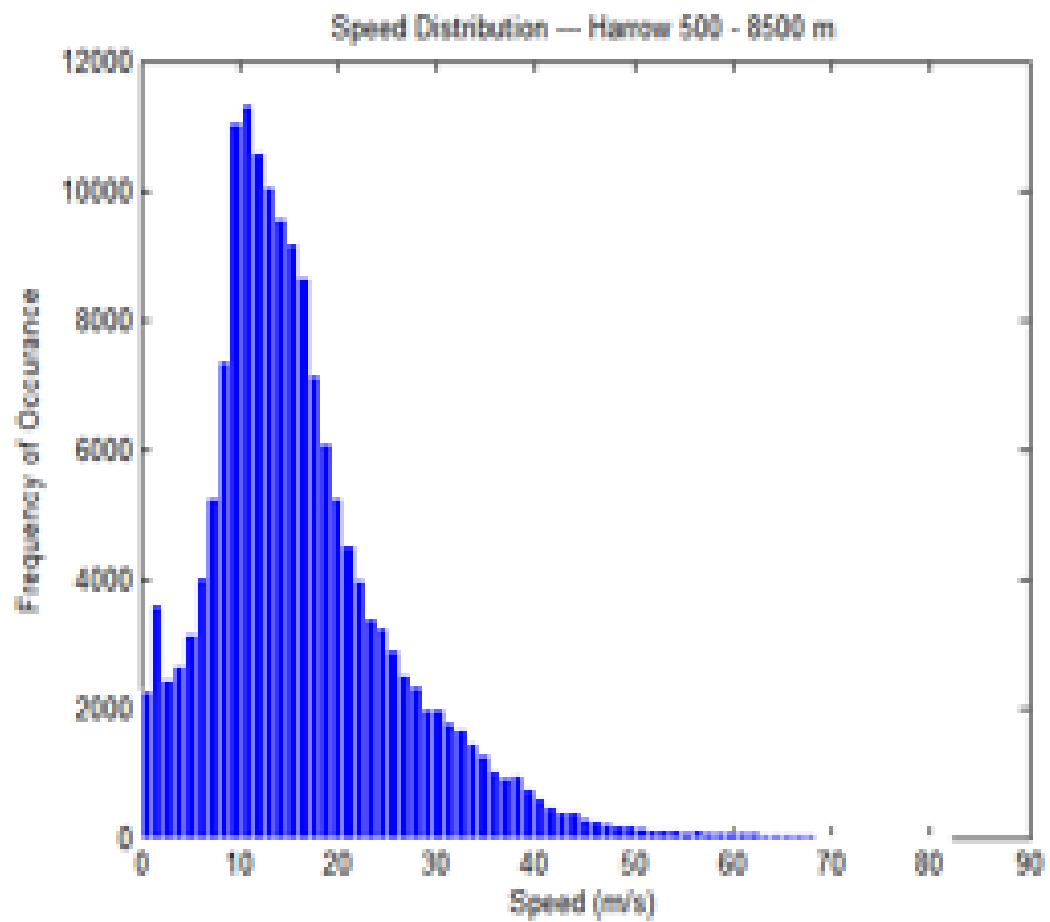


Figure 2.6: A probability distribution of wind speeds at the Harrow profiler for 7 months in 2010 for all 500 m increments between 500 m and 8500 m.

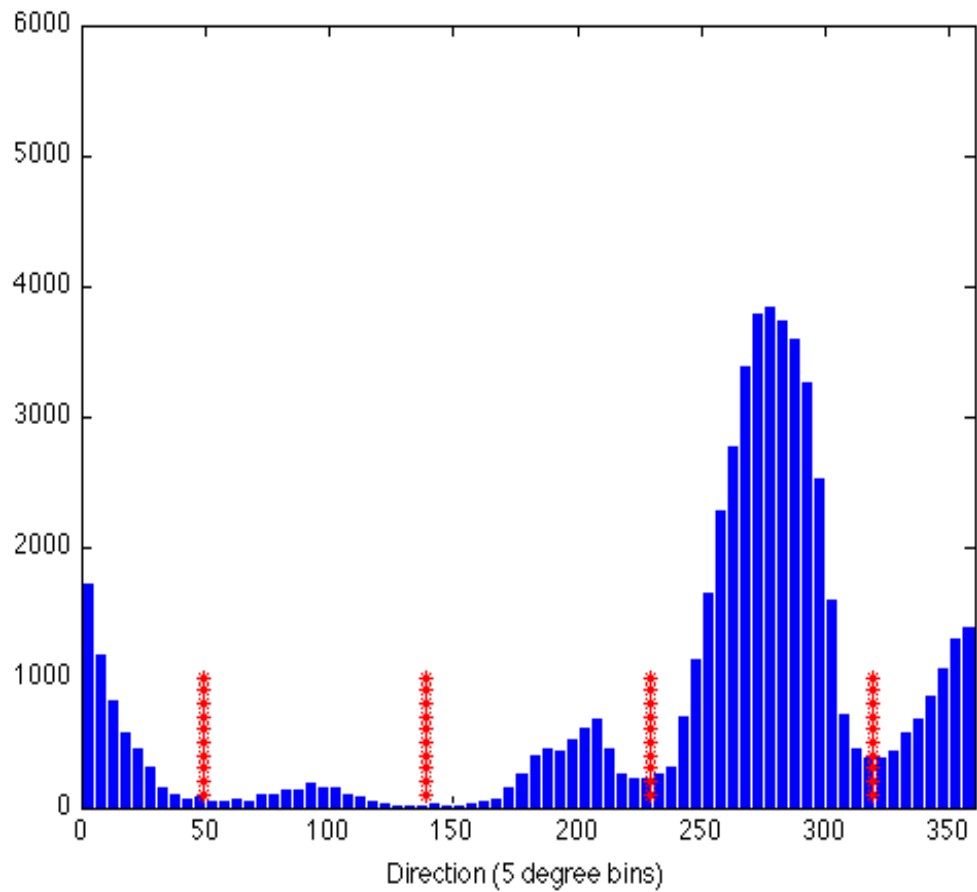


Figure 2.7: A probability distribution of wind directions at the Harrow profiler for 7 months in 2010 for all 500 m increments between 500 m and 8500 m. The red asterisks show the orientation of the antenna arrays .



Figure 2.8: A picture of the Harrow profiler from Google Earth and the orientation of the antenna is highlighted in red.

the sensitivity was decreased to create the direction distribution in Figure 2.9.

In the directional distribution in Figure 2.9 the minima in the frequency no longer occur at the location of the antenna and the shape of the directional distribution is what is expected. Comparing this figure to Figure 2.7 one will notice much more data which is a result of the new method recovering more data. Figure 2.9 has about 94 % of possible hourly data while Figure 2.7 has about 65 % of possible hourly data which demonstrates how much data the old method was missing.

Next, consider the distributions of the spaced antenna data at Harrow. Figure 2.10 shows the speed distribution of the spaced antenna data for 7 months of 2010 at Harrow.

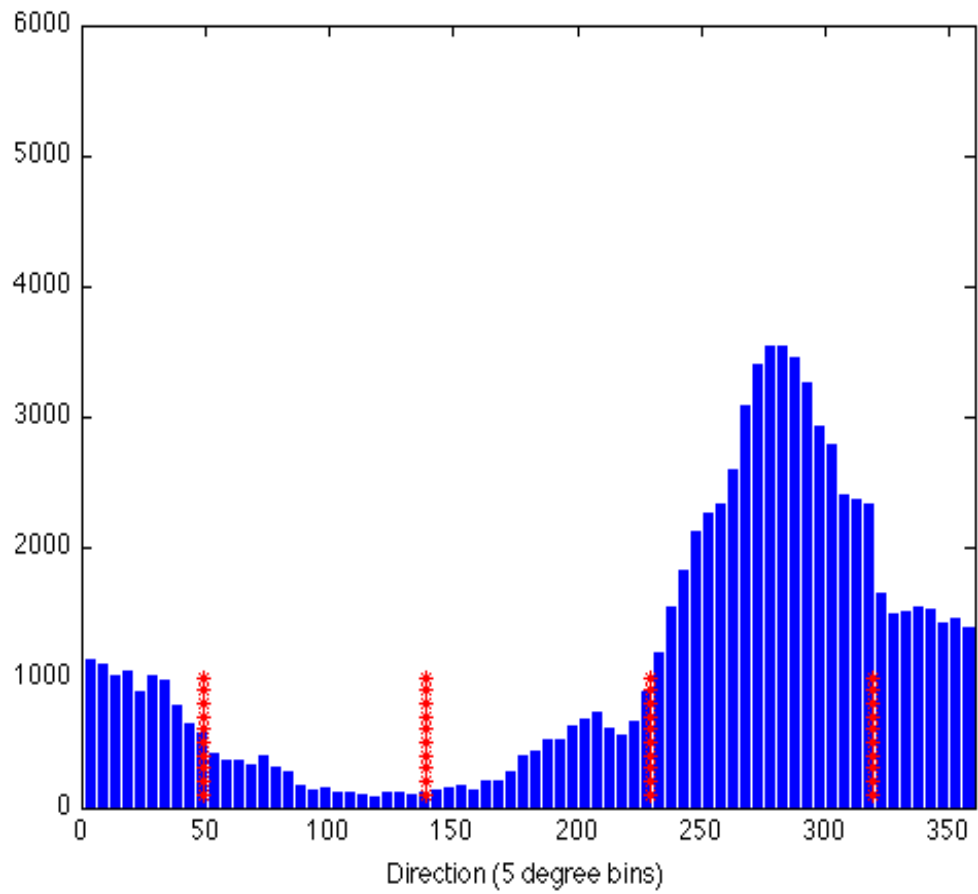


Figure 2.9: Directional distribution of Doppler data for 7 months of 2010 at Harrow showing the four orientation of the radar antenna in red asterisks.

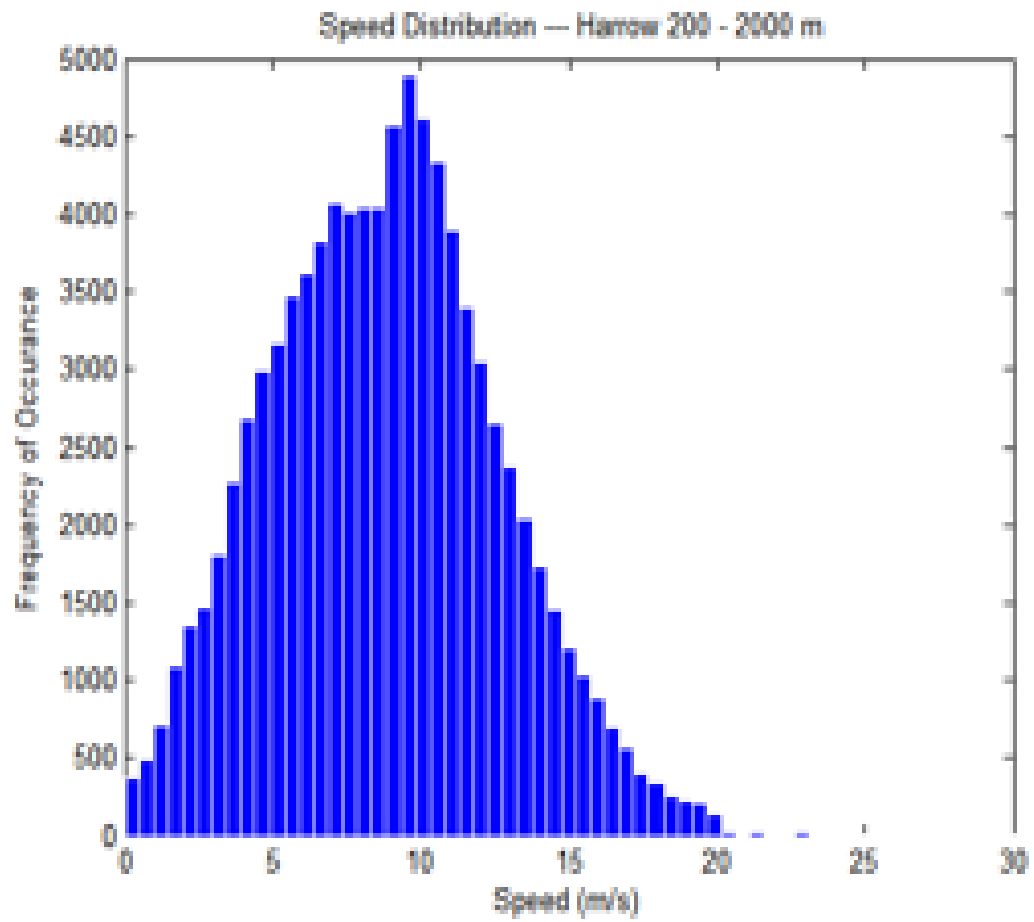


Figure 2.10: The wind speed distribution for 7 months of data using the space antenna method at Harrow in 2010.

This speed distribution looks typical of a wind speed distribution in southern Ontario and is similar to the shape of the Doppler speed distribution with the exception of the absence of higher speeds in the Doppler data due to the higher measurement elevation. For the spaced antenna directional distribution similar distribution to the Doppler directional distribution shape in the Figure 2.11.

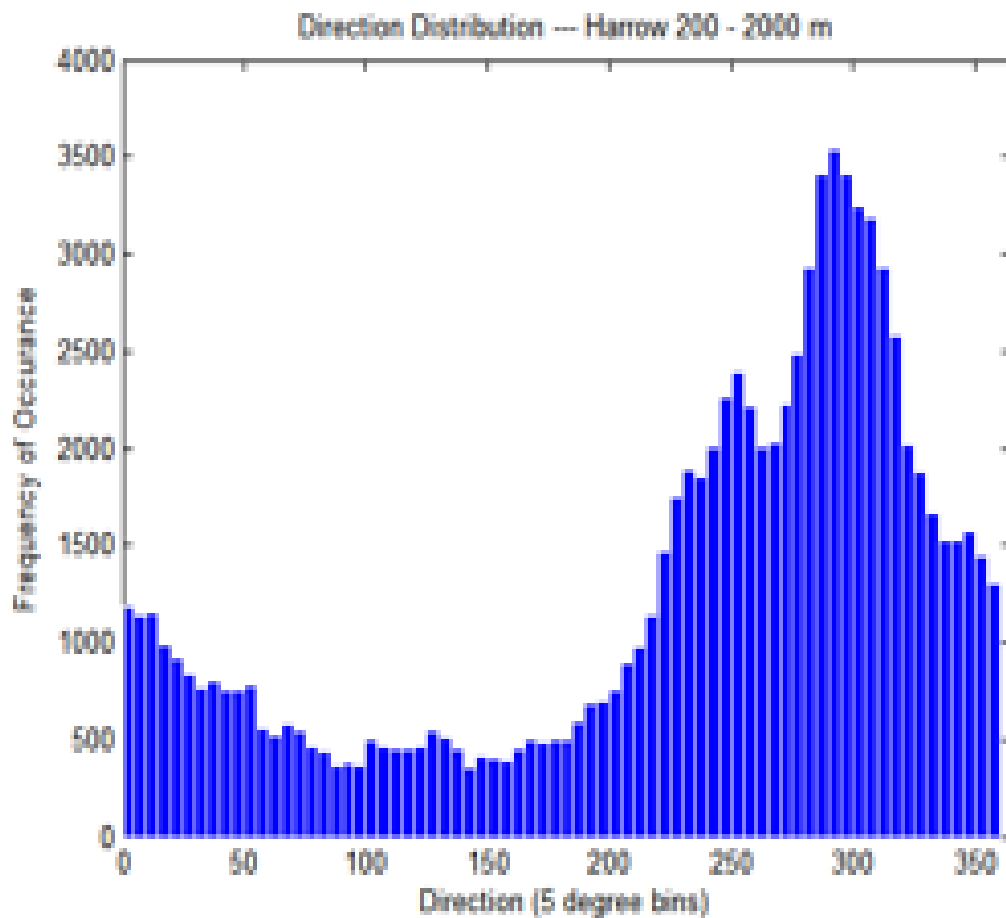


Figure 2.11: Wind direction distribution for 7 months of data using the spaced antenna method at Harrow in 2010.

In Figure 2.11 there is a slightly less predominate westerly component than in the doppler data. This is expected since the spaced antenna method only includes the low levels and west winds are less dominate in the lower atmosphere.

### **2.3 Comparing with Models**

Some of the data from all the operational wind profilers have been obtained by CMC for potential data assimilation in a research version of the GEM regional model but no decision has been made to assimilate this data into the operational GEM model yet. To see how the current operational model is doing against the profiler data, wind speed and wind directional data will be compared against forecast data from the operational Canadian GEM regional model with 15 km horizontal resolution. These forecasts are 48 hour forecasts that are output every 3 hours. In order to compare wind profiler data with the model forecasts, the model forecasts need to be interpolated to the location of the profiler. First a inverse linear distance weighted interpolation is done between the four model grid points surrounding the location of the profiler as in the Figure 2.12.

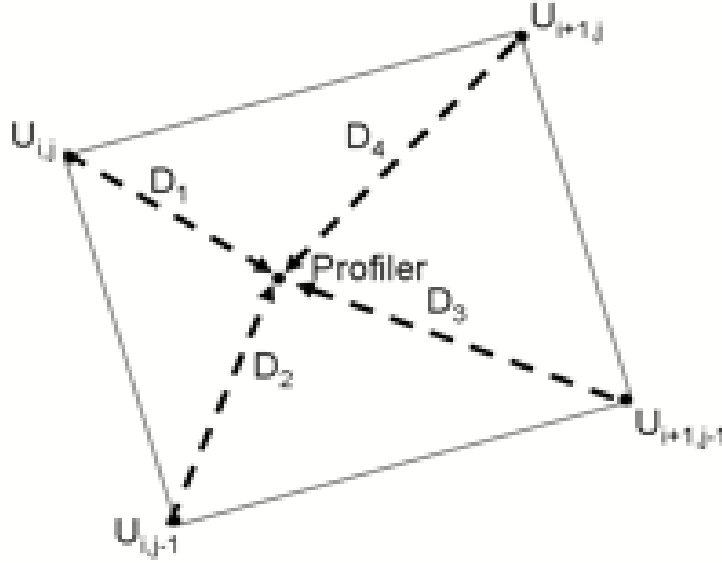


Figure 2.12: A schematic of a model grid cell in the solid lines with a  $U$  wind speed at each corner. The black dot shows location of the profiler and the broken lines show distances from each corner needed to interpolate the model forecast to the location of the profiler location.

In this figure, the  $U$ s are the four nearest model grid location to the profiler and the  $D$ s are the distances between the model grid point and the profiler. Given this

diagram in Figure 2.12, the model estimate ( $U_{Model}$ ) at the profiler is given by

$$U_{Model} = \frac{U_{i,j} \left( \frac{1}{D_1} \right) + U_{i,j-1} \left( \frac{1}{D_2} \right) + U_{i+1,j-1} \left( \frac{1}{D_3} \right) + U_{i+1,j} \left( \frac{1}{D_4} \right)}{\frac{1}{D_1} + \frac{1}{D_2} + \frac{1}{D_3} + \frac{1}{D_4}}. \quad (2.1)$$

Equation 2.1 can be used directly for wind speed but for direction the sine and cosine components need to be considered. Inverse weighting has been used instead of bilinear interpolation because the GEM model runs on an irregular grid making bilinear interpolation unsuitable as a interpolation method. In the vertical, a linear interpolation is done between the nearest two model geopotential levels to each

pre-determined wind profiler level. The vertical interpolation is given by

$$U(H) = (1 - w) \bullet U_m(k) + w \bullet U_m(k + 1)$$

$$w = \frac{H - Z(k)}{Z(k+1) - Z(k)} \quad (2.2)$$

where  $H$  is the height of a particular profiler level,  $U_K$  is the model estimation below  $H$ ,  $U_{k+1}$  is the model estimation above  $H$ ,  $Z_K$  is the the height of  $U_{M_k}$  and  $Z_{k+1}$  is the height of  $U_{M_{k+1}}$ . Once the model estimates have been interpolated to the exact location and height of the profiler measurement, the model estimates can be directly compared to the measurements from the profiler. To assess the differences between the model and profiler measurements the mean absolute error (MAE) and mean bias will be calculated. In comparing the wind between model estimates and profiler measurements, it will assumed the profiler measurements are perfect, even though the profilers have small errors associated with their measurements. The MAE is given by

$$MAE = \frac{\sum_{i=1}^n |(p(i) - m(i))|}{n} \quad (2.3)$$

where  $p(i)$  is the wind measurement and  $m(i)$  is the model estimate of the wind. In this equation  $n$  is taken to be the number of 3 hour outputs of the model in the 48 hour forecast ( $n=16$ ). The mean bias is given by

$$Bias = \frac{\sum_{i=1}^n (p(i) - m(i))}{n} \quad (2.4)$$

where  $p(i)$ ,  $m(i)$  and  $n$  are as defined above.

## 2.4 Results

In this study, model forecasts will be compared for 5 different profilers; Harrow, Egbert, Gananoque, Negro Creek and Walsingham. Most weather models including the GEM model are set up to ingest observations to form initial conditions at the 0 forecast hour, or analysis. From this initial state, the model moves forward in time by solving equations simulating the atmosphere to create forecasts. In comparing the profiler measurements to the GEM model output, data can only be compared every 3 hours since that is the frequency of the GEM model output that is archived. In Figure 2.14, the profiler measurements are compared to the GEM model 3-48 hour forecasts and analysis. The profiler measurements will be compared to the analysis and 3 - 48 hour forecasts (17 three hour forecasts) for the GEM model initialized at 00 UTC for a 12 month period from April 2011 through March 2012. This period was chosen due to the longest consecutive period when the 5 chosen profilers were running and model data were available. In Figure 2.13 are the return rates at 500 m intervals from 1000 m up to 12000 m for all 5 profilers for the period being investigated. These profilers do measure winds at 500 m however, this level is considered a research level and the quality is sometimes questionable and therefore left of this analysis.

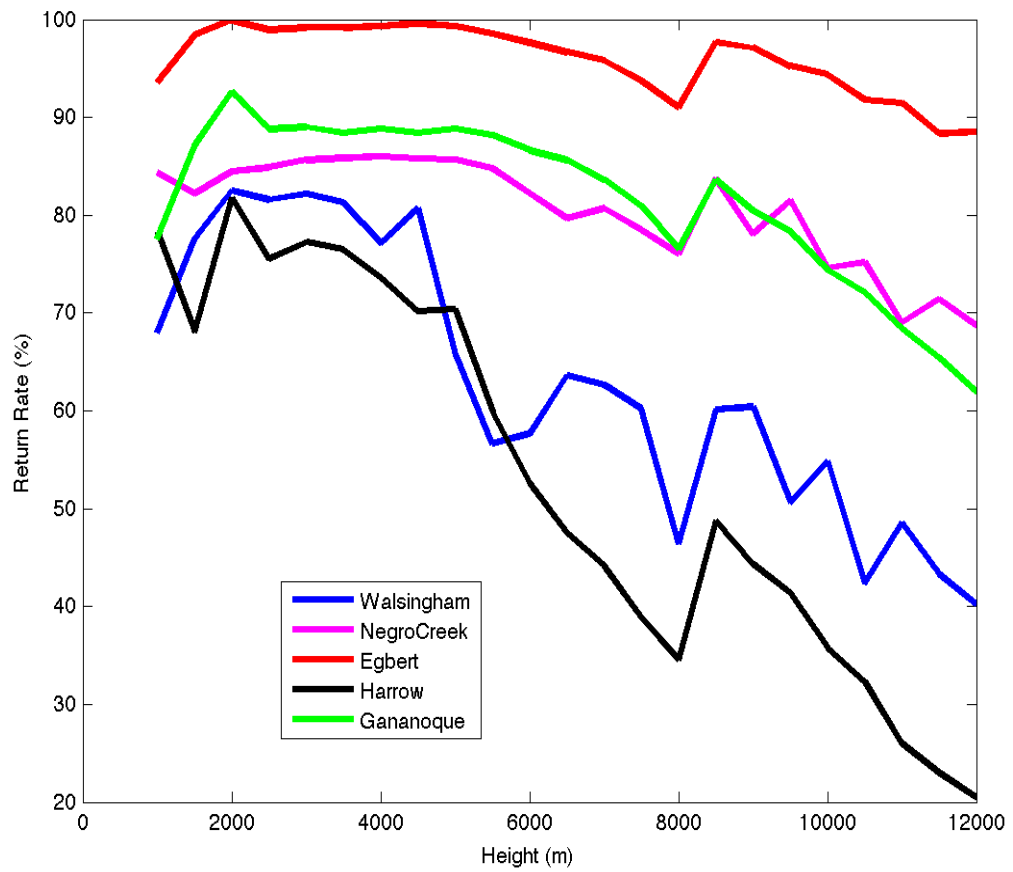


Figure 2.13: The return rates for five profilers for the 12 month period. In cases when an entire month of profiler data is missing, it is omitted in the return rates but when less than a consecutive month is missing, it has been included in the return rates.

In Figure 2.13 the return rates of data are shown for each of the 5 different profilers being investigated in this study. The return rates are generally constant up to 8 km but gradually decrease above about 8 km due to wireless frequency constraints leading to reduced frequency to noise ratios. These constraints are set by the spectrum allocation division of Industry Canada, which defines the frequencies on a case-by-case basis. The current frequency of the profilers is the highest that could be allocated for this project. In some cases the profilers have operational issues that cause lower return rates, and in the case of Harrow, the significant air traffic heading to and from the Detroit airport cause major interference and data loss at the upper levels. In this figure, all profilers show a local minima in data at 8km which is expected in order to achieve optimum signal. The profiles use a variety of modes; for example at lower heights monopulses are used while at upper heights complementary codes are used and the transition level is 8 km. Making the transition smooth is always difficult because the upper method can't really get below about 8 km due to the nature of pulse-coding while the lower signal drops off significantly between 5-7 km which explains the drop in data at 8km.

The errors or differences between profiler measurements and model predictions were investigated for each 3 hour interval and no large differences were found between the 3 hour forecast and 48 hour forecasts even though one would expect forecast error to increase with time. One theory for the cause of little growth in errors

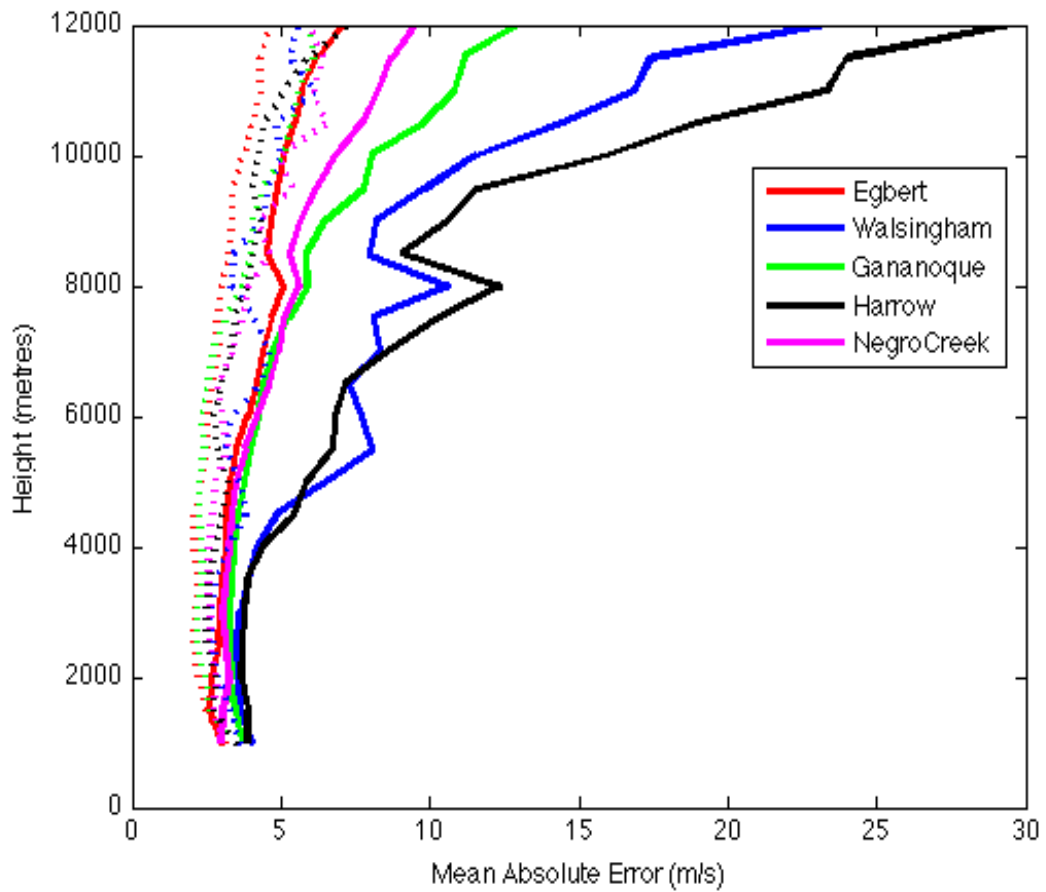


Figure 2.14: The mean absolute error (MAE) in wind speed between the profiler data and GEM model data. The solid line are the MAE between profiler measurements and 3-48 hour GEM forecasts while the broken lines are the MAE between the profiler measurements and the GEM analysis..

with forecast time is that often large outliers account for much of the error and these outliers seem to occur at similar frequency for all forecast hours. For these reasons, errors for between measurements and model will be shown with all forecast hours lumped together. In Figure 2.14, the mean absolute error (MAE) between profiler measurements and GEM model forecasts are shown. The analysis MAE is shown in broken lines and is fairly consistent for all the profiler sites and generally lower than the MAE for the 3-48 hour forecasts which are shown as solid lines. It is not surprising that the MAE is less for the analysis than the 48 hour forecasts since the analysis is when the model ingests observations to initialize the forecast. The MAE increases with height for the 3-48 hour forecasts but one should into account that wind speeds increase significantly as shown in Figure 2.15. The error increases significantly at Harrow and Walsingham with height, likely a result of a couple of factors. Referring to Figure 2.13 the return rates drop off significantly with increasing height at these two locations so there are fewer measurements to go into the MAE so that outliers are more likely to skew the data. As well, from Figure 2.13 the low return rates of data could suggest that the data present may be of lower quality than if there were high return rates. At the other three sites MAE is significantly lower especially above 4000 m which appears to be proportional to the higher return rates in Figure 2.13 .

Figure 2.15 shows the MAE in wind speed between profilers and GEM model data

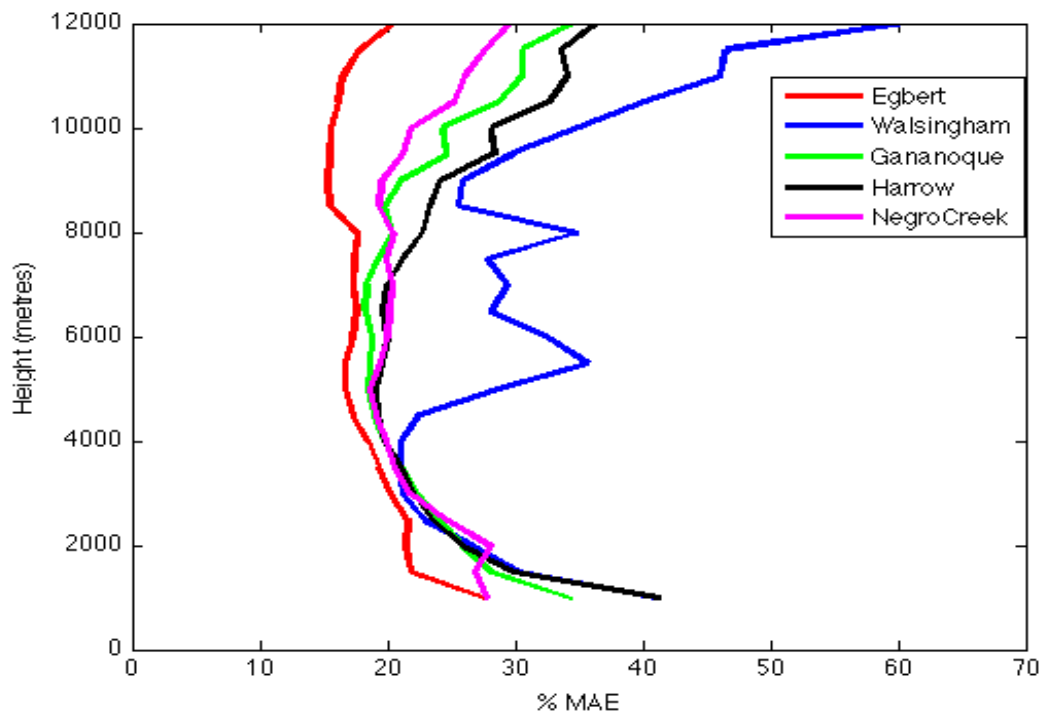


Figure 2.15: The mean absolute error (MAE) between the profiler data and GEM model data in wind speed as a percentage of the average measured wind speed at each level.

for 3-48 hour forecasts as a percentage of the measured wind speed at each level. For each profiler but Walsingham, the percentage error is relatively constant except for slight increases at the low and high levels. Walsingham has much higher percentage error in wind speed at the mid and upper levels which may be a result of the profiler being near the Lake Erie shore and in ability of models to predict wind speeds as well near bodies of water.

In Figure 2.16, the bias between the model analysis and profiler measurements are shown in broken lines while the solid lines represent the bias between the model forecasts and the profiler measurements. Generally the bias in the analysis and 48 hour forecasts show similar results but the analysis seems to have more bias overall. This is likely a result of comparing only one measurement to one model data point so there is much less data averaging than in the 48 hour forecasts. Egbert and Gananoque have very little bias up to about 8 km. Harrow and Walsingham have a positive bias which suggests that the model is over predicting wind speed at these two sites, while a negative bias below 8 km suggests the model is under predicting the wind speeds at NegroCreek. Between 8 km and 10 km the bias is negative for all profilers suggesting the model is over predicting the winds at these levels. This is not surprising since this is the locale of the jet stream and models are known to have a hard time predicting its exact location and speed. Above 10 km, the model under predicts the wind speed at all five profiler locations which may be a result

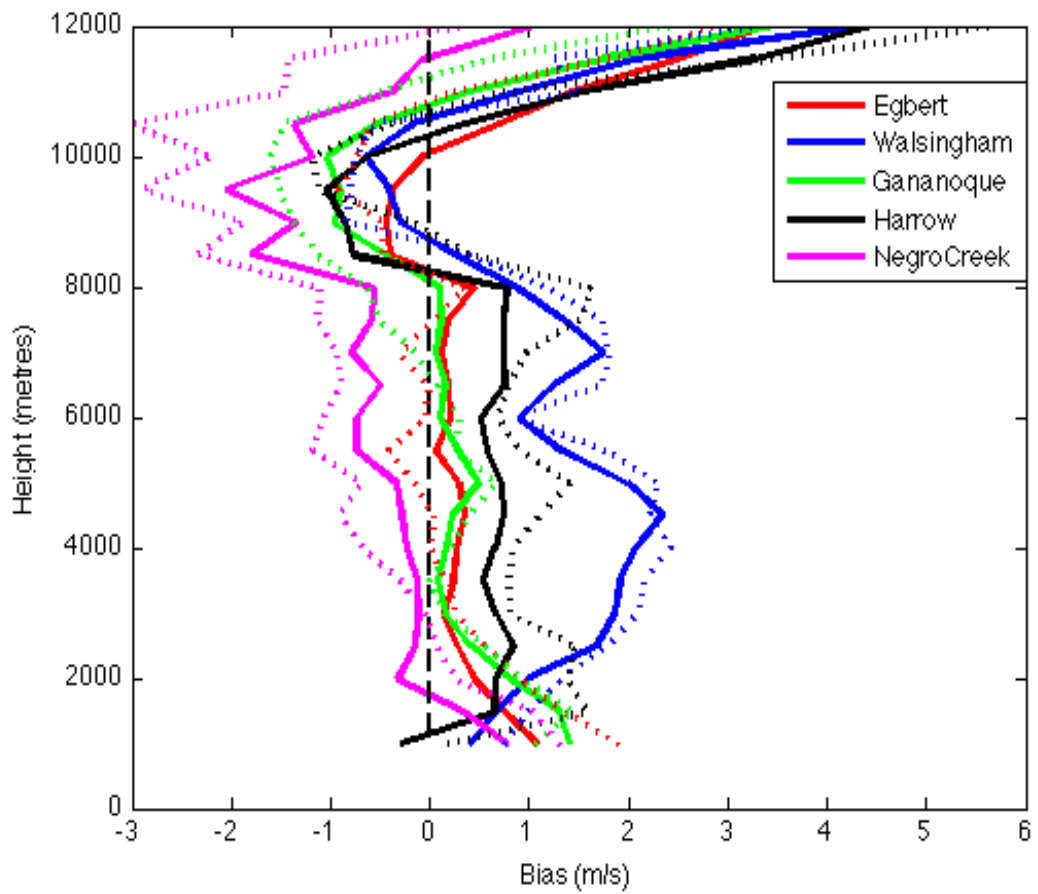


Figure 2.16: The wind speed bias (as defined in Equation 2.4) in the GEM model compared to each of the wind profilers. The broken lines are the model analysis and the solid lines are the model 3 - 48 hour forecasts.

of the model estimating the jet stream at the wrong altitude assuming the OQ-net data are correct. Now that the MAE and Bias have been investigated for wind speed at the five different wind profilers, the same can be done for wind direction. The mean absolute error of wind direction between the GEM model and each of the 5 profilers is shown in Figure 2.17.

In Figure 2.17 there are only slight deviations in the direction error between the analysis and the forecasts and similar trends between the two. A trend that is notable with all the data is the error decreases with height which makes sense since winds are far less variable at higher altitudes meaning wind direction is more constant and easier to forecast. In Figure 2.17, Egbert, Walsingham, Harrow and Gananoque all have similar errors while NegroCreek has about a 10 to 15 degree larger error from about 1000 m right up to 12 000 m. One possible reason for this larger error is the location of NegroCreek, situated somewhat between Lake Huron and Georgian Bay. A location between two bodies of water like this would make for large swings in wind direction something that is difficult to forecast. Another possible reason for larger errors at NegroCreek is that it is further away from flight paths from which wind data are assimilated in the models to increase the accuracy. This provides additional motivation to use profiler data in the models to increase their accuracy.

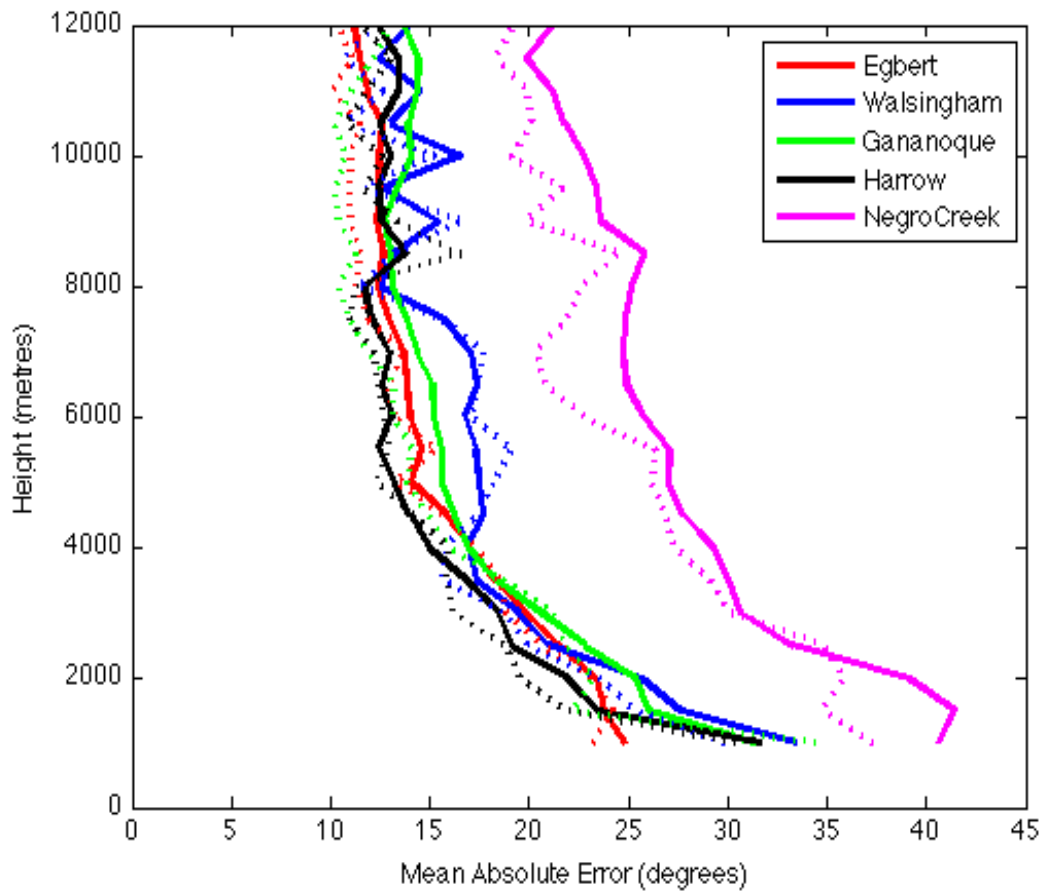


Figure 2.17: The MAE in wind direction for each of the five profilers compared with GEM model analysis in broken lines and 48 hour forecasts in solid lines.

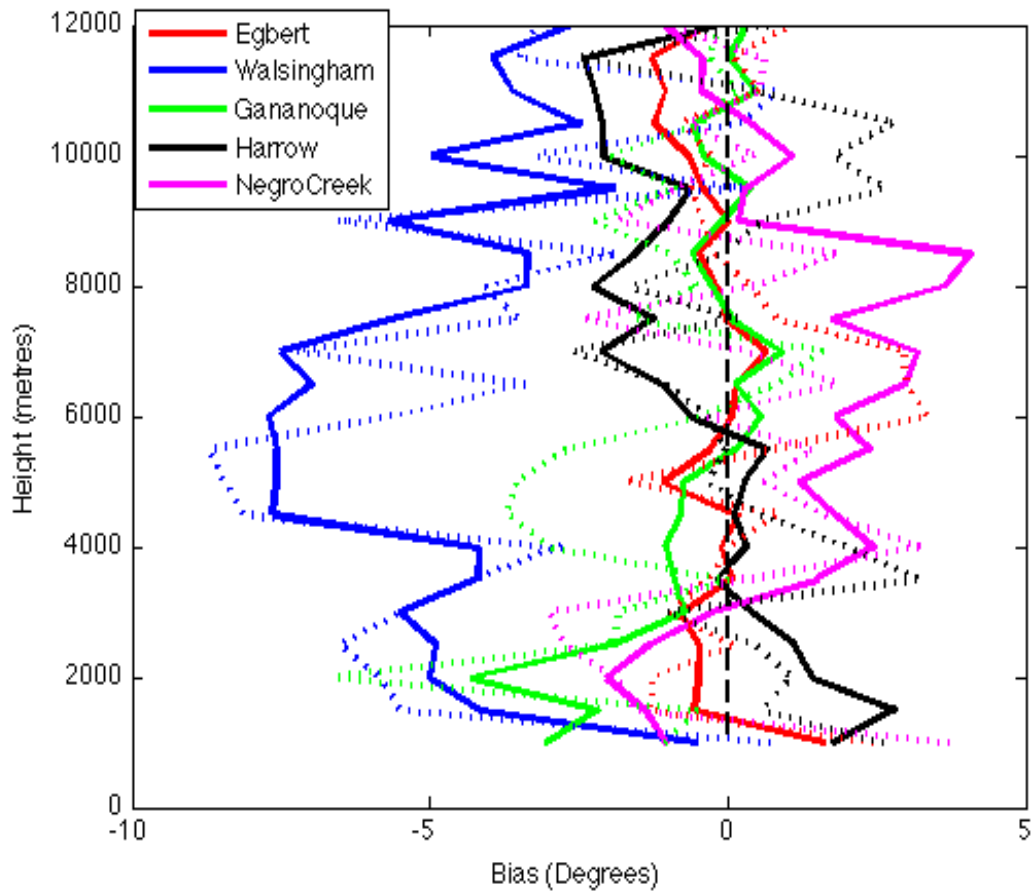


Figure 2.18: The bias in wind direction between the GEM model analysis and the 48 hour forecasts compared with each of 5 profilers.

In Figure 2.18, the in wind direction bias is shown between the GEM model and data from the 5 profilers. The bias in the GEM model analysis relative to data at each of the 5 profilers seems to follow the bias in the 48 hour GEM forecasts pretty well with a few exceptions. The GEM model shows similar and fairly low bias at

Egbert, Harrow and Gananoque compared with the measured wind profiler data. The bias at NegroCreek is negative closer to the surface and changes to a positive bias at 4000 m up to 8000 m before moving to very little bias at the upper levels. In the context of wind direction and the way bias has been defined in Equation 2.4, a negative bias suggests the model is backing the winds too much while a positive bias suggests the model is veering the winds too much. In the case of wind direction at Walsingham, the bias is negative through the entire column from 1000 m through 12000 m which is likely a result of being so close to the lake shore of Lake Erie and the model having a bias of over water wind direction assuming the OQ-net measurements are correct.

## 2.5 Comparing Data to Radiosonde

Finally, in the analysis of the wind profiler data, the data at Harrow can be compared with radiosondes from Detroit airport to help validate the data. In Figure 2.19 is a vertical profile of wind speed at Harrow from the profiler, the GEM model and the Detroit radiosonde.

In Figure 2.19, the wind speed profiles are shown from the Detroit radiosonde in blue, the Harrow profiler in green and the GEM 00 Z analysis in red on November 14, 2009 at 00Z. The measured wind speed profile at the Harrow profiler matches the measured profile at the Detroit radiosonde which is located about 50 km south west

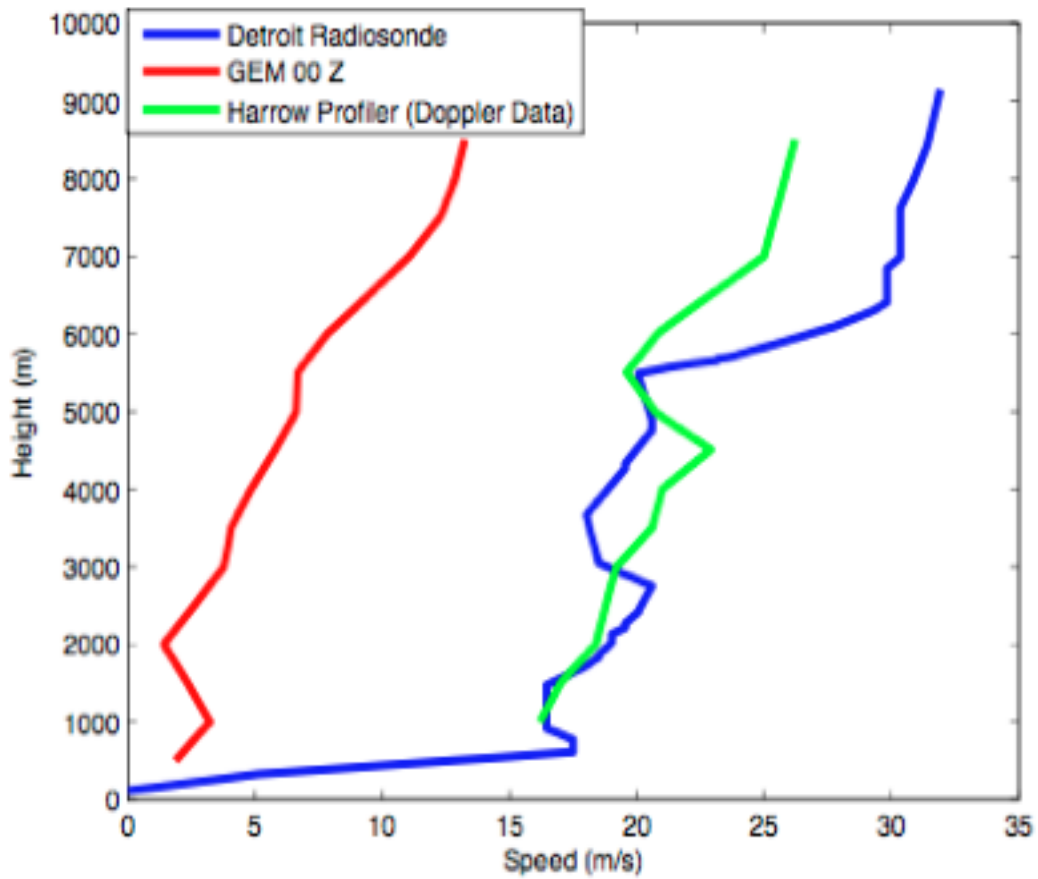


Figure 2.19: Vertical profiles of wind speed for the Harrow wind profiler, GEM 00Z analysis and the Detroit Radiosonde on November 14, 2009 at 00Z.

of the profiler site. The GEM model is on the other hand lower by about 10 m/s which shows large the difference between model and measurements. Although this may be an extreme case, several examples were examined at and these differences are not uncommon. Given these large differences such as in Figure 2.19, between the Harrow profiler and the GEM model, the large MAE is not surprising in Figure 2.17.

In Figure 2.20, the direction profiles are shown from the Detroit radiosonde in blue, the Harrow profiler in green and the GEM 00 Z analysis in red on November 14, 2009 at 00Z. The Harrow profile differs very little from the Detroit radiosonde but both differ significantly from the profile generated from the GEM 00 Z analysis. The GEM model differs from the other profiles by up 100 degree at some points in the profile showing how much the model can differ from the measurements and help explain the large direction MAE in Figure 2.17.

As another validation site, the Maniwaki radiosonde is about 12 km southwest of the Aumond wind profiler. Figure 2.21 shows a vertical profile of wind speeds of the Aumond wind profiler, GEM analysis and the Maniwaki Radiosonde on September 4, 2010 at 00Z.

The Aumond wind profiler, GEM analysis and the Maniwaki Radiosonde all match fairly well and each show the low level wind jet although each vary it in height. The model profile matches the radiosonde quite closely compared to the Detroit

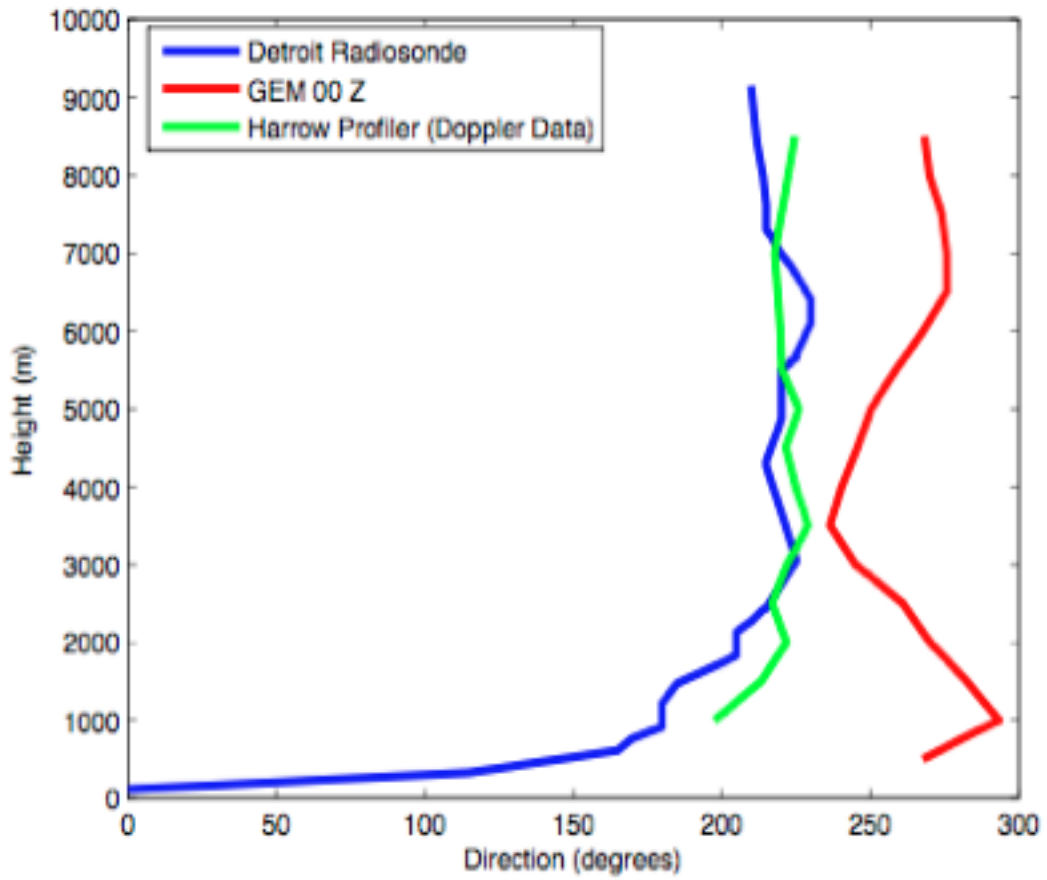


Figure 2.20: Vertical profilers of wind direction for the Harrow wind profiler, GEM 00Z analysis and the Detroit Radiosonde on November 14, 2009 at 00Z.

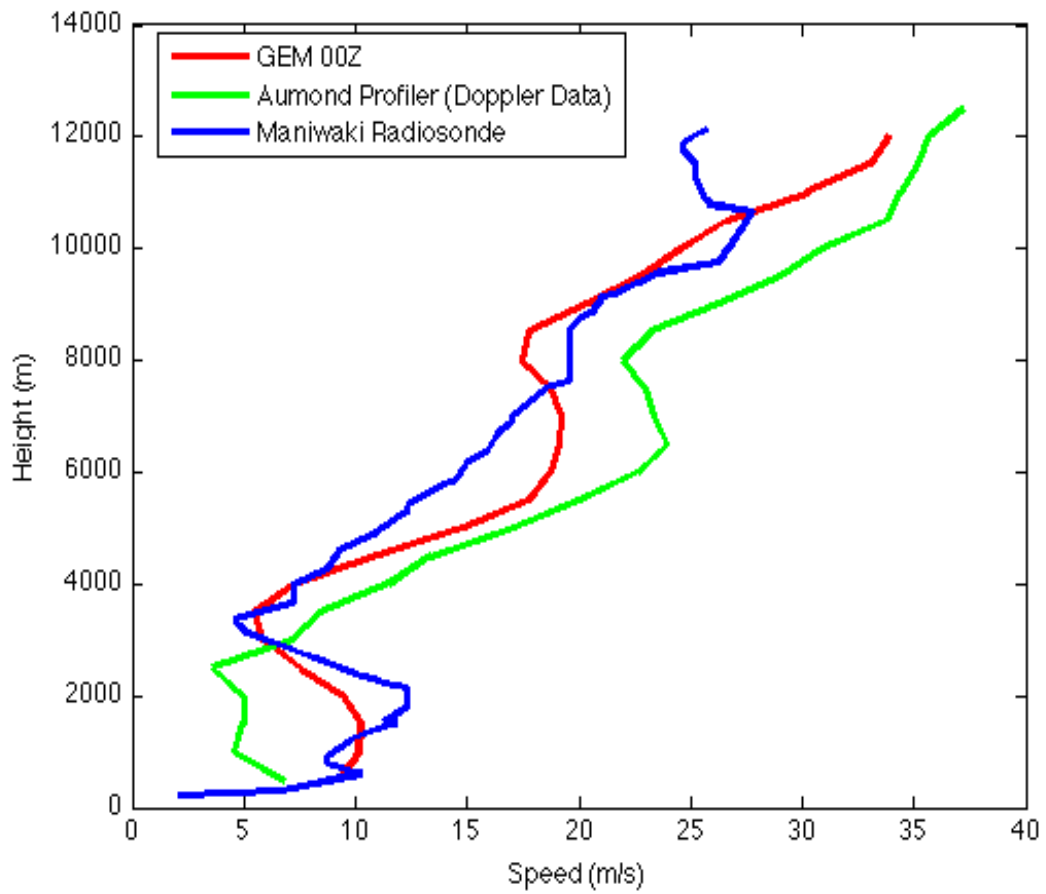


Figure 2.21: Vertical profilers of wind speed for the Aumond wind profiler, GEM 00Z analysis and the Maniwaki Radiosonde on September 4, 2010 at 00Z.

case but may be a result of being further from the a large body of water. Although the vertical profile of the Aumond profiler is slightly further from the Maniwaki profile, it can still be considered accurate taking into account the distance between the two and the difference between the hourly average and a single sample for the radiosonde.

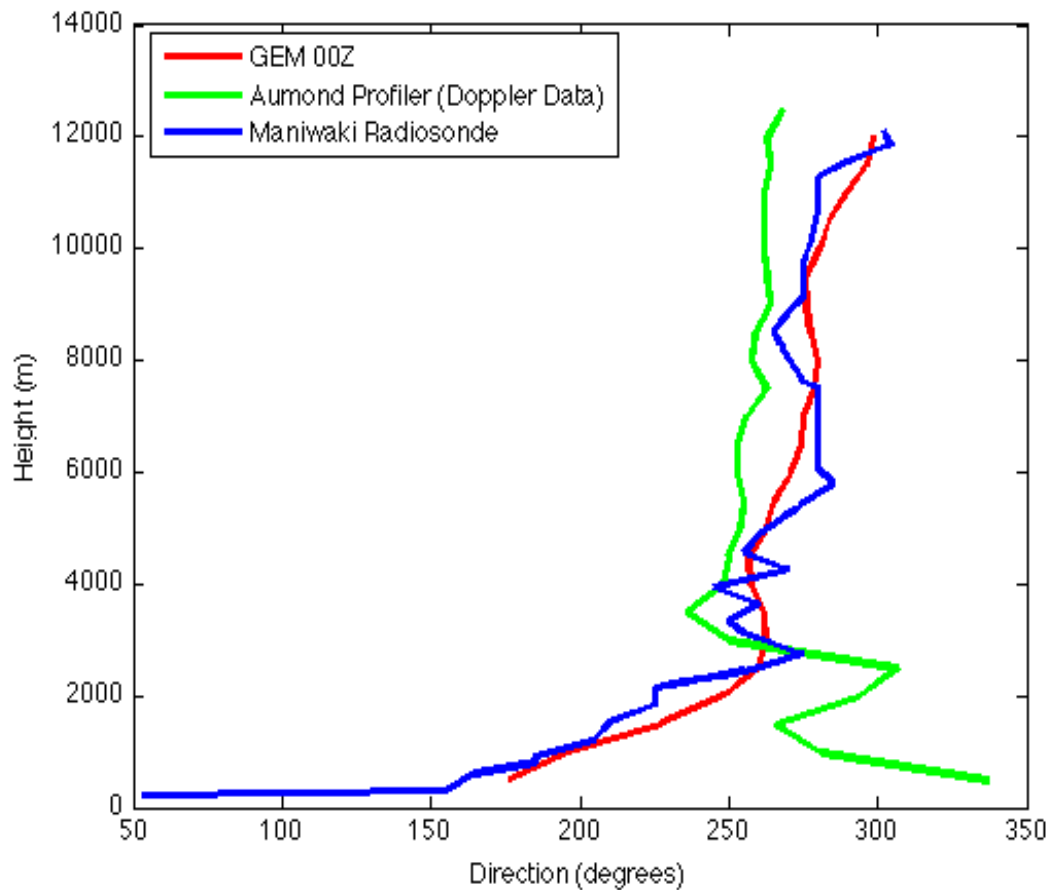


Figure 2.22: Vertical profilers of wind direction for the Aumond wind profiler, GEM 00Z analysis and the Maniwaki Radiosonde on September 4, 2010 at 00Z.

In Figure 2.22, the directional profile of the Aumond wind profiler, GEM 00Z analysis and the Maniwaki Radiosonde are very similar except that the Aumond profiler shows about 50 - 100 degree difference at the surface. It does show the sharp change in direction at 2500 m. The lowest level of these wind profilers is still a research level and may help explain the large deviation in wind direction.

Figures 2.19 through 2.22 show an initial snap shot into profiler and radiosonde comparisons but the work by Zheng Qi Wang et al. in [25] shows a year's worth of radiosonde and profiler comparisons. Figure 2.23 compares wind speed and direction from the Aumond wind profiler and radiosonde profiles Maniwaki for the period of May 2012- April 2013. The differences in wind speed in the top panel and wind direction in the lower panel are comparable to the differences in the individual profiles shown above. A similar comparison was done for Harrow and the Detroit radiosonde by Zheng Qi Wang et al. showing similar results

## **2.6 OQ-net Summary**

Although there are some deviations between the radiosonde and the wind profilers, overall the agreement is quite good, showing the accuracy of the wind profilers can be trusted. The OQ-net is a powerful resource to help understand the meteorology of Southern Ontario and help improve the forecasts. The large differences shown in this investigation, especially in the GEM model analysis help make a strong case

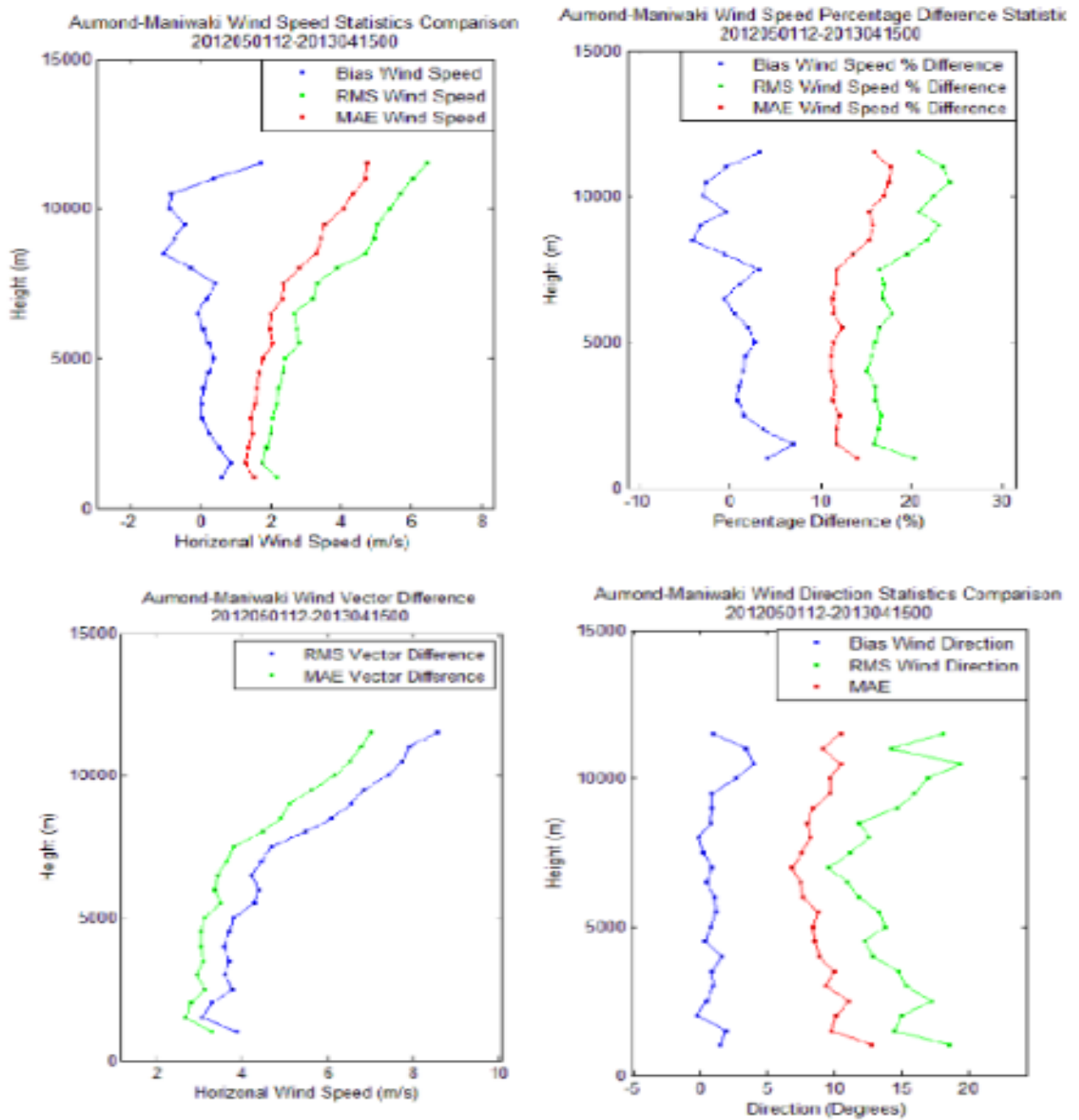


Figure 2.23: Summary statistics of differences between winds measured at the Aumond wind profiler and radiosonde profiles from Maniwaki. May 2012- April 2013. This Figure is from work by Zheng Qi Wang et al. in [25]

to continue work to use data from the OQ-net in the data assimilation process for the GEM model to help correct these errors. Other work is being done to use the data from the OQ-net as an entire network to help predict severe weather in the region.

## **3 Investigating a Possible Wind Energy Site in Lake Ontario**

### **3.1 The Site**

Looking at the Canadian wind energy atlas produced by CMC, the Great Lakes hold an excellent wind energy resource as shown in Figure 3.1 [4]. Figure 3.1 is a map of the 50 m mean wind speed for all of Canada run at 5 km resolution. This map clearly shows the high wind speeds throughout the Great Lakes. This wind resource is untapped and up until the past few years was largely un-explored. Although the entire Great Lakes have a great wind energy potential, the Canadian side of the lakes statistically will have the best wind resource because the prevailing wind direction is south - south west which allows the winds to ramp up, taking advantage of the long over-water fetch. Toronto Hydro decided to study the wind resource near the northern shore of Lake Ontario just east of the city of Toronto as shown in Figure 3.2.

Mean Wind Speed at 50 m above ground  
Vitesse moyenne du vent à 50 m au dessus du sol

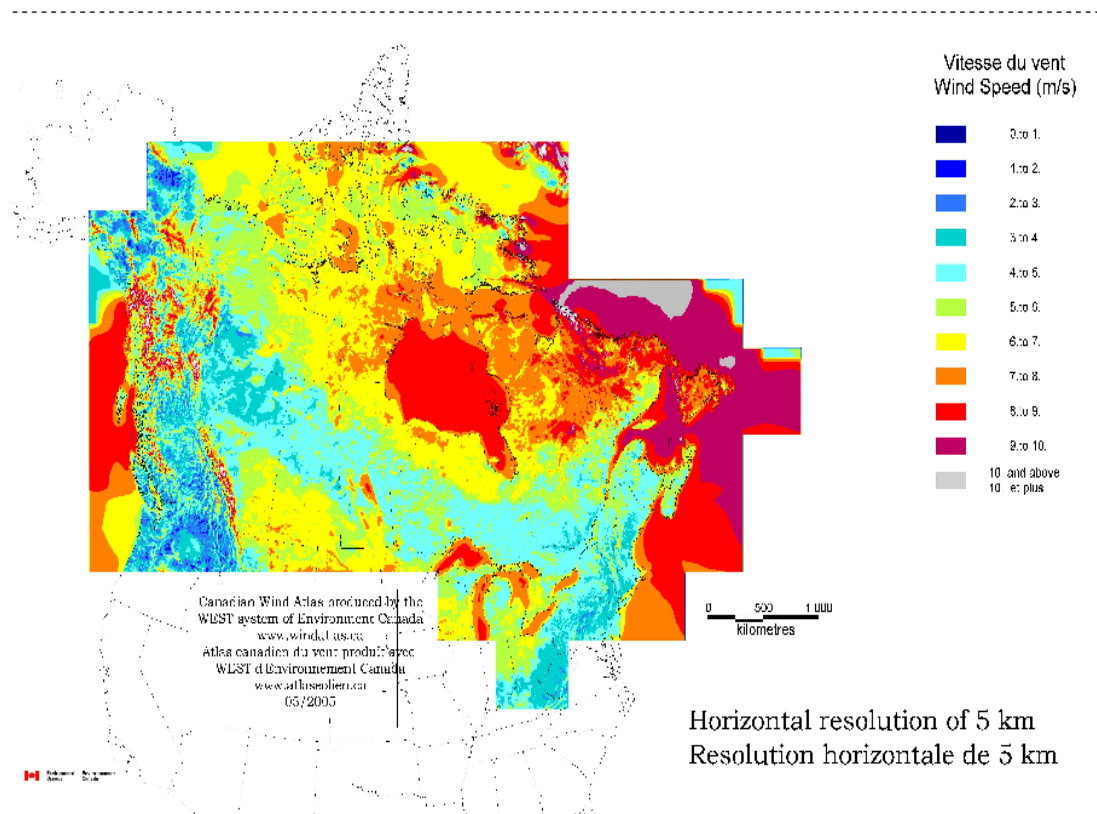


Figure 3.1: A map of the 50 m mean wind speed for all of Canada run at 5 km resolution by CMC [4].

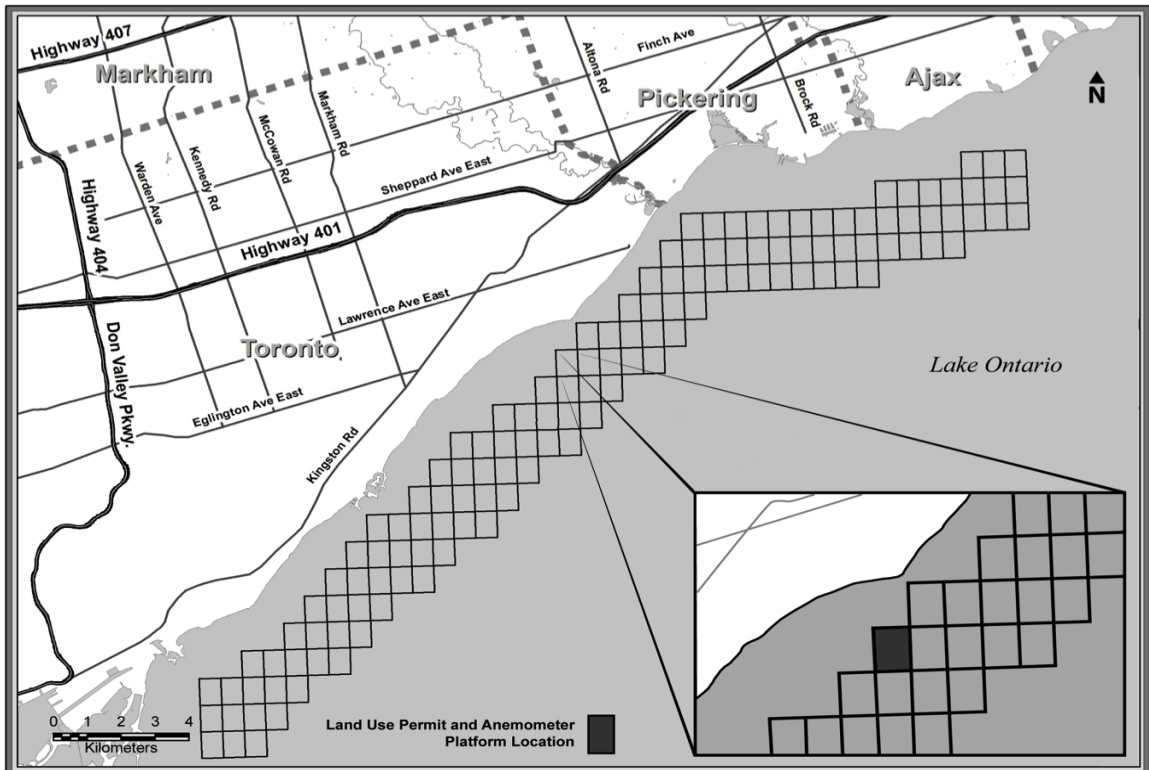


Figure 3.2: Location of the study area for a potential wind farm proposed by Toronto Hydro and the darkened cell is the location chosen for the Lidar and Anemometer platform.

They chose to use a lidar to make wind measurements at 6 levels above a platform, as well as allowing York University to install platform level anemometers, humidity, temperature and pressure sensors. The lidar that was chosen is the ZephIR with range of 10 m through 150 m. The platform shown in Figure 3.3. It used a cell phone for communication of the data while small wind turbines and solar panels were used to power the lidar and communications. The lidar was programmed to measure wind speed and direction at 17, 30, 45, 60, 90 and 120 m above the water surface. The platform sits about 7 m above the lake surface. The in-situ wind, air temperature, pressure and relative humidity measurements are approximately at 7 m above the water surface.

The lidar makes a measurement every 3 seconds for one of the levels and does this continuously for 10 minute intervals from which it computes a 10 minute average for each level using all available measurements during that period. Each level can have up to 33 measurements in 10 minutes but weather conditions along with other problems often decrease the number of measurements significantly. The software computes a 10 minute average so long as there is at least one measurement. Problems can arise though when there are low numbers of measurements and a 10 min wind speed average that is inaccurate can occur. For this reason further quality control is needed to ensure the each 10 minute average is reliable. The method that has been developed here looks at probability distributions of the ratio of consecu-



Figure 3.3: The Toronto Hydro platform in location denoted in Figure 3.2. The #1 shows the small wind turbines for power, #2 is an anemometer, # 3 is the Lidar and #4 is the solar panels for power.

tive points in time at each level. This method looked both at the point before and after each measurement in time. Through careful analysis and looking at different cases, it has been determined that the top 1% of ratios of consecutive points in time at each level are likely inaccurate and these data will be filtered out.

Measurements started in June 2010 but the lidar was removed in July 2011 for repair and due to many delays was not operational again until May 2012. Using all available lidar data for 14 months from June 2010 through July 2011, probability distributions of consecutive 10 minute wind speed averages show that for levels 120, 90, 60, and 45, 99 % of the data has a ratio of less than 1.6 or greater than 1/1.6 while this ratio is 1.7 for the levels 30 m and 17 m. The first 14 months were chosen to obtain these ratios because that was when there was best data recovery. Although this may filter out the occasional accurate 10 minute wind average during severe weather or a frontal passage this is considered minimal. The plot in Figure 3.4 shows a one day time series at 120 m of the filtered and non filtered data. In Figure 3.4 the red points are unfiltered while the green are the data after they have been run through the process described above. In this case, there are 2 points which have been filtered out and it is clear why these points have been removed.

Table 3.1 shows the % of missing data for each of the 25 months (although for 9 months there are no measured lidar data) for the raw data and filtered data at the 120 m level. The other levels are similar. The 120 m level is chosen to show the

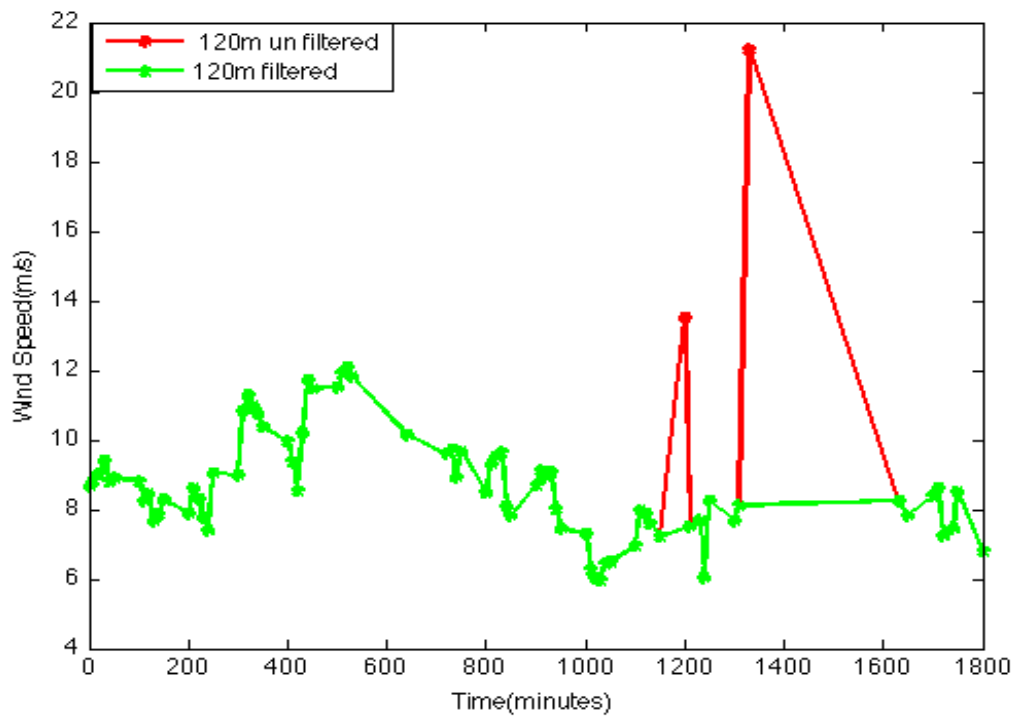


Figure 3.4: A time series of the 10 minute wind speed for December 27, 2010 at 120 m lidar level. The green series is the filtered data and the red series is the unfiltered data.

<b>Month</b>	<b>Raw Data</b>	<b>Filtered Data</b>
June 2010	97.55	96.55
July 2010	99.00	98.05
August 2010	95.63	95.30
September 2010	90.12	89.75
October 2010	94.67	94.20
November 2010	92.85	92.18
December 2010	96.06	95.79
January 2011*	36.42	36.35
February 2011*	64.59	62.24
March 2011	67.75	64.26
April 2011	48.85	41.61
May 2011	78.72	78.01
June 2011	93.45	92.82
July 2011*	29.84	29.73
August 2011	0	0
September 2011	0	0
October 2011	0	0
November 2011	0	0
December 2011	0	0
January 2012	0	0
February 2012	0	0
March 2012	0	0
April 2012	0	0
May 2012	76.89	75.14
June 2012*	61.42	61.21

Table 3.1: Percentage of raw measured data at 120 m as well as data after the filtering process described has been executed. The \* shows months where the lidar was down for part of the month.

return rates because this is the highest lidar level and has the lowest data return, so return rates increase slightly at lower levels. The filtered percentage of data return is on average about one percent less than the raw data return rate. This is expected based how the filtering is defined. Some months the data are worse than others such as April 2011 when about 7 percent of the data have been filtered out as inaccurate data. This is not surprising because there the wind shield wiper to keep the lidar lens free of rain was stuck in the middle of the lens during this month. In this quality control process, any wind speeds that have been rejected for being inaccurate by the process described above also have the corresponding wind direction with the same time stamp rejected.

Monthly averages of the 90 m winds initially computed by Toronto Hydro Lidar software seemed to not recognize missing data and the software appears to take these missing measurements as zero wind speeds when calculating monthly averages. For months like July 2010 when data return was near 100%, this mis-calculation has little effect, but for months like April 2011 when data return was under 50 %, the average initially calculated by the Toronto Hydro software was much lower than the available measurements show.

In an effort to provide a full data set to provide the best possible estimation of monthly averages and power estimations, missing data from the 90 m lidar level are being estimated using 2 combined methods. The first method looks to see if

four or more measurement levels ( from the 6 lidar levels + 7 m met station) are available at a given time in which case a power law fit and a log fit are done for the available data and error is calculated for each fit. The fit with the least error is then used to estimate wind speed at 90 m. If less than 4 measurements are available, the 90 m wind speed is estimated using the 7 m data from the met station at platform level. This estimation is done by calculating the ratio of 90 m to 7 m measured wind speeds for each time when both the data are available. For any times when the 90 m wind speed is missing, it can be estimated using the 7 m wind speed and this ratio. This ratio of 90 m to 7 m wind speed is calculated 4 different ways, the first using 22.5 degree wind direction sectors and shown in Figure 3.5.

For onshore directions (112.5 - 225 degrees) the profile has adjusted to be almost in equilibrium with the underlying surface. In contrast, offshore flow the low level winds (7 m) have started to accelerate over the smoother water surface and the 90 m level shows less acceleration and the wind speeds are more characteristic of over land values. As a result,  $\frac{U_{lidar}}{U_{met}}$  is slightly lower for offshore flows. This is what is shown in Figure 3.5. The data used in Figure 3.5 are all 10 minute averages for 14 months from June 2010 to July 2011 when both the 90 m lidar and 7 m anemometer wind speeds are available. The error bars show 1 standard deviation around the average ratio and the error bars that show negative are to be consistent when in reality no ratio can be negative. The large ratios are caused mainly by

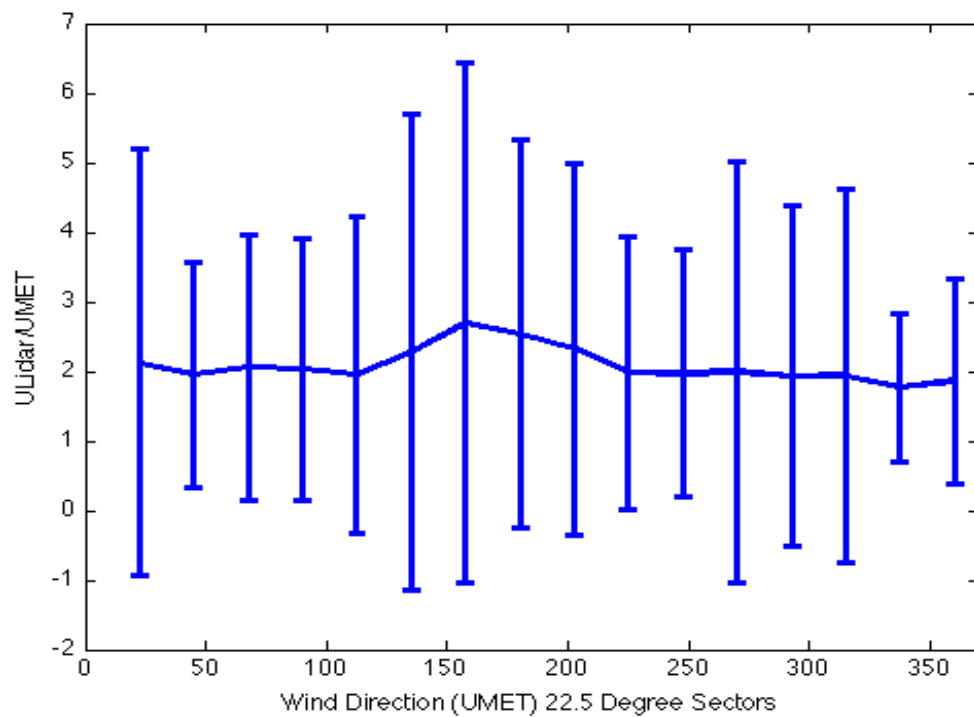


Figure 3.5: The ratio's of the 90 m wind speed to the 7 m met. station wind speed by 22.5 degree wind direction sectors for 14 months of data from June 2010 to July 2011. The error bars show 1 standard deviation above and below the mean ratio.

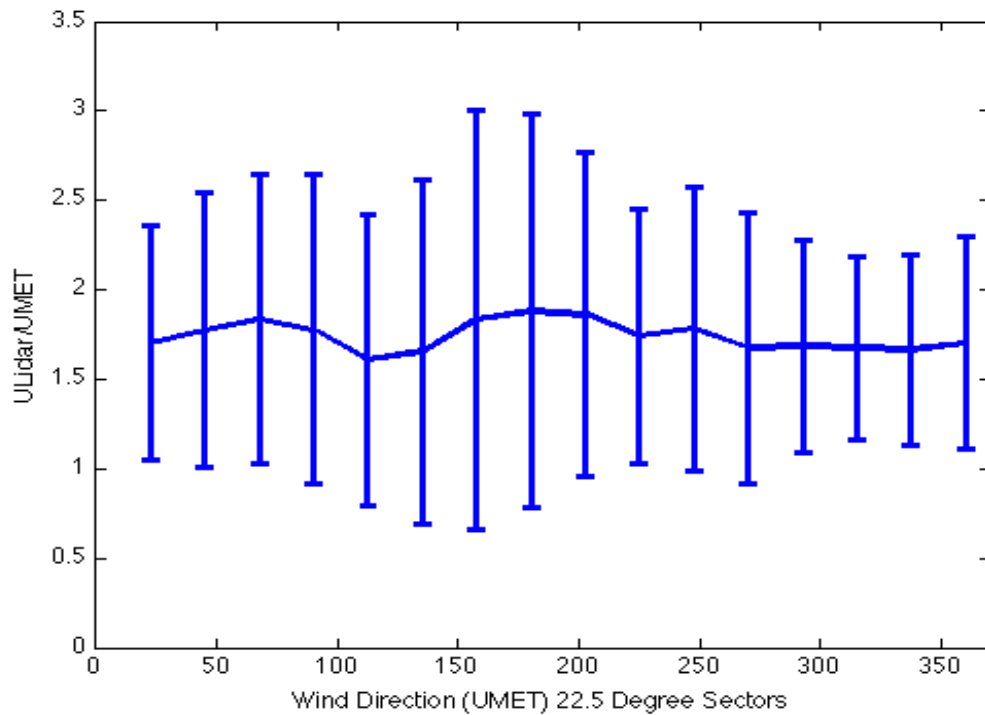


Figure 3.6: The ratio's of the 90 m wind speed to the 7 m met. station wind speed by 22.5 degree wind direction sectors for 14 months of data from June 2010 to July 2011. In this figure all times when the met wind speed is less than 1m/s are excluded. The error bars show 1 standard deviation above and below the mean ratio

very low 7 m wind speeds which cause large errors. For example one instance was found when the 7 m wind speed was 0.1 m/s and 90 m wind speed was 4 m/s giving a ratio of 40. Arguably the anemometer cannot measure wind speeds less than 1 m/s accurately. Figure 3.6 shows the ratio between 7 and 90 m wind speeds for all 10 minute averages between June 2010 to July 2011 excluding 10 minute intervals

when the 7 m wind speeds are less than 1 m/s. Similar to Figure 3.5, the ratios increase for directions of 112.5 to 225 degrees as a result of the long over water fetch for these directions. Comparing the Figure 3.5 to Figure 3.6, the ratios between 7 m and 90 m wind speeds are similar but the error bars in Figure 3.6 are much smaller which show that wind speeds of less than 1 m/s create outliers that increase the standard deviation significantly. To investigate a slightly different approach to calculating ratios between the 7 m wind speeds and 90 m wind speeds, Figure 3.7 shows the ratios that have been calculated using wind speed bins instead of wind direction sectors.

Figure 3.7 shows the ratio between 7 m and 90 m wind speeds for 14 months of data from June 2010 to July 2011 calculated using 17 wind speed bins based on 7 m wind speeds.. The wind speed bins were 0 - 0.5 m/s, 0.5 - 1 m/s, 1 m/s intervals between 1 and 15 m/s and 15 - 40 m/s with the error bars showing 1 standard deviation above and below the mean ratio. The ratio and error bars decrease with increasing wind speeds except when they increase for high wind speeds slightly. The large ratios and error bars at low wind speeds help motivate excluding instances when wind speeds are less than 1m/s at 7 m. Finally the two methods of ratio calculation can be combined to calculate the wind speed ratio between 7 m and 90 m wind speeds using wind speed bins and wind direction sectors and this is shown in Figure 3.8.

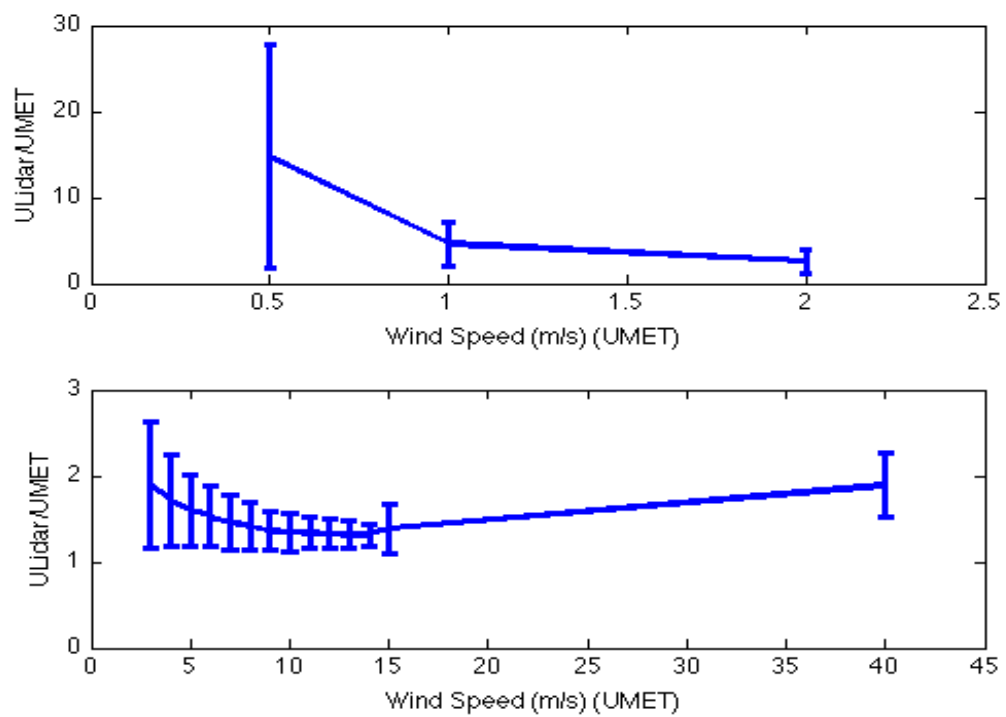


Figure 3.7: This figure shows the ratio's of the 90 m wind speed to the 7 m met. station wind speed by wind speed sectors for 14 months of data from June 2010 to July 2011. The error bars show 1 standard deviation above and below the mean ratio.

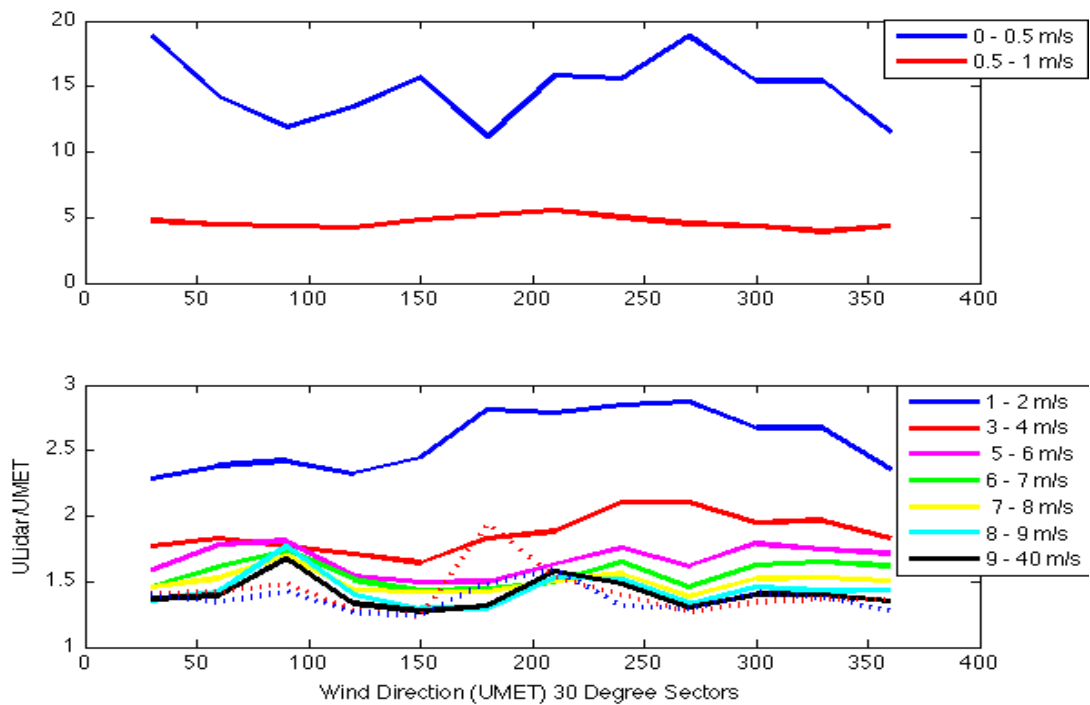


Figure 3.8: The ratio's of the 90 m wind speed to the 7 m platform level wind speed by wind speed and wind direction sectors for 14 months of data from June 2010 to July 2011. The error bars have been omitted in this figure to avoid clutter but the errors are similar to Figure 3.6 and Figure 3.7.

Figure 3.8 shows ratios calculated using wind speed bins and wind direction sectors or 14 months of data from June 2010 to July 2011. The error bars have been omitted to avoid cluttering the figure, but the errors show similar trends to those methods using just wind speed bins or wind direction sectors. The wind direction sectors have been changed slightly to 30 degree sectors instead of 22.5 degrees and the upper sector of wind speed has been changed to 9- 40 m/s instead of 15 - 40

m/s. These changes have been to ensure that data are not too scarce in some of the sectors. Similar trends are seen in the ratios with double sectoring where the ratios decrease with increasing wind speed.

### **3.2 Filling in Missing Data**

The objective of any wind resource assessment campaign is to achieve 100 % data return, but this is challenging for an offshore site like the one being investigated here, and as seen in Table 3.1 was not achieved. Even with ever improving technology, offshore wind resource instruments face really harsh conditions and in northern regions like Lake Ontario during winter, wind can create freezing spray and coat any object in its way in a thick layer of ice. Not only can this create operational issues for instrumentation and communication, it makes access and maintenance of any equipment, dangerous, costly and sometimes impossible, in part because of ice build-up on the access ladder to the platform.

As mentioned previously, the lidar is set up to measure 6 levels (17, 30, 45, 60, 90 and 120 m) plus a platform level anemometer at 7 m above the water. The lidar is configured to make measurements at one level every 3 seconds and output 10 minute averages at each level. If there are not enough measurements to go into the 10 minute average at a particular level there will be a gap in the data. In other instances there may be operational issues and data all levels for a particular time

or period may be missing. Figure 3.9 shows a profile when all 7 levels are available.

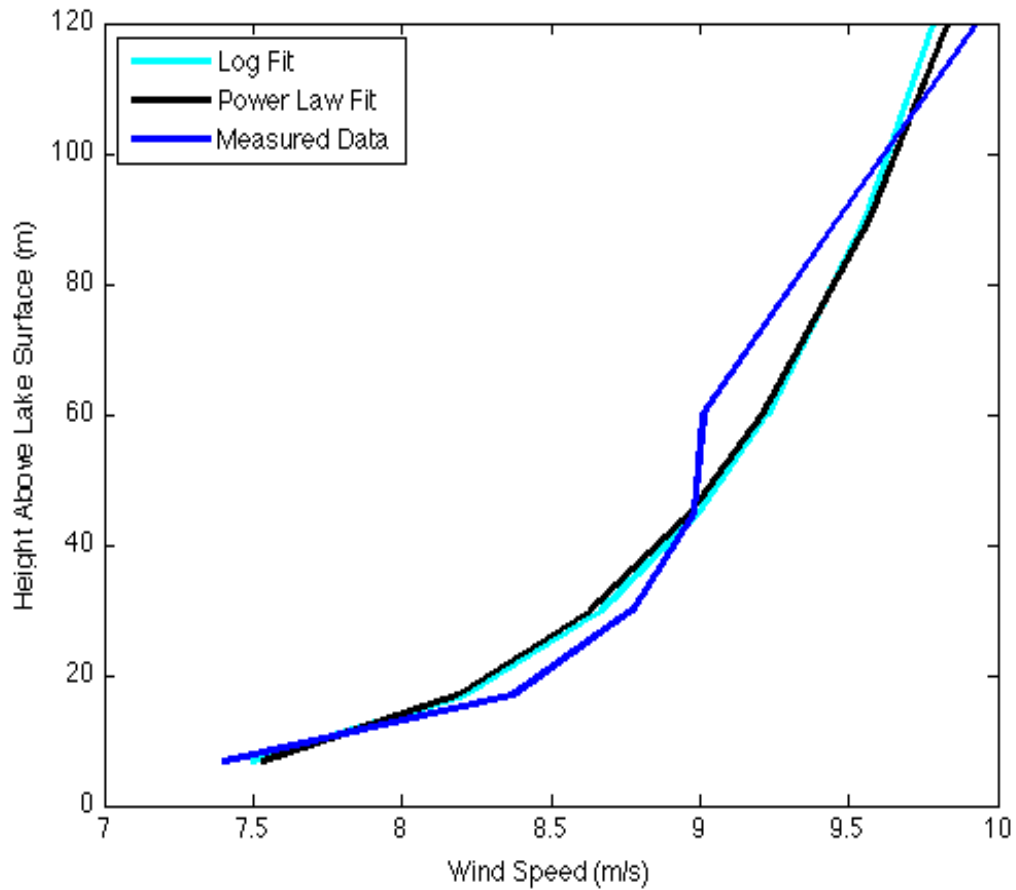


Figure 3.9: A case when all the wind speed levels have been measured (in blue) and the boundary layer is neutrally stratified. As a reference the log profile fit is in cyan and a power law fit in black

Figure 3.9 shows a wind profile on December 1, 2010 at nearly midnight when the wind speeds are relatively high. Using the log fit as a reference, this profile is almost logarithmic, which is expected given the time of day and the wind

speed. At high wind speeds and at night, conditions are almost neutrally stratified and the wind profile is logarithmic [10]. On the other hand Figure 3.10 is somewhat unstable. Figure 3.10 is a wind profile from early September 2010 during the day

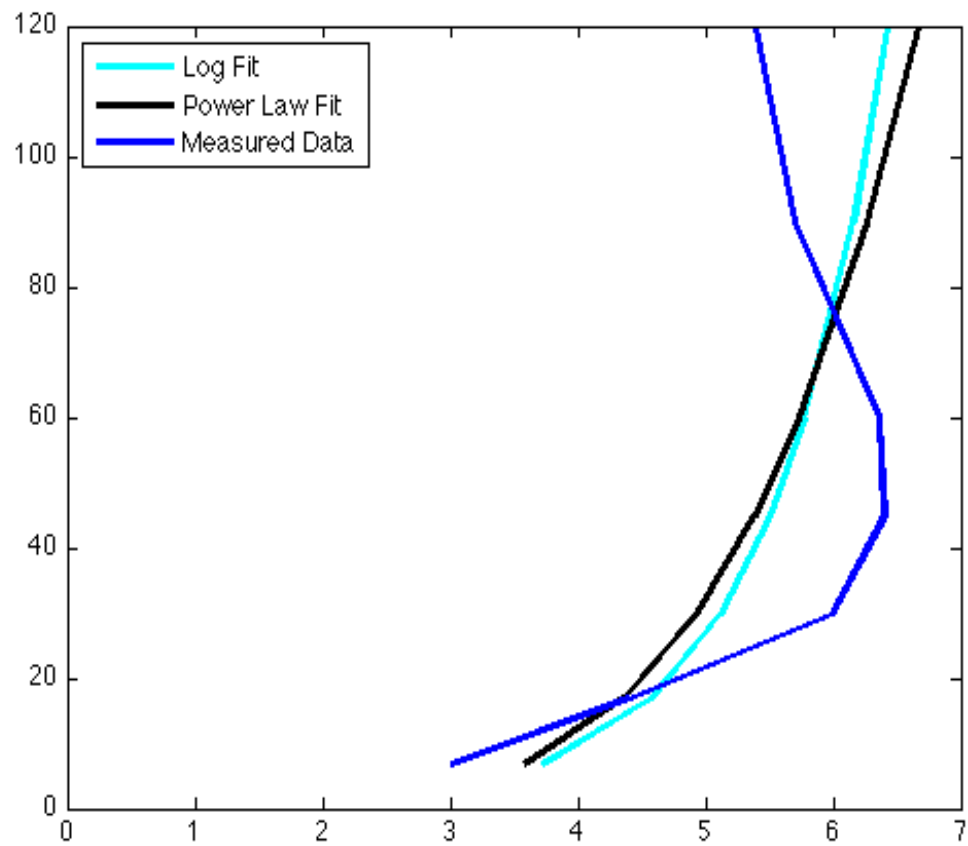


Figure 3.10: A case when all the wind speed levels have been measured (in blue) and the boundary layer is unstable. As a reference the log profile fit is in cyan and a power law fit in black

when the boundary layer is unstable. Since conditions are unstable and wind speeds

are relatively low, it is not surprising this profile is not logarithmic.

To address the problem of missing data, methods have been formulated to deal with the two cases of missing lidar data when: a) some levels are available but not all; b) all lidar levels are missing. In cases where there are less than 4 levels that have been measured, the missing levels are estimated using the platform level wind speed and direction dependant ratios that have been computed for all available times within 14 months when the platform level wind speed and a particular level is present. In cases where at least 4 of 7 possible measured wind levels are available, a power law and logarithmic fit are made with the available data. The fit with the least absolute mean error is used to estimate the missing level. Figure 3.11 shows a case when only the 7 m wind speed and 17 m wind speed have been measured so using the methodology described, the missing upper levels have been estimated using the ratios from Figure 3.6 and the 7 m wind speed.

In Figure 3.11, the lidar levels above 17 m have been estimated using ratios from Figure 3.6 and provide a reasonable profile up to 120 m. Some would argue that the log or power law fit could be better in this case, but given only 2 measured levels, doing a log or power law fit up to 120 m data cannot be justified. The other possible case is shown in Figure 3.12.

This is a case when 5 of the lowest measured points are available and the upper two missing levels have been estimated using the best of the log and power law

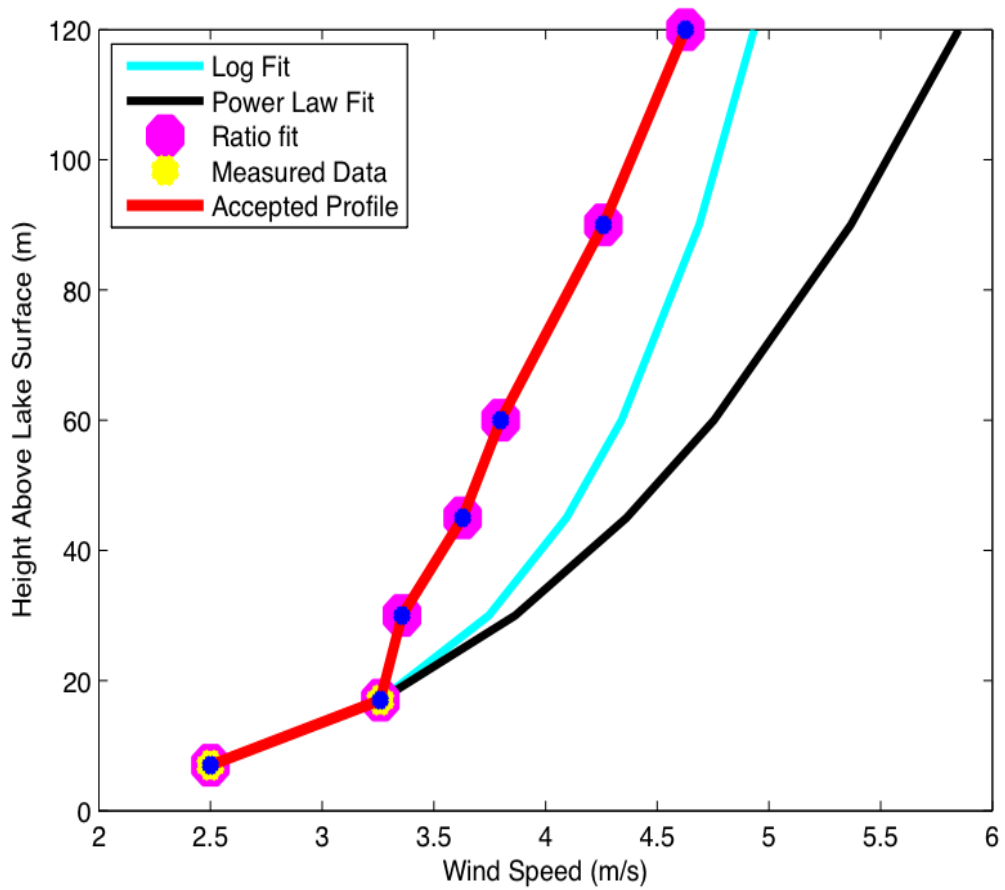


Figure 3.11: A case when all the wind speed levels are missing except the 7 m and 17 m levels. The log profile fit to these two levels is in cyan, the power law fit in black and profile using the ratios from Figure 3.6 in red.

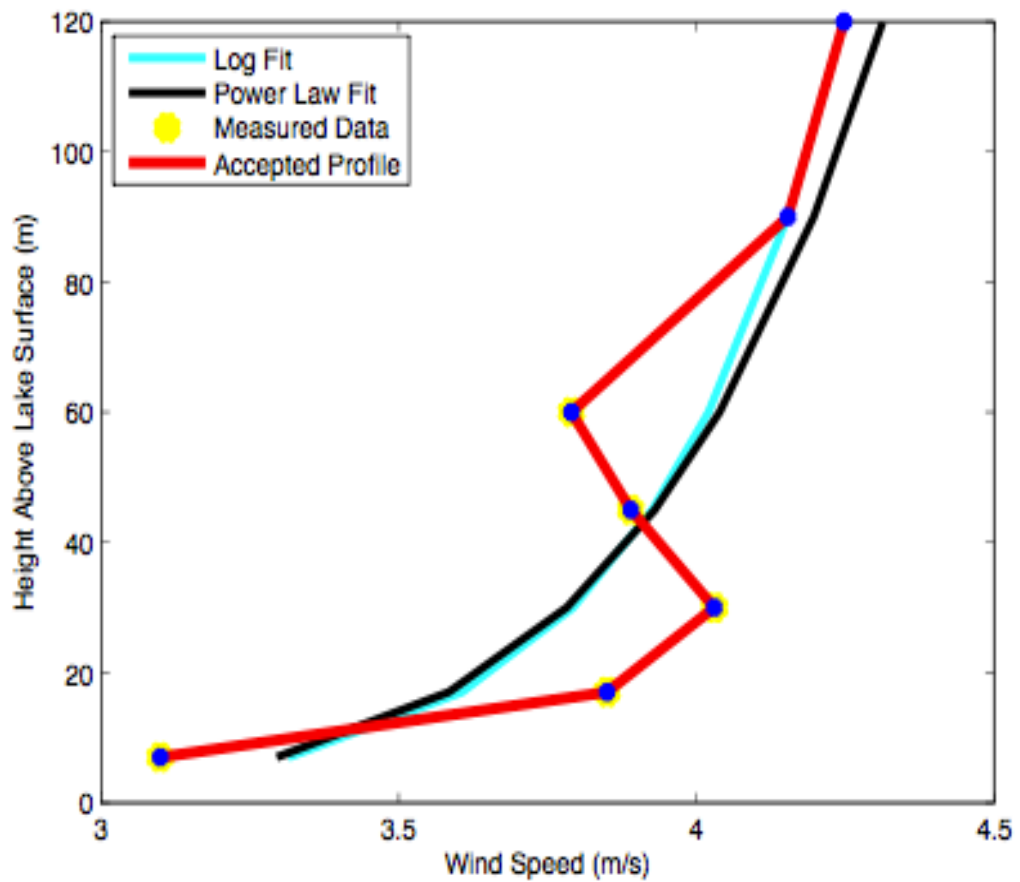


Figure 3.12: A case when the lower 5 levels are present with 90 m and 120 m missing. The log profile fit to these two levels is in cyan, the power law fit in black and profile using the ratios from Figure 3.6 in red. For this case the log profile is deemed the best fit and used as the accepted profile.

fit. In this case the log profile provides the best fit. This profile is during the daytime hours in July, so it is not surprising the profile shape is not logarithmic given low wind speeds and time of day. To make defining each method of filling in data easy to refer to, they will be defined as Method 1 through 4 as in Table 3.2 .

Method	1	2	3	4
Raw data	X	X	X	X
Wind Directional Ratios	X			
Wind Directional Ratios $U_7 > 1$		X		
Wind Speed Ratio			X	
Wind Directional and Wind Speed Ratio				X

Table 3.2: Methods of filling in data is defined. Method 1 (M 1) is raw data plus estimated data using directional ratios, Method 2, (M 2) is raw data plus estimated data using directional ratios excluding when 7 m wind speeds are less than 1 m/s, Method 3 (M 3) is raw data plus estimated data using wind speed bins, Method 4 (M 4) is is raw data plus estimated data using wind speed bins and wind direction ratios.

### 3.3 Monthly Averages

In Table 3.3, the averages of 25 consecutive months at the Toronto Hydro platform are shown for the 7 m met station and 90 m lidar level calculated from raw data and using methods 1 through 4. The months when the 90 m raw column is blank are months when the lidar was out of service. The errors on each of the averages for methods 1-4 are the errors from inclusion of the estimated data using 7 m winds and 90 m/7 m wind speed ratios with standard deviations. These errors are calculated

Month	7 m R	90 m Raw	90 m M 1	90 m M 2	90 m M 3	90 m M 4	90 m RR
Jun. 2010	3.61	6.03	6.09 ± 0.02	6.09 ± 0.00	6.10 ± 0.01	6.10 ± 0.01	96.5
Jul. 2010	3.13	5.68	5.67 ± 0.02	5.66 ± 0.00	5.68 ± 0.02	5.67 ± 0.02	98.1
Aug. 2010	3.86	6.23	6.20 ± 0.05	6.19 ± 0.01	6.22 ± 0.03	6.21 ± 0.06	95.3
Sept. 2010	4.30	7.13	7.11 ± 0.08	7.07 ± 0.03	7.07 ± 0.02	7.07 ± 0.05	89.7
Oct. 2010	4.51	7.62	7.48 ± 0.05	7.46 ± 0.01	7.48 ± 0.03	7.48 ± 0.03	94.2
Nov. 2010	4.69	7.56	7.16 ± 0.11	7.13 ± 0.04	7.17 ± 0.06	7.17 ± 0.07	92.2
Dec. 2010	5.13	7.46	7.38 ± 0.06	7.35 ± 0.02	7.34 ± 0.04	7.34 ± 0.01	95.8
Jan. 2011	4.61	6.77	7.94 ± 1.32	7.20 ± 0.42	6.90 ± 0.85	6.84 ± 0.40	36.3
Feb. 2011	5.67	8.16	9.23 ± 0.67	8.80 ± 0.25	8.29 ± 0.44	8.27 ± 0.20	62.2
Mar. 2011	5.23	8.58	8.45 ± 0.59	8.20 ± 0.21	8.11 ± 0.47	8.12 ± 0.24	64.2
Apr. 2011	4.96	9.00	9.40 ± 1.09	8.73 ± 0.38	8.30 ± 0.59	8.30 ± 0.43	41.6
May 2011	3.41	6.50	6.38 ± 0.431	6.22 ± 0.14	6.30 ± 0.55	6.29 ± 0.31	78.0
Jun. 2011	3.40	6.39	6.26 ± 0.06	6.25 ± 0.03	6.28 ± 0.06	6.27 ± 0.10	92.8
Jul. 2011	3.33	5.81	6.28 ± 1.16	5.81 ± 0.41	5.84 ± 0.77	5.85 ± 0.63	29.7
Aug. 2011	3.26	-	6.47 ± 2.10	5.61 ± 0.70	5.76 ± 1.62	5.71 ± 1.08	0
Sept. 2011	3.96	-	8.11 ± 2.13	6.96 ± 0.73	6.59 ± 1.81	6.62 ± 0.83	0
Oct. 2011	4.61	-	9.50 ± 2.10	8.22 ± 0.72	7.44 ± 1.74	7.38 ± 0.74	0
Nov. 2011	4.69	-	9.46 ± 2.13	8.23 ± 0.71	7.43 ± 1.36	7.47 ± 0.71	0
Dec. 2011	4.94	-	9.93 ± 2.14	8.62 ± 0.68	7.71 ± 0.98	7.61 ± 0.55	0
Jan. 2012	5.98	-	12.12 ± 2.19	10.41 ± 0.73	8.89 ± 0.64	8.89 ± 0.49	0
Feb. 2012	5.40	-	10.94 ± 2.20	9.42 ± 0.73	8.25 ± 0.51	8.18 ± 0.49	0
Mar. 2012	4.65	-	9.27 ± 2.02	8.11 ± 0.72	7.52 ± 1.00	7.44 ± 0.87	0
Apr. 2012	4.75	-	9.17 ± 1.91	8.11 ± 0.65	7.48 ± 1.14	7.44 ± 0.67	0
May 2012	2.86	5.64	5.45 ± 0.03	5.23 ± 0.09	5.45 ± 0.02	5.45 ± 0.01	75.1
Jun. 2012	3.90	6.48	6.82 ± 0.56	6.59 ± 0.19	6.54 ± 0.21	6.55 ± 0.26	61.2

Table 3.3: Monthly wind speed averages in m/s at the Toronto Hydro platform at 7 m and 90 m. At 90 m, monthly averages are for raw data, raw data plus estimated data using Method 1 (M 1), raw data plus estimated data using Method 2, (M 2) raw data plus estimated data using Method 3 (M 3) and raw data plus estimated data using Method 4 (M 4). The 90 m RR is the lidar data return rates at 90 m.

by weighting the standard deviations of these ratios based on the percentage of estimated data within each month.

In months when raw data return is high, the monthly 90 m averages are similar for all methods while months when the data return is low, the monthly averages can vary noticeably. In months when the missing data percentage is high, there is no expectation that raw monthly average is the true monthly average as shown in Salmon and Taylor [20]. To decide which method is most accurate in calculating a representative average wind speed, the errors incurred from estimating 90 m wind speeds using 7 m wind speeds are considered. Overall, the errors on the monthly averages using method two are lowest which means the 7 m winds are best correlated to 90 m winds using wind direction and although no estimated data are a replacement for measured data, this method can be considered as the best method to estimate missing data in this case.

## **4 Estimating Energy at the Toronto Hydro Site**

### **4.1 MCP Statistics for Toronto Hydro Platform based on 1989-2011**

Measure-Correlate-Predict (MCP) is a method commonly used in the wind energy industry to do long term wind predictions based on a nearby reference site that has measured wind data for a significant length of time in the past (usually a minimum of 15 years). This reference site must be concurrently measuring wind speeds for the time the target site is collecting wind measurements in order to do a the correlation. This concurrent overlap period is usually a minimum of one year but the longer the concurrent period; the more confidence placed on the correlation [5]. In this study, the Toronto Hydro research platform (THRP) will be the target site and the Meteorological Service of Canada (MSC) site at Toronto Island Airport (YTZ) will be the reference site. It is about 24 km southwest of the platform according to Google Earth and measures hourly winds at 10 m. The period that will be

used for correlation is June 2010 through May 2011 during which the lidar on the THRP was running. This period was used since the second year of lidar operation only consisted of data in the summer and would introduce a seasonal bias. For this period, five methods of correlation have been used from which two have been chosen to do long term wind and energy estimations using data from YTZ back to 1989. The correlation will be done using 90 m winds from the lidar and 10 m winds from YTZ. In order to use winds from any MSC site including Toronto Island, the data must be "whitened"; a process used to modify the original measured winds. MSC wind speed is originally measured in knots and then converted to km/h and rounded to the nearest integer, so when the wind speeds are converted back to knots or m/s accuracy is lost. This whitening process takes the wind speed integer in km/h and converts it to knots and adds a random number between  $+/- 0.5$  knots in an attempt to recover a continuously distributed measured wind speed. This process is quite common in the wind energy industry and was recommended through correspondence with Jim Salmon of Zephyr North Limited. Its worth noting that the meteorological station on Toronto Island has changed locations 3 different times in since 1987 and these changes are shown in Table 4.1.

Although the location of the reference site has changed 3 times since 1987 as shown in Table 4.1, it is nearly impossible to know if there were any sheltering effects in the past to influence the wind measurement. For this reason, this location change

Station Name	Latitude	Longitude	Elevation
Toronto Island Airport 1987-2006	Latitude: 43° 37'43.000" N	Longitude: 79° 23'42.000" W	Elevation: 76.50 m
Toronto City Centre (YTZ) 2006-2009	Latitude: 43° 37'43.000" N	Longitude: 79° 23'42.000" W	Elevation: 76.80 m
Toronto City Centre (YTZ) 2009-2013	Latitude: 43° 37'39.000" N	Longitude: 79° 23'46.000" W	Elevation: 76.80 m

Table 4.1: The location of the reference site and changes in the Toronto Island location since 1987.

is noted but the wind speeds are in no way altered in this study to compensate for this move.

The correlation period is 12 months, from June 2010 to May 2011 and the data at the lidar includes the measured data along with any that has been estimated due to missing lidar data.

The first and most basic method of correlation is the simple ratio (SR) in which the wind speeds at the target site and reference site are averaged and a simple ratio is obtained for the concurrent period defined above. Using the assumption that this ratio applies to long term wind speeds; the long term target wind speeds are calculated using the product of this simple ratio and the wind speed at the reference site. Given the concurrent period of June 2010 through May 2011, the simple ratio is 1.70.

The second method of correlation is linear regression in which linear coefficients between wind speeds at the target and reference sites are produced for 16 equal wind 22.5 degree wind direction sectors. The 16 wind direction sectors are based upon the wind direction at the reference site with the direction at the target site assumed the same. Long term target site wind speeds are then predicted using these direction dependant transfer coefficients and wind speeds directions from the reference site.

In Table 4.2, the regression statistics are shown for the linear regression MCP

Direction	22.5	45	67.5	90	112.5	135	157.5	180	202.5	225	247.5	270	292.5	315	337.5	360
slope	1.04	1.04	1.23	1.21	1.42	1.32	0.92	1.04	1.46	1.24	0.88	0.83	0.93	0.77	0.93	0.81
intercept (m/s)	2.60	3.04	0.50	0.55	0.85	0.99	2.33	1.99	1.07	2.47	3.38	2.90	2.63	3.60	3.44	3.90
data	122	218	498	1087	380	90	121	194	591	428	641	709	1058	730	780	393
r-squared	0.44	0.36	0.63	0.60	0.57	0.23	0.15	0.34	0.61	0.59	0.50	0.52	0.57	0.36	0.40	0.22

Table 4.2: Regression constants (rows 2 and 3) for each of the 16 equal 22.5 degree wind direction sectors ending with the direction in the first row of column. The fourth row is the number of hourly wind measurements going into each correlation and the fifth row is the r-squared value, a measure of how strong the correlation is.

method with 16 equal 22.5 degree wind direction sectors. In this table the r-squared values vary from 0.15 to 0.63 but many of the low r-squared values are in sectors with a low frequency of wind measurements. As a general trend, when the number of measurements increases, the r -squared value increases so this means for those wind directions that occur most frequently, the long term estimation should be a better measure of the actual wind speeds.

The third method is the matrix method and is similar to the linear regression method but is further divided into wind speed bins based on wind speeds at the reference site. In this study the wind speed bins are set at 1 m/s in size while direction sectors are kept at 22.5 degrees [19]. To define this method let A be the reference site and B be the target site. If  $d_{ij}$  is the relative frequency of concurrent occurrences of i at A and j at B then:

$$F_i = \sum_{j=1}^J d_{ij} \quad (4.1)$$

$$G_j = \sum_{i=1}^I d_{ij} \quad (4.2)$$

In these equations wind categories are a joint distribution of wind speed classes and wind direction sectors, so  $I=J=527$  [19]. Using the information from Equation 4.1, the coefficient matrix  $c_{i,j}$  is defined by

$$c_{ij} = \frac{d_{ij}}{F_i} \quad (4.3)$$

This coefficient ( $c_{ij}$ ) is calculated using short term data of concurrent data at A and B and then can be used to estimate the long term wind speeds  $g_j$  at the target site by

$$g_j = \sum_{i=1}^I c_{ij} f_i \quad (4.4)$$

where the ( $c_{ij}$ ) is summed over  $i$ . and  $f_i$  is the long term data at the reference site A. Here,  $g_j$  is the long term climatology at the target site or in other words the frequency that wind speed will occur in each wind speed bin and wind direction sector.

The fourth method is the Variance Ratio Method (VRM) which produces linear relationships that force the short term predicted values to have the same mean and variance as the short term observed values [18]. These means and variances are calculated for data that have been divided in 16 wind direction sectors using the wind direction at the reference site for the concurrent period of the target and reference site defined above. If the variance of the predicted wind speed at a target site is  $\sigma^2(\hat{u}_t)$ , in linear model form  $\sigma^2(\hat{u}_t) = \sigma^2(mu_r + b) = m^2\sigma^2$ , then  $\sigma^2(\hat{u}_t) = \sigma^2(\hat{u})$  by setting  $m^2 = \sigma^2(u_t) = \sigma^2(u_r)$  [18]. Given these means and variances, the long - term target wind speed is predicted using

$$\hat{u}_t = [\mu_t - \frac{\sigma_t}{\sigma_r}\mu_u] + \frac{\sigma_t}{\sigma_r}\mu \quad (4.5)$$

where subscripts t and r represent target and reference sites,  $\mu$  is the mean,  $\sigma$  is the

standard deviation and  $u$  is the wind speed. In this method any wind speeds that are predicted less than zero are set to zero while the long term wind directions at the target site is set to those at the reference site. The specific means and variances are shown in Table 4.3.

In Table 4.3 the means and standard deviation in m/s are shown for the 12 month concurrent period at both the target site and reference site for each of the 16 direction sectors. Using this table and Equation 4.5, the long term wind speeds at the target site can be calculated.

The fifth method is All Direction Regression (ADR) which is similar to the linear regression method except the following differences: a) The target and reference wind are not segregated into wind direction sectors; all directions are correlated together. b) Wind speeds are correlated for four averaging periods; hourly (no averaging needed), daily, 3-day and monthly. c) Since there are 4 averaging periods, the long term estimations using the linear coefficients for each averaging period and wind speeds from the reference site will produce 4 different estimates for the target site.

Using the 5 MCP methods outlined above, the short term and long term monthly wind speed averages can be calculated. The short term monthly wind speed averages will be using Toronto Island data from June 2010 through May 2011; the same period used to produce the MCP coefficients. The long term monthly wind

Direction	22.5	45	67.5	90	112.5	135	157.5	180	202.5	225	247.5	270	292.5	315	337.5	360
10 m mean	4.41	5.00	5.97	5.21	3.56	2.74	2.64	3.50	4.30	4.76	5.49	5.73	5.49	4.48	4.46	4.20
90 m mean	7.20	8.29	7.83	6.86	5.90	4.61	4.78	5.64	7.36	8.35	8.23	7.63	7.67	7.04	7.57	7.28
10 m standard deviation	1.48	1.75	2.82	2.70	1.92	1.15	1.17	1.46	1.99	2.74	3.35	3.14	2.86	2.18	1.84	1.39
90 m standard deviation	2.31	3.07	4.36	4.23	3.60	3.16	2.81	2.63	3.74	4.39	4.17	3.59	3.49	2.78	2.67	2.37

Table 4.3: Statistics for the VRM MCP method at 90 m for the Toronto Hydro platform (target site) and Toronto Island (reference site).

	Hourly	Daily	3 Day	Monthly
Slope	1.00	1.18	1.21	1.21
Y-intercept (m/s)	2.48	1.59	1.45	1.41
R-Squared	0.51	0.72	0.75	0.87

Table 4.4: Statistics for the all direction MCP method at 90 m for the Toronto Hydro platform (target site) and Toronto Island (reference site).

speed averages will use 21 years from Toronto Island between January 1989 and December 2009. Table 4.5 shows the short term monthly wind speed averages.

Table 4.5 shows the monthly averages and annual average for each of the MCP based on 1 year of data from June 2010 through May 2011. The purpose of doing a short term analysis using MCP is to see how well these methods can recalculate the monthly wind speed averages. All the annual wind speed averages in Table 4.5 are within 1 m/s of the actual wind speed average with the linear regression and variance mean method recreating the actual mean very well. The matrix method seems to predict a fair bit lower wind speed than the other methods which may seem odd given this method is the similar to the linear regression method. The problem with the matrix method is that when 1 year of data is split into wind direction sectors and wind speed bins, it spreads the data thin in many of the individual elements of the matrix and with less data in each element there will be more scatter and correlations will provide less accurate estimations. Looking at individual monthly wind speed averages shows more deviation from the actuals

	SR	LR	Matrix	VRM	hourly	1 day	3 day	Monthly	1st year 90 m	YTZ 10 m
January	10.07	8.49	7.98	8.87	8.29	8.54	8.75	8.62	7.19	6.28
February	8.45	7.54	7.94	7.62	7.40	7.45	7.72	7.45	8.80	5.87
March	8.83	7.86	7.84	7.99	7.53	7.67	7.49	7.73	8.17	5.41
April	8.18	7.31	7.59	7.40	7.08	7.14	6.98	7.26	8.67	5.15
May	7.62	6.94	7.28	6.84	6.61	6.84	6.90	6.84	6.18	4.46
June	7.01	6.66	5.80	6.44	6.25	6.51	6.56	6.42	6.11	3.89
July	5.53	5.86	5.68	5.43	5.60	5.40	5.30	5.37	5.66	3.72
August	6.74	6.41	5.81	6.17	6.33	6.22	6.13	6.23	6.19	3.70
September	7.59	6.89	6.23	6.80	6.73	6.76	6.67	6.84	7.08	4.10
October	7.79	7.52	6.41	7.14	6.96	6.97	6.95	6.99	7.46	4.67
November	8.46	8.17	6.73	7.48	7.16	7.31	7.30	7.46	7.30	5.37
December	9.28	8.81	6.82	8.26	7.78	8.00	7.80	8.06	7.46	5.94
Annual Mean	7.96	7.22	6.57	7.20	7.06	7.04	7.10	6.98	7.19	4.88

Table 4.5: Monthly wind speed averages (m/s) using the five MCP methods outlined in this study for the period of June 2010 through May 2011. The abbreviations are as follows; Simple Ratio (SR), Linear Regression (LR), Matrix Method. Hourly, 1 day, 3 day and monthly refer to the different regression schemes within the All Directions,(AD) method, 1st year refers to Measured + estimated data from June 2010 - May 2011, Toronto Island (YTZ 10 m)

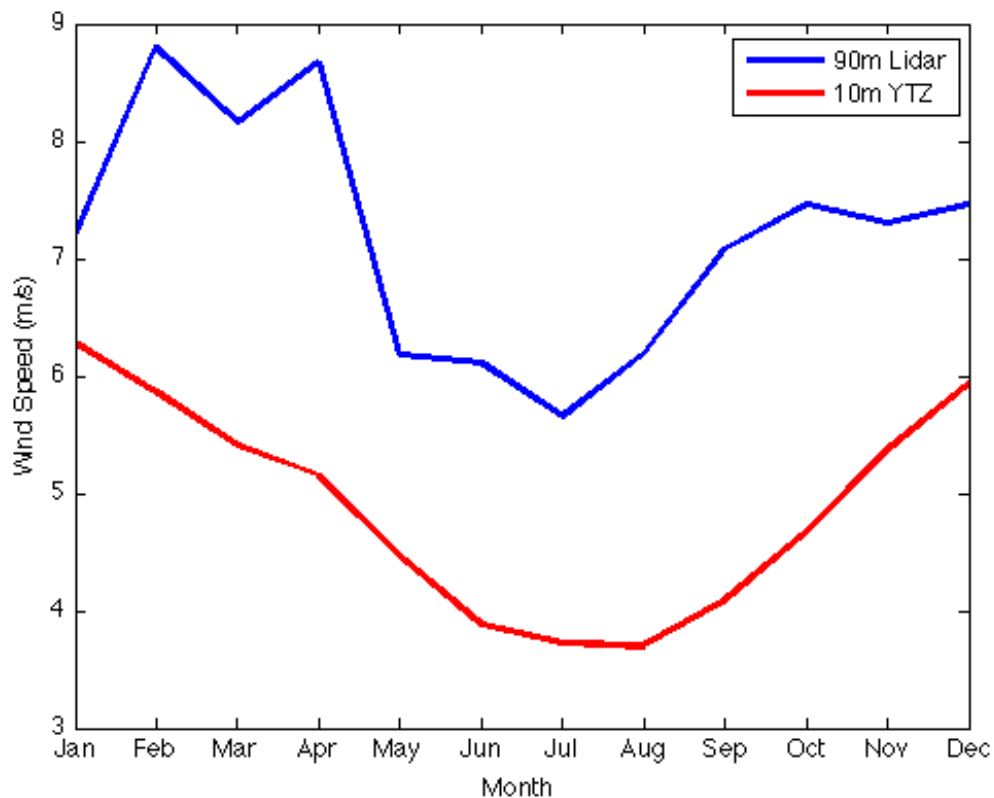


Figure 4.1: The 90 m lidar and 10 m Toronto Island (YTZ) monthly wind speed averages for the period of June 2010 – May 2011.

means but this is expected given seasonal variations. To help visualize how the 90 m lidar winds compare to 10 m winds at Toronto Island, Figure 4.1 shows the monthly wind speed averages for both from Table 4.5.

Figure 4.1 shows that the monthly wind speed averages for the 90 m lidar follow similar trends to the 10 m YTZ monthly wind speed averages. There seems to be a spike in the 90 m winds for the months of February, March and April which could

be related to low data return during these months.

Turning to the long term averages using data from Toronto Island from January 1989 through December 2009, Table 4.6 shows long term annual monthly averages for the 90 m wind speeds at the site of the Toronto Hydro Platform using the same 5 MCP methods.

This period was chosen because the quality of the data at Toronto Island before 1989 seemed to be less reliable. In Table 4.6 all the annual wind speed means are higher than the actual wind speed mean measured from June 2010 through May 2011 except for the hourly all direction method. This analysis would suggest that overall, the year of June 2010 through May 2011 was slightly lower wind speed than the past years since 1989. To investigate this further, Table 4.7 will look at the monthly and annual wind speed averages at Toronto Island to see how representative the year of June 2010 through May 2011 is compared to the past 21 years. Table 4.7 is 24 years of monthly wind speed averages at Toronto Island, the reference site for the MCP analysis at the Toronto Hydro platform. The 12 months which are highlighted in bold are the months used to do the MCP analysis. Comparing these 12 months to the 24 year monthly averages, only five months within the 12 months highlighted are higher than the 24 year average. As well the 12 month average of both years used in the MCP is lower than the 24 year annual average. This evidence supports that the data during the 12 months used in the MCP analysis is actually

	SR	LR	Matrix	VRM	AD - hourly	AD - 1 day	AD - 3 day	AD - Monthly
January	10.66	8.69	7.96	9.17	8.41	8.96	8.99	9.04
February	9.98	8.28	7.95	8.62	8.02	8.43	8.45	8.54
March	9.20	7.780	7.86	8.08	7.50	7.87	7.91	7.98
April	8.75	7.54	7.62	7.72	7.24	7.59	7.623	7.68
May	7.59	6.75	7.29	6.66	6.28	6.76	6.78	6.83
June	6.60	6.21	6.95	5.89	5.84	6.13	6.15	6.14
July	6.32	6.10	6.72	5.75	5.79	5.91	5.89	5.93
August	6.29	6.13	6.61	5.78	5.79	5.89	5.87	5.90
September	6.97	6.53	6.91	6.34	6.16	6.33	6.30	6.39
October	7.98	7.06	7.41	7.02	6.59	7.01	7.06	7.09
November	9.13	7.74	7.53	7.93	7.31	7.82	7.84	7.94
December	10.12	8.32	7.72	8.70	8.03	8.52	8.60	8.63
Annual Mean	8.30	7.26	7.38	7.30	6.91	7.27	7.29	7.34

Table 4.6: Monthly wind speed averages (m/s) using the 5 MCP methods outlined in this study for the period of January 1989 through December 2009. The abbreviations are as follows; Simple Ratio (SR), Linear Regression (LR), Matrix Method, All Directions,(AD).

Year	J	F	M	A	M	J	J	A	S	O	N	D	12 month
1989	7.15	6.08	5.39	4.33	4.27	3.77	3.64	4.16	4.28	4.99	6.79	5.68	5.04
1990	6.12	5.62	5.33	4.83	4.93	4.36	3.82	3.92	4.18	4.6	5.44	6.25	4.95
1991	6.84	5.51	5.36	5.22	4.43	3.60	3.79	3.72	3.85	3.77	5.28	5.42	4.73
1992	5.37	4.86	5.17	4.51	4.32	3.77	3.63	3.78	3.92	4.77	5.59	5.81	4.63
1993	5.80	5.83	5.05	4.96	4.40	4.17	3.17	2.15	3.12	4.65	5.05	4.56	4.41
1994	5.54	5.47	4.70	5.14	3.82	3.83	3.34	3.25	3.53	3.45	5.08	4.66	4.32
1995	6.40	6.21	4.68	5.61	4.37	4.02	3.71	4.21	4.23	5.48	6.01	6.30	5.10
1996	5.78	6.08	6.15	5.59	4.10	3.92	3.94	3.58	4.73	5.23	5.03	5.60	4.97
1997	7.69	5.95	6.03	4.91	5.08	3.55	3.83	4.01	4.44	4.44	5.45	5.74	5.10
1998	6.14	4.95	5.77	4.78	4.44	3.97	3.93	3.89	3.88	4.89	5.34	6.12	4.84
1999	7.22	5.33	5.73	5.35	4.15	3.85	4.16	3.67	4.28	4.62	5.29	5.95	4.97
2000	6.01	5.81	5.20	5.14	4.47	4.29	3.90	3.63	4.33	4.05	5.82	5.94	4.88
2001	5.80	6.14	5.86	4.91	4.42	3.70	4.14	3.71	4.14	4.98	5.02	5.66	4.87
2002	6.94	6.70	6.56	4.70	5.11	3.89	3.82	3.80	3.84	5.06	5.60	6.58	5.21
2003	6.74	6.64	5.03	5.74	5.18	4.34	3.55	3.53	4.76	4.37	5.84	5.43	5.10
2004	6.82	5.72	5.25	5.10	4.33	4.00	3.85	3.62	3.91	5.21	4.84	6.68	4.94
2005	5.44	4.79	5.18	5.10	4.07	3.56	3.86	3.75	4.12	4.62	6.52	6.64	4.80
2006	5.77	6.69	5.01	5.40	4.51	3.92	3.73	3.86	4.55	5.07	4.16	6.76	4.95
2007	5.80	7.50	5.91	5.68	3.66	3.91	3.23	4.22	3.81	4.59	5.21	6.13	4.97
2008	6.49	6.12	5.34	5.06	4.78	3.77	3.48	3.52	3.78	4.48	4.96	6.62	4.87
2009	6.02	5.27	4.95	6.14	4.90	3.60	3.66	3.63	4.36	4.80	4.50	6.26	4.84
2010	5.93	4.97	5.20	4.82	4.49	<b>4.13</b>	<b>3.26</b>	<b>3.97</b>	<b>4.47</b>	<b>4.59</b>	<b>4.98</b>	<b>5.47</b>	4.69
2011	<b>4.96</b>	<b>5.98</b>	<b>5.29</b>	<b>5.99</b>	<b>4.33</b>	4.28	3.64	3.67	4.33	4.74	4.90	5.32	4.79
2012	6.06	5.58	5.61	5.05	3.83	4.36	3.61	3.79	3.55	5.05	4.84	5.49	4.73
mean	6.20	5.83	5.41	5.17	4.43	3.94	3.70	3.71	4.10	4.69	5.31	5.88	4.86

Table 4.7: 10 m monthly average wind speed (m/s) at Toronto Island from 1989 through 2012. The months highlighted in bold are the 12 months used in the MCP analysis.

lower than 24 year average which correlates with Table 4.6 showing slightly higher annual wind speed averages than the short term wind speed average.

As an alternative to MCP analysis using the reference site at Toronto Island, the wind energy industry has found value in correlating with high resolution model data using re-analysis data as input. VORTEX , a company in Europe provides 3 km resolution data at a chosen site. In this case a 10 year time series was obtained for the location of the Toronto Hydro platform at a height of 100 m. Using the software at Zephyr North Canada, a second MCP analysis has been done using the VORTEX 10 year time series. In this MCP analysis, the 120 m lidar level has been used for correlation. A full analysis using the VORTEX will not be done as for Toronto Island, but a summary of important results will be shown. Table 4.8 shows the details of the linear regression MCP method using VORTEX data for the period of June 2010 through May 2011.

It is difficult to compare the constants of Table 4.8 to those in Table 4.2 using Toronto Island as a reference site, but it is worth noting that the r-squared values in Table 4.2 are overall higher showing a better correlation. Regression data from the all direction MCP method using VORTEX data as the reference site is shown in Table 4.9.

Again it is tough to compare constants between all direction MCP method using the VORTEX data and Toronto Island data but comparing the r-squared values

Direction	22.5	45	67.5	90	112.5	135	157.5	180	202.5	225	247.5	270	292.5	315	337.5	360
slope	0.63	0.63	0.92	0.92	1.01	0.73	0.68	0.44	0.59	0.77	0.61	0.53	0.83	0.72	0.49	0.52
intercept (m/s)	2.79	3.55	1.58	1.92	1.89	3.10	2.55	4.45	2.72	3.71	4.65	4.36	2.44	2.88	4.35	4.03
data	289	227	193	406	329	124	56	48	63	344	632	544	368	512	778	524
r-squared	0.25	0.28	0.41	0.34	0.55	0.30	0.33	0.07	0.28	0.37	0.23	0.18	0.33	0.27	0.19	0.16

Table 4.8: Regression constants (rows 2 and 3) for each of the 16 equal 22.5 degree wind direction sectors ending with the direction in the first row of column based on VORTEX data as a reference site. The fourth row is the number wind measurements going into each correlation and the fifth row is the r-squared value, a measure of how strong the correlation is.

	hourly	Daily	3 day	Monthly
Slope	0.68	1.00	1.14	1.15
Y-intercept (m/s)	3.04	0.89	-0.11	-.16
R-Squared	0.28	0.65	0.68	0.50

Table 4.9: Statistics for the all direction MCP method at 120 m for the Toronto Hydro platform (target site) and VORTEX data at 100 m.

shows that the MCP method using Toronto Island as a reference site has better correlation with the Toronto Hydro platform site at 120 m

Using the MCP software from Zephyr North Canada, the short term and long term mean wind speeds at the Toronto Hydro Platform are shown in Table 4.10. In this case, short term covers the period of June 2010 through May 2011 while longterm covers June 2002 through May 2012.

	SR	LR	Matrix	VRM
Short Term	7.64	7.63	7.63	7.63
Long Term	7.51	7.91	7.57	7.54

Table 4.10: The annual wind speed averages (m/s) using the VORTEX MCP analysis. The abbreviations are as follows; Simple Ratio (SR), Linear Regression (LR), Matrix Method, All Directions,(AD)

Comparing the short term and long term wind speed averages using VORTEX as a reference site (Table 4.10) to those using Toronto Island as a reference site (Tables 4.5 and 4.6), those using VORTEX produce higher mean wind speeds for all 4 methods in Table (4.10). Given that the reference site of Toronto Island produced better correlations than using VORTEX in the MCP analysis, Toronto is considered

the most accurate and this is verified by reproducing short term mean wind speed most accurately.

## 4.2 Wind Characteristics

Wind varies greatly with location and these variations are important to consider in addition to the wind resource when planning any wind farm. This is especially true for offshore wind farms where the length of the over water fetch can play a large role in the wind dynamics and wind resource. In Figure 6.1 the location of the Toronto Hydro Platform is shown along with arrows separating long and short over water fetch. Figure 6.1 shows that for winds with a direction 80 through 220 degrees, the over water fetch is significant, at least 50 km. Figure 4.3 shows a wind rose with frequency of wind direction and as well as wind speed for the period of June 2010 through May 2011.

In Figure 4.3 a significant portion of the winds lie in the region of the wind rose which is considered to have a long over water fetch and appear to contain the highest wind speeds. To investigate how the wind profiles of long over water fetch compares to short over water fetch compare, 10 minute lidar profile has been grouped into long over water fetch and short over water by surface wind direction as described above. The lidar profiles for each of the two groups have been averaged to show the difference in short fetch versus long fetch over water as in Figure 4.4.



Figure 4.2: Location of the Toronto Hydro platform with the black arrows show the directions between which winds are considered to have a long over water fetch (80 through 220 degrees). Winds coming from 221 degree to 79 degrees are considered to have a short over water fetch.

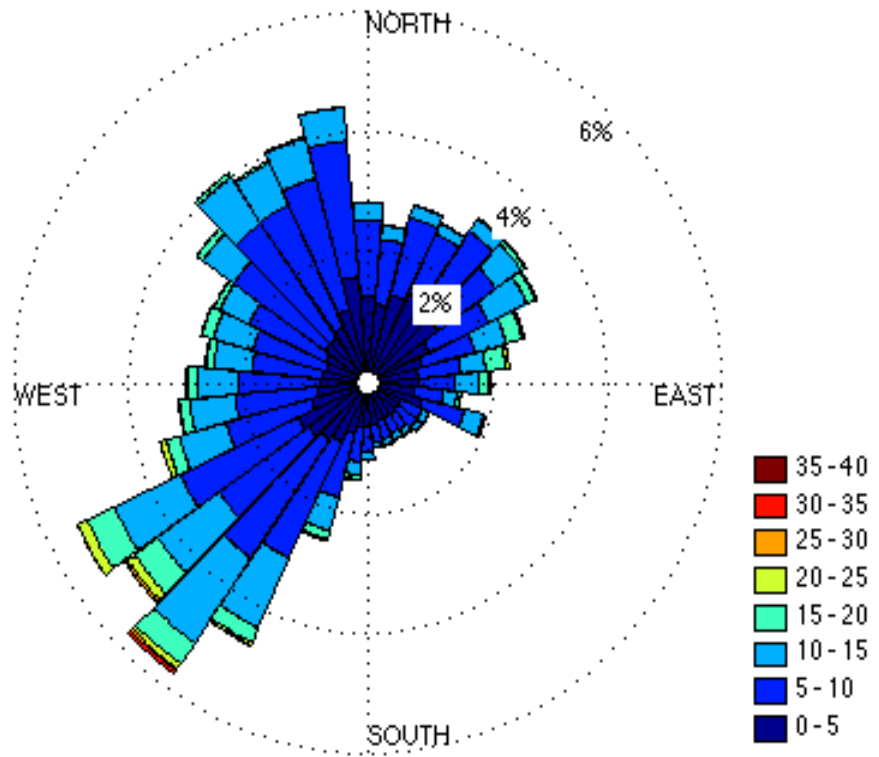


Figure 4.3: Wind rose showing frequency of wind direction and wind speed for June 2010 - May 2011. The colour coded legend shows wind speed ranges in m/s.

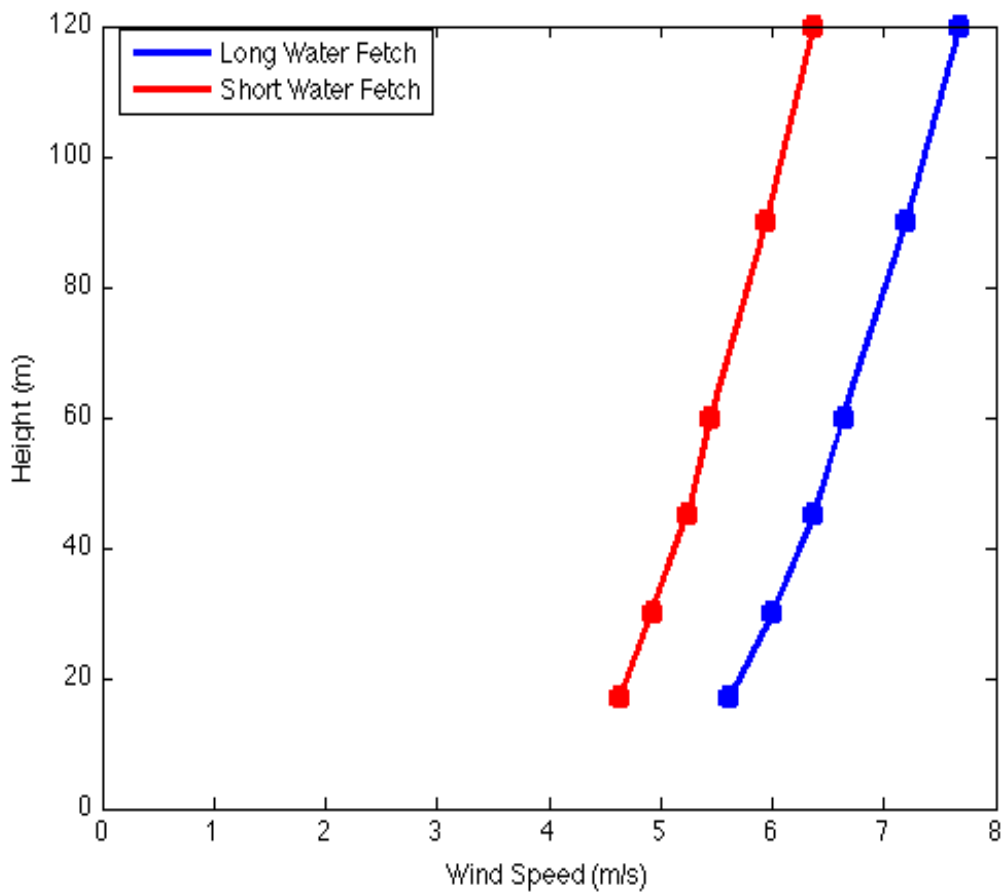


Figure 4.4: Average wind profile at the Toronto Hydro platform for a long over water fetch in red (wind directions 80 - 220 degrees) and short over water fetch in blue (wind directions 221 - 79 degrees). This is for the period June 2010 until May 2011.

In Figure 4.4 the averaged vertical profile is shown for the long over water fetch in blue and short over water fetch in red. The shorter over water fetch profile is about 0.78 m/s less than the longer fetch profile showing the offshore directions produce stronger wind speed. Looking at Figure 4.3, a significant portion of the winds are in the directions which are considered long over water fetch which correspond to the green profile in Figure 4.4. This shows that on average when winds are coming from the offshore wind direction, it is expected the wind speed will be close to 1 m/s faster.

Figure 4.5 is the same data as Figure 4.4 with a vertical scale plotted as logarithmic so that the roughness length ( $z_0$ ) can be estimated. Given the log wind profile

$$u_z = \frac{u_*}{\kappa} \ln\left(\frac{z}{z_0}\right) \quad (4.6)$$

where  $z$  is the height of wind speed  $u_z$ ,  $\kappa$  is the Von Karman constant and  $u_*$  is the friction (or shear) velocity ( $ms^{-1}$ ). This log wind profile assumes neutral stability, but is often a good assumption for unstable conditions. Neutral stability often occurs when temperature is not a large contributing factor which often occurs in high winds or under heavy cloud [23]. Unstable conditions usually occur during the day time hours when heating occurs at the surface and causes the air to rise. Equation 4.6 is less accurate during when the boundary layer is stable when air is cooled from below and this creates a more linear wind profile [23]. Given Equation 4.6, the anti log of the y-intercept linear fits in Figure 4.5 will give an estimation

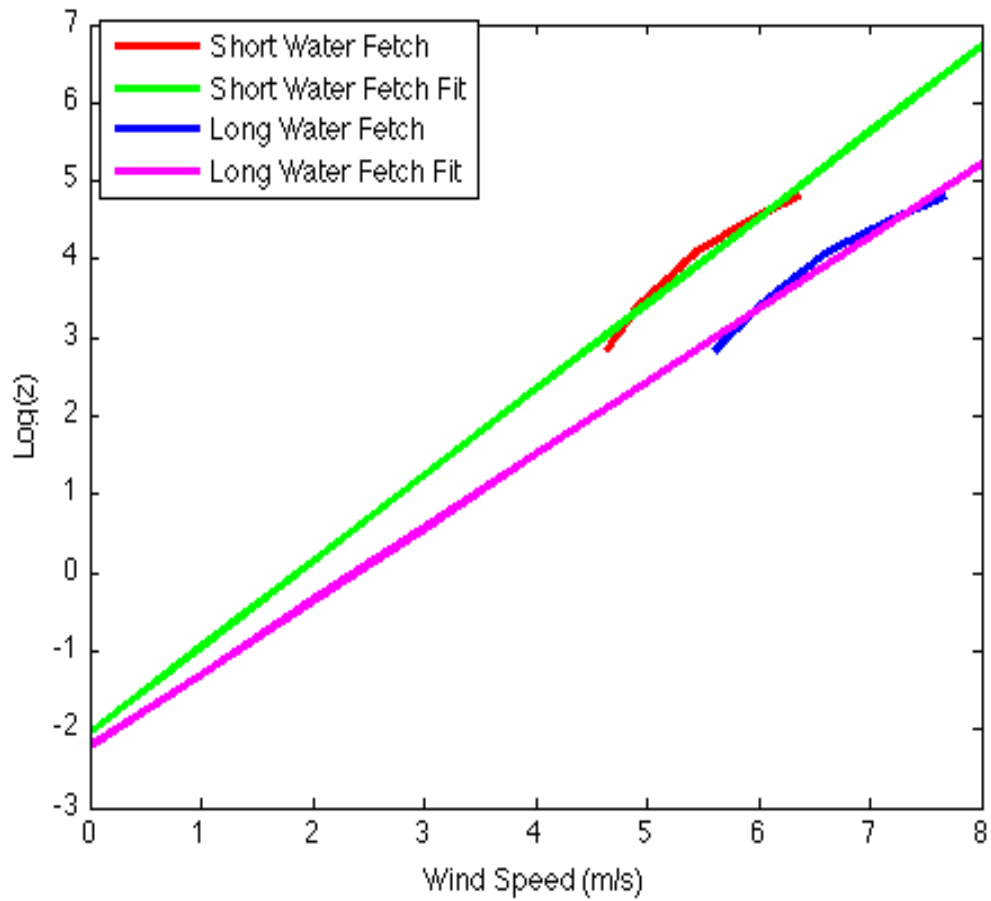


Figure 4.5: Average wind profile at the Toronto Hydro platform for a long over water fetch in red (wind directions 80 - 220 degrees) and short over water fetch in blue (wind directions 221 - 79 degrees) with a vertical log scale. This is for the period June 2010 until May 2011.

of the surface roughness of each profile. The y-intercept of the of the short over water fetch and long over water fetch are -2.04 and -2.21 respectively corresponding to surface roughness of 0.009 and 0.006 m respectively. The slightly higher surface roughness for the short over water fetch likely due to the upper levels having not fully converted to the over water regime.

Now that an estimation of the surface roughness has been obtained, the depth of the internal boundary layer (IBL) can be calculated using a equation derived by Panofsky and Dutton [21]. The depth of IBL is given by

$$1.25\kappa\left(\frac{x}{z_{0D}}\right) = \frac{\delta}{z_{0D}}\left[\ln\left(\frac{\delta}{z_{0D}}\right) - 1\right] + 1 \quad (4.7)$$

where  $\kappa$  is the von Krmn,  $x$  is the distance from the roughness change,  $\delta$  is the depth of the IBL and  $z_{0D}$  is the downstream surface roughness. Since the internal boundary layer is formed in this case from wind blowing from land to water, the short over water fetch  $z_{0D} = 0.009$  m is used and  $x=1100$  m (distance from the shoreline to platform) is used. Using an iterative method the depth of the IBL is found to be 69.2 m showing that the two upper levels of the lidar are actually above the IBL. One assumption here is  $x = 1100$ , which is the closest point from the platform to shore, but the profile used to calculate  $z_{0D}$  is for a range of directions, some having a larger  $x$  value which would result a slightly higher IBL.

## 5 Wind farm design

Despite a moratorium on all offshore wind farms on the Canadian side of the Great Lakes, this section will look at two potential wind farm designs in the area of the Toronto Hydro platform. There has been talk about if the moratorium is ever lifted, there will be a 5 km buffer zone around the shoreline where no wind farms can be built. To comply with this potential buffer zone, the potential wind farm designs will have wind turbines no closer than 5 km from the shore. This 5 km buffer zone will greatly complicate this project as water depths drop off significantly beyond 4 km offshore in this location making it more difficult and costly to build a wind farm. However, this study is not focused on the economics of this project but more the wind resource. This wind farm design is going to be a 90 MW wind farm comprised of 30 - 3 MW Siemens wind turbines with a power curve as shown in Figure 5.1

Figure 5.2 shows a possible single array wind farm design for the Toronto Hydro site offshore of the Scarborough Bluffs. A1 represents the location of the Toronto

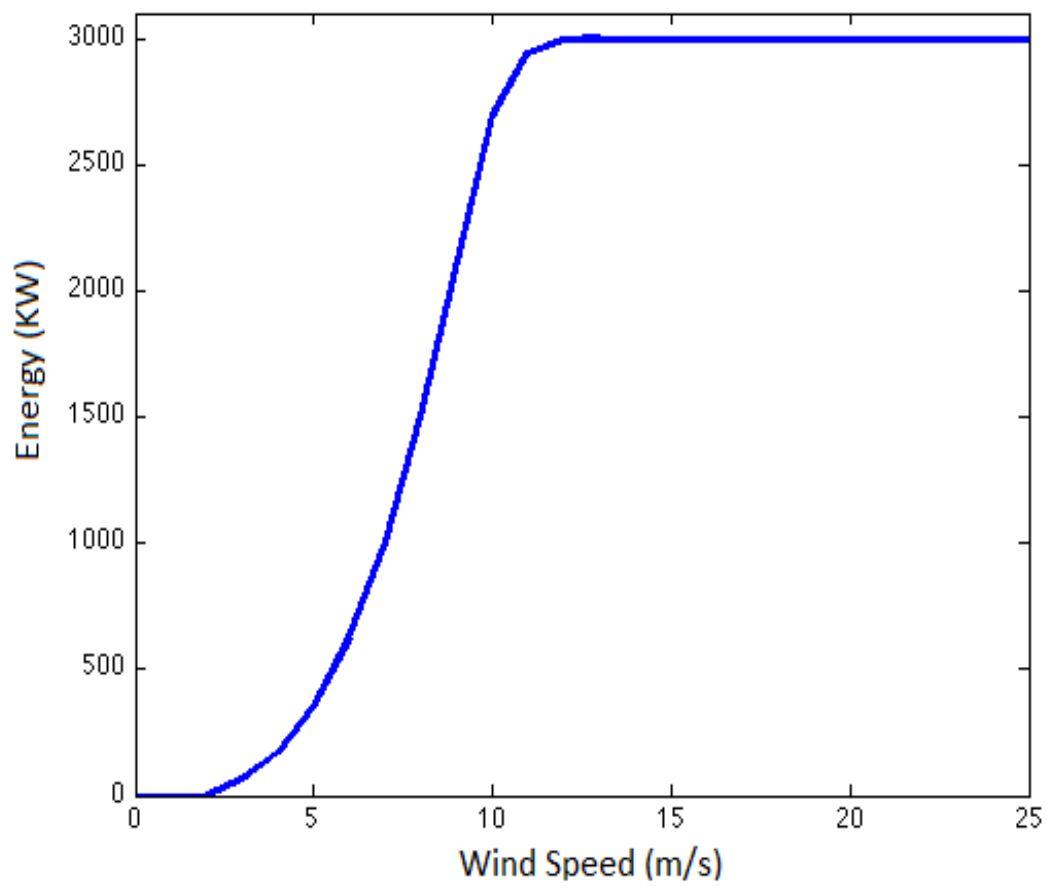


Figure 5.1: The power curve for a 3 MW Siemens wind turbine.

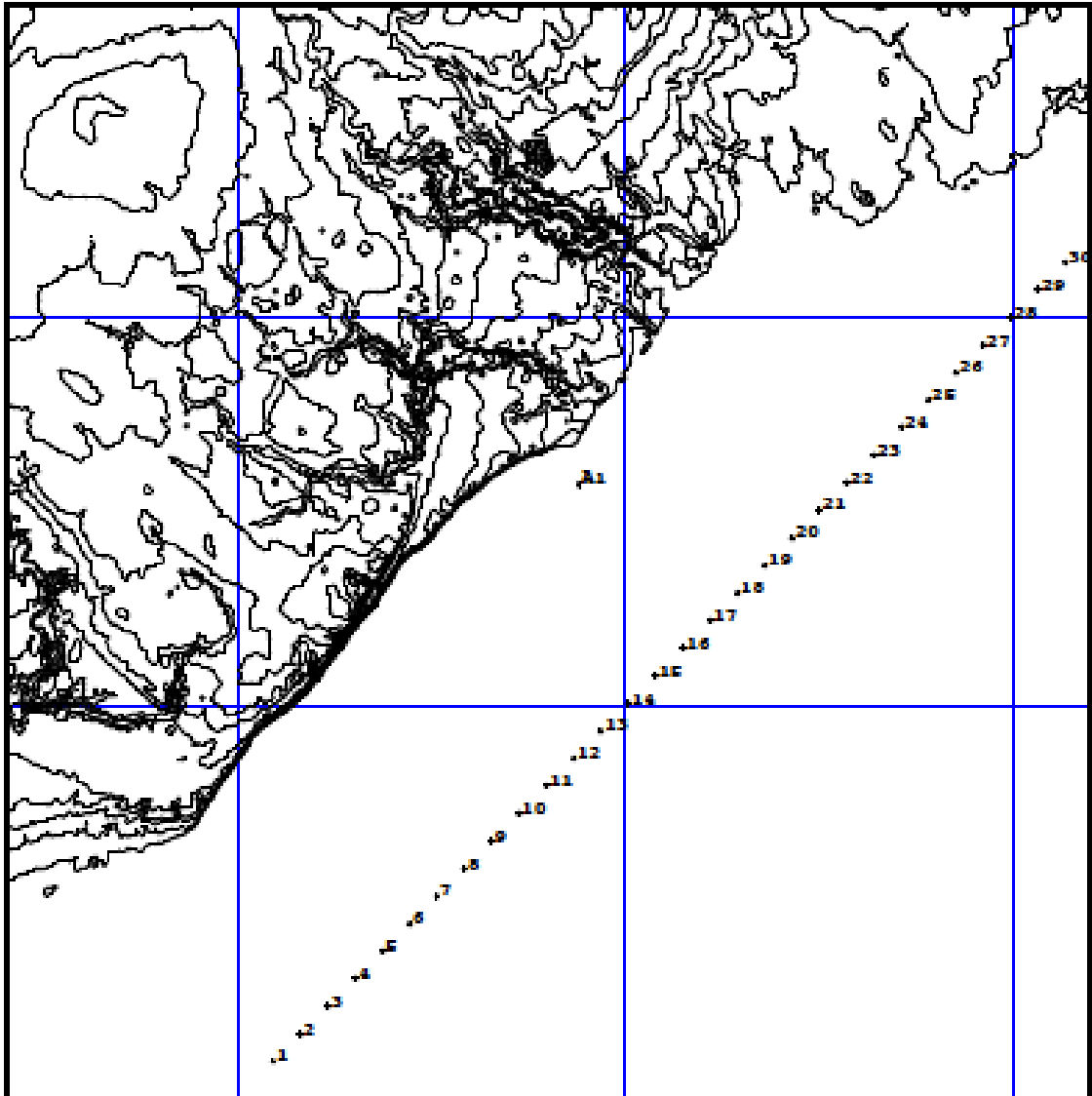


Figure 5.2: A potential single array wind farm design created in the program Wind Farm. The A1 represents the location of the Toronto Hydro platform while the numbers 1-30 show the location of individual wind turbines in this design. Each grid box is 5 km with the x axis representing east - west directions and the y axis north - south direction..

Hydro Platform, while numbers 1-30 show the location of individual wind turbines in this design. The wind turbines have been placed at least 5 km from the lake shore to comply with the potential 5 km buffer zone. The turbines in this single array design are placed about 1 km apart or 10 rotor diameters. The second design is a double array of wind turbines as shown in Figure 5.3 where each row is comprised of 15 wind turbines. The two rows in the double array are the same length as the single array, therefore the turbines are placed about 2 km apart.

Using the program Wind Farm and data from June 2010 through to May 2012, energy calculations can be done for each wind farm design. This will not only show the wind energy potential of this site but it will show if there is any advantage to a single or double array wind farm. The annual energy as well as the wake losses and terrain effects will be investigated in Figure 5.4.

Figure 5.4 shows energy calculations for both 80 m and 99.5 m hub height wind turbines for both the single array and double array wind farm design. In the top panel is the annual energy that would be produced by each of the wind farm designs sectored by wind direction. Although difficult to see, the broken line slightly above the solid line, showing the 99.5 m hub height turbine produces slightly more energy than the 80 m hub height turbine as expected. The second panel shows the percentage change in total energy as a result of terrain effects. This plot shows that the terrain contribution to the energy output increases to a maximum of almost

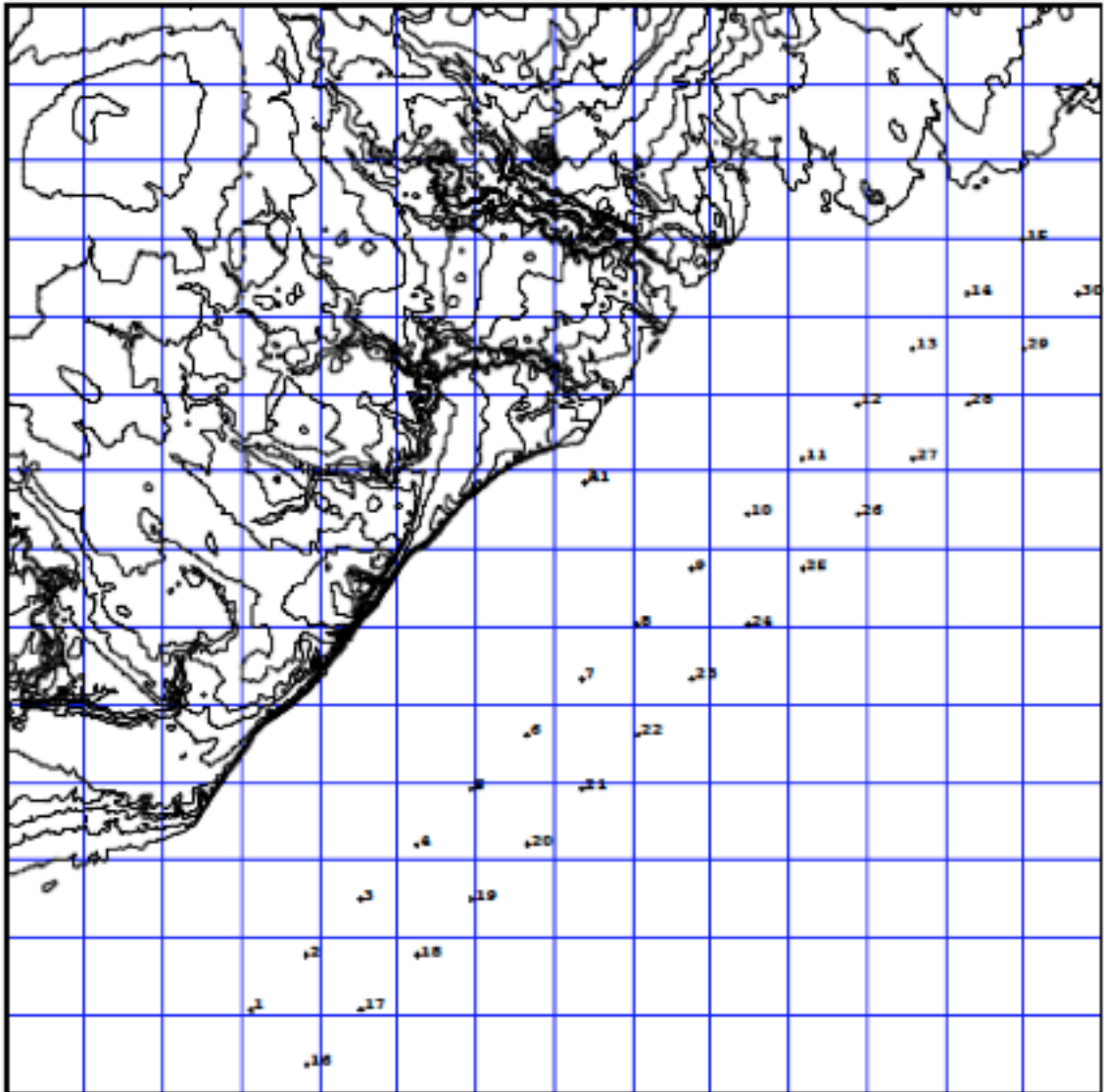


Figure 5.3: A potential double array wind farm design created in the program Wind Farm. The A1 represents the location of the Toronto Hydro platform while the numbers 1-30 show the location of individual wind turbines in this design. Each grid box is 5 km with the x axis representing east - west directions and the y axis north - south direction..

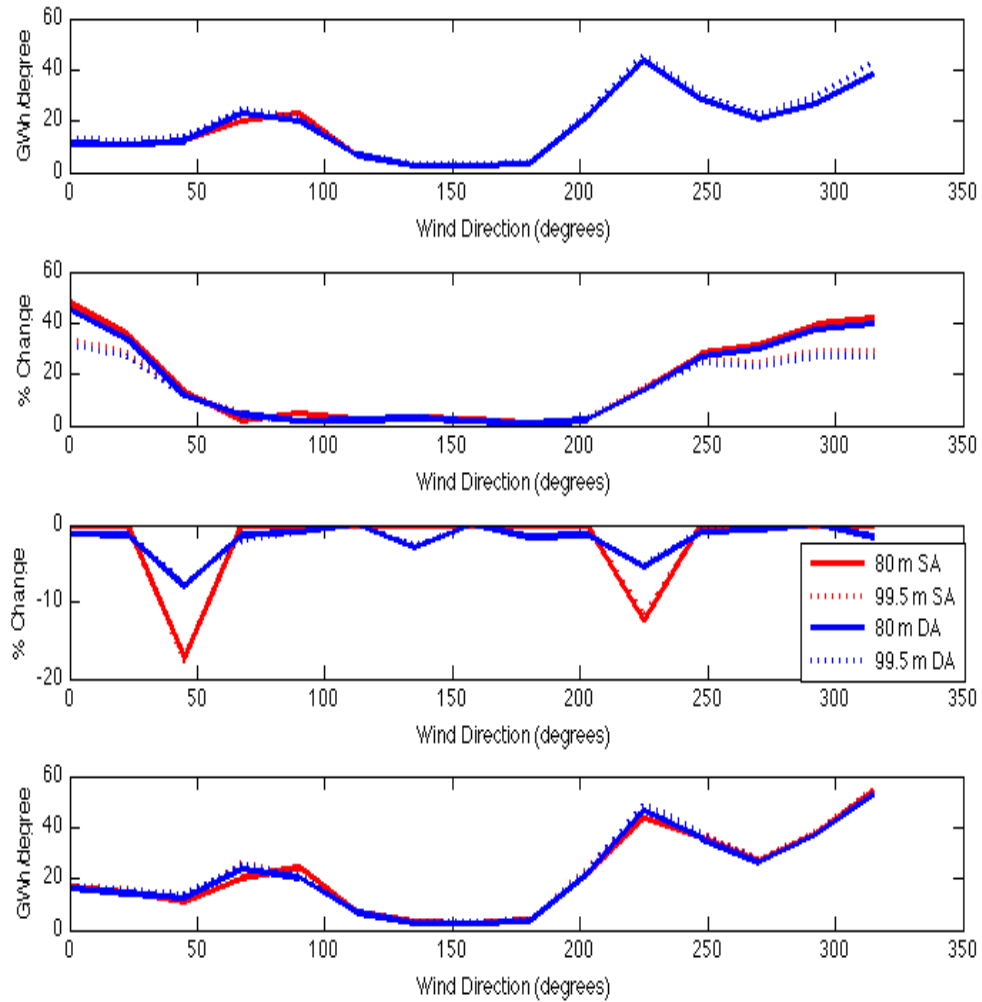


Figure 5.4: 4 panel figure comparing energy estimations using 2 years of data from the Toronto Hydro Platform (Measured + estimated) for the single array design and double array design with 80 m and 99.5 m hub height. The top panel shows energy estimations without considering wake effects and terrain effects by 22.5 degree wind direction sectors. The second panel shows the increase in energy as percentage caused by topographical effects by 22.5 degree wind direction sectors. The third panel shows the decrease in energy as percentage caused by wake effects by 22.5 degree wind direction sectors. The fourth panel shows the total energy estimation considering both wake effects and terrain effects by 22.5 degree wind direction sectors.

50 % for directions when the wind is blowing directly off the land and decreases to zero as the wind blows directly off a long over water fetch. The 80 m hub height has the more speed up because it takes some time for the wind to respond to the roughness change and the lower to the waters surface, the less time needed to respond to this roughness change. This increase is due to the met tower being closer to the shoreline than the turbines. Winds within the internal boundary layer will continue to adjust to the smoother water surface as air travels from the lidar location to the farm site further offshore. The two 99.5 m hub height designs see even less increase because the higher wind turbines are likely less in the internal boundary later than at 80 m hub height. The third panel shows the percentage loss due to wake effects. The largest loss due to wake losses is when the wind is blowing at 45 degrees or 225 degrees a result of the wind being directly parallel to the array. For the single array there are only wake losses for the two directions and there is nearly no difference in wake losses between the 80 m hub height and 99.5 m hub height. The double array shows less than half the wake losses for the directions of 45 and 225 degrees because the rows of turbines only have half the number of turbines however, the double array designs sees small wake losses for all directions. The average wake loss for the single array is 2.36 % over all directions while the double array has a average wake loss of 1.5 % showing the double array experiences slightly less wake loss compared to the single array. The fourth panel

shows the total energy of each wind farm design including wake losses and terrain effects. The only notable difference between the double array and single array is at directions 245 and 315 degrees. The single array shows slightly more energy at 315 degrees because of the greater increase due to terrain effects while the double array shows slightly more energy at 225 degrees because it has less wake losses compared to the single array. The annual energy production will be investigated numerically in Table 5.1.

Figure 5.5 shows the wake loss, increase due to terrain and total energy for each of the 30 wind turbines in each design (refer to Figure 5.2 and Figure 5.3 to see turbine numbers). In the top panel, the percentage gain due to terrain effects for each of the 30 turbines is shown. The single array turbines have relatively constant gain for the first 23 turbines but then the gain due to roughness changes because the turbines get closer to the shoreline moving east (but still greater than 5 km from the shoreline). The double array wind farm design shows the same pattern as the single array design in that for each row the percentage gain due to terrain is relatively constant for the first 11 turbines of each row from west to east as the turbines get closer to the roughness change (but still greater than 5 km from the shoreline). The second row of turbines show higher gain due to terrain which is a result of the turbines being further from the shore and terrain gains increase moving further from the abrupt change in surface as the internal boundary layer

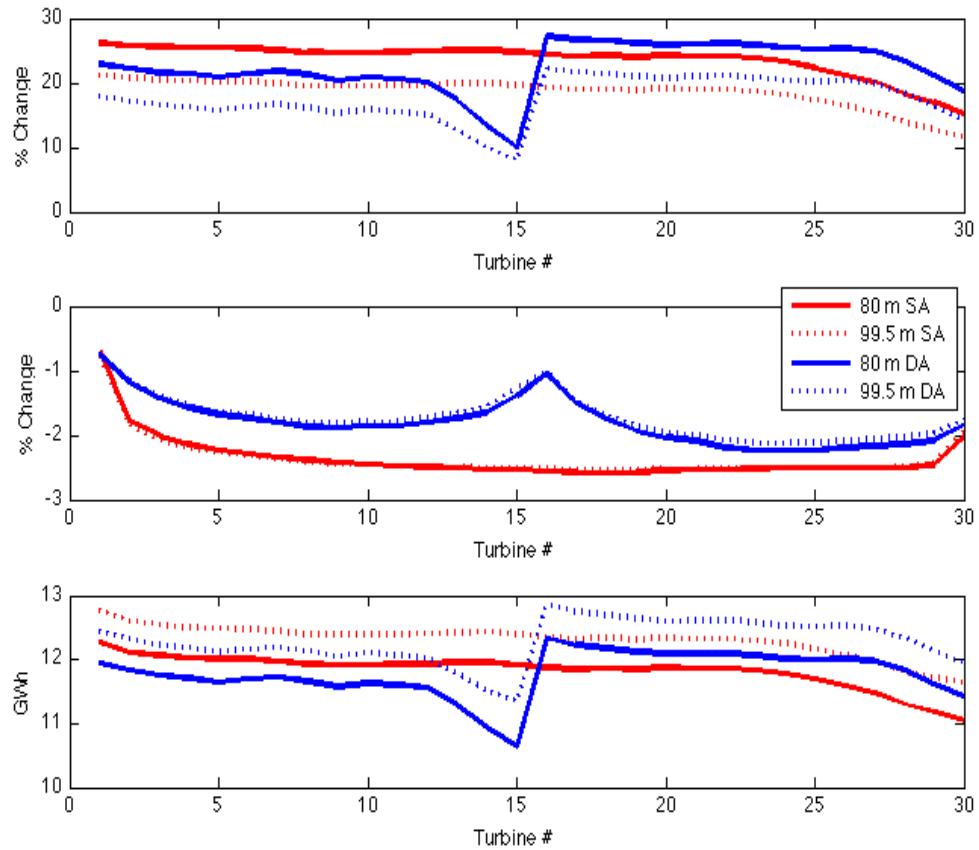


Figure 5.5: 3 panel figure comparing energy estimations for individual wind turbines within the wind farm design using 2 years of data from the Toronto Hydro Platform (Measured + estimated) for the single array design and double array design with 80 m and 99.5 m hub height. The top panel percentage loss due to wake effects for each of the 30 wind turbines. The second panel shows the increase in energy as a percentage caused by topographical effects by 22.5 degree wind direction sectors. The third panel shows the total energy estimation considering both wake effects and topographical effects by 22.5 degree wind direction sectors for each of the 30 wind turbines.

evolves. Figure 5.5 also shows that the 80 m turbine wind farm design has more percentage growth than the 99.5m which is a result of the turbine being higher and therefore there being less in the internal boundary layer. In the second panel is the percent wake losses for each wind turbine in each wind farm design. In the single array design there is very little difference between the 80 m and 99.5 m hub height turbine and the wake losses are relatively constant for all turbines except less for the couple of turbines on each end of the array. In the case of the double array, a similar pattern occurs to the single array for each row of turbines (turbine 1-15 and turbine 16-30). The second array of turbines has slightly higher wake losses because the winds blowing from the north west to south east are frequent than the wind from south east to north west, and the more frequent the winds, the more wake loss. The third panel shows the total energy produced by each wind turbine in each wind farm design. The annual energy of the single array designs is relatively constant for the first 23 wind turbines between 12 and 13 GWh but the energy drops off significantly for turbines 24 through 30 where the turbines see far less topographic increase as seen in panel two of Figure 5.5. The total energy of each turbine in the double array shows a similar shape to the single array for each row in that the total energy is relatively constant in the first 11 turbines of each array and the energy tapers off for the last 4 turbines in each row as terrain change gains decrease.

To look at exactly how each wind farm design compares, Table 5.1 shows the annual energy after wake losses and terrain gains of each wind farm.

Table 5.1 shows the annual energy for the single array and double array wind farm designs for both 80 m and 99.5 hub height. For the 80 m hub height single array, annual energy has been calculated for 97 % , 100 % and 103 % of wind speeds to see how sensitive the wind farm would be to small variations in wind speed. Comparing the annual energy of 80 m hub height wind farm designs with 100 %, the single array shows just under 1 GWh more energy than the double array meaning there is very little difference between the two designs. The 99.5 m hub height for both the single array and double array shows about 14 GWh more than the respective design with 80 m hub height. Its worth noting that these energy estimations have a certain level of uncertainty carried over from uncertainty in wind speed. In the case of the 80 m hub height design when the winds are increased and decreased by 3 %, the annual energy is altered by about 4-5 % which makes sense since at these wind speeds, a wind turbine curve can be approximated as linear. Only at the high and low ends is the power curve non - linear.

With the annual energy estimations for each wind farm design, the capacity factor can be calculated using

$$\text{Capacity Factor} = \frac{\text{Annual Energy Output}}{(365 \text{ days}) \times (24 \text{ hours/day}) \times (\text{Power})}. \quad (5.1)$$

Using the 100 % of wind speed, the capacity factors of the single array are 44.9 %

Wind Farm Design	80 m 100 %	80 m 103 %	80 m 97 %	99.5 m 100 %	99.5 m 103 %	99.5 m 97 %
Single Array	354.8	369.8	340.2	369.2	384.0	354.6
Double Array	353.3	-	-	368.5	-	-

Table 5.1: The annual energy for the single array and double array wind farm design in GWH. For single array design, annual energy has been calculated for 97 % of wind speed, 100 % of wind speed, and 103 % of wind speed. For the double array, only the total energy for the 100 % wind speeds are shown.

and 46.8 % for 80 m and 99.5 m hub heights respectively. These capacity factors are fairly high, usually 30 - 40 % are considered good for a wind farm.

## 6 Wind Forecasting with Wind Energy

### Applications

In Ontario, wind energy is an increasing source of power to the energy grid. In 2012, the wind energy capacity in Ontario of 1511 MW or about 3 % of the energy supply as seen in Figure 6.1 [15]. With this increasing amount of wind energy, the problem the Independent Electricity System Operator (IESO) of Ontario has to deal with is that wind energy varies with the wind speed, not the energy demand, so wind power is said to be non-dispatchable. In an effort to try to manage this variability, on November 1st, 2011, the Market Rule for Centralized Forecasting came into effect, requiring all wind facilities 5 MW or greater to register and participate in the service [15]. The centralized forecast system requires each wind energy facility in Ontario to report detailed information about the location of each wind turbine, realtime energy output and weather conditions at the wind farm. This information is reported to the IESO to be used as input in the province wide forecasting system in an effort to improve the wind energy forecasts in Ontario.

# Energy Output by Fuel Type (2012)

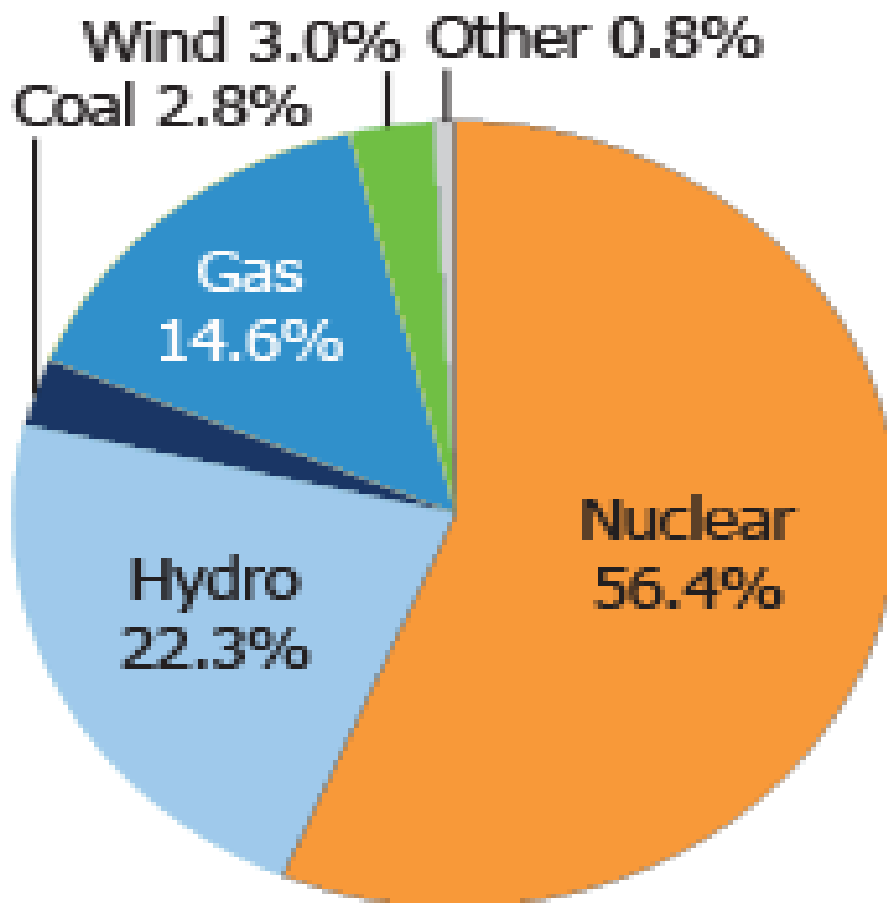


Figure 6.1: The fuel types and percentages used to feed Ontario energy demand in 2012 [15].

## 6.1 Accuracy of Current Weather Models

One may ask why can't the wind speeds of current weather models be used for forecasting the wind energy output for Ontario. In principle, available wind energy varies according to the wind energy equation

$$P = \frac{1}{2}\rho Av^3 \quad (6.1)$$

where  $P$  is power,  $\rho$  is air density,  $A$  is the swept area of the blades of the wind turbine, and  $v$  is wind speed. However, not all of this possible amount of power can be extracted by a wind turbine. A German physicist Albert Betz concluded in 1919 that no wind turbine can convert more than  $16/27$  (59.3%) of the kinetic energy of the wind into mechanical energy turning a rotor[11]. However, the real life limit is between 0 - 50 % (where zero percent is when  $U > 25m/s$  and the turbine is shut down). Other losses that make the real life limit lower than the Betz limit come from accounting for the strength and durability of the wind turbine and the losses incurred from the turbine generator, bearings and gear box. If air density is considered constant in short time intervals, wind power varies with the cube of wind speed. So this means, in any energy forecast, actual errors in wind speed forecasts can be amplified in wind power error by a factor of 3. To see what kind of errors the current models produce for wind energy forecasts, this study will look at cases at the Toronto Hydro platform using forecasts from the GEM 15 km regional

model and a WRF model run at 1.5 km horizontal resolution. These errors will be shown both as errors in wind speed and energy using a typical wind turbine curve.

### **6.1.1 Wind Speed and Direction Comparisons with GEM**

In Chapter 2, the GEM 48 hour forecasts along with analysis were compared to upper air measurements from the OQnet wind profilers. In this study the GEM regional forecasts will be compared to the Toronto Hydro lidar data to see how the GEM model performs at low levels. Figure 6.2 shows the mean absolute error and bias in wind speed at levels 17 - 120 m between the Toronto Hydro lidar measurements and the GEM 48 hour forecasts as well as the GEM analysis for data from June 2010 to May 2011. These errors are calculated using the same methods outlined in Chapter 2 and the Toronto Hydro data are measurements and estimated data and similar to Chapter 2, the lidar measurements are assumed to be correct.

Figure 6.2 shows the mean absolute error and bias between Toronto Hydro data and the GEM model. In the left panel of the plot the mean absolute error is just over 2 m/s at 17m and increases to about 3 m/s at 120 m for the 48 hour forecasts, while the error is very similar for the analysis. The bias shows about 0.5 m/s at 17 m increasing to nearly 1.4 m/s at 120 m for the 48 hour forecasts while the analysis bias is slightly less at all levels. Using the bias definition from Chapter 2,

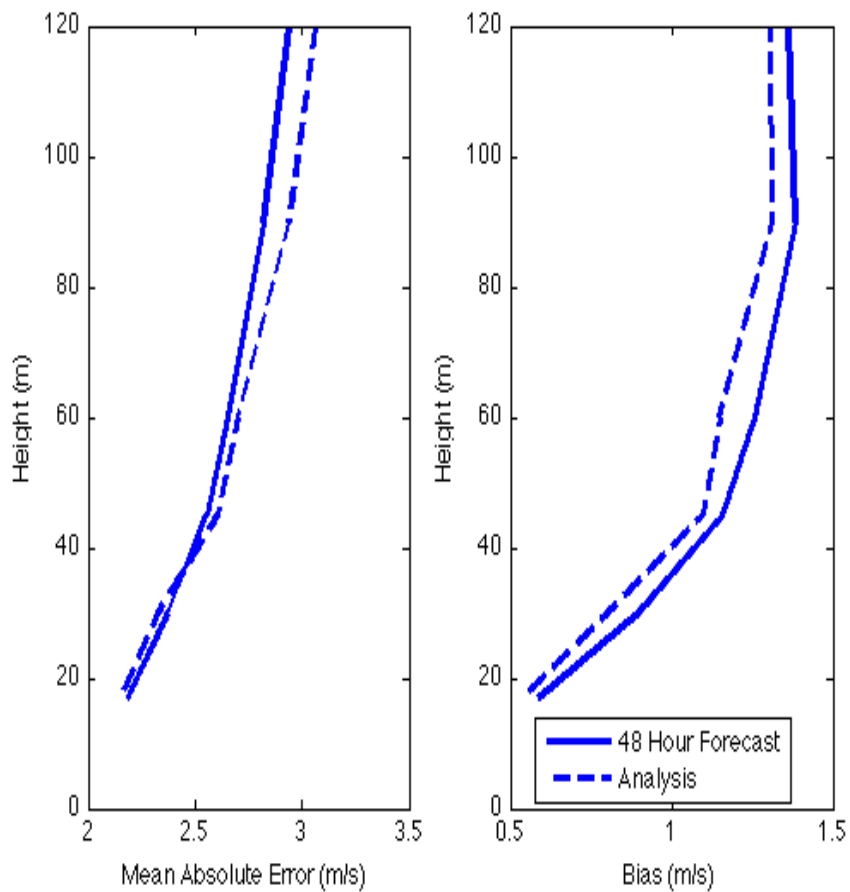


Figure 6.2: The MAE (observation - model) between the Toronto Hydro 6 lidar levels compared with the GEM analysis and 3 - 48 hours forecasts in solid lines and GEM analysis in broken lines for 1 year of data from June 2010 through May 2011. The left panel shows the mean absolute errors at each level while the right panel shows the bias.

the positive bias in the speed at all levels shows that the GEM model nearly always under predicts the wind speed at the location of the Toronto Hydro platform. The strong positive bias can partially be explained through the orientation of the GEM grid. Through the linear interpolation of the 4 surrounding grid cells, 2 of these cells are over land so the lower model wind speeds would be impacted and likely decreased by the effect of higher surface roughness.

Figure 6.3 shows the mean absolute error and bias in wind direction between the Toronto Hydro lidar measurements and the GEM 48 hour forecasts and GEM analysis for data from June 2010 to May 2011.

In Figure 6.3 the mean absolute error is relatively constant at just over 40 degrees for the GEM 48 hour forecasts at all levels and about 45 degrees for the GEM analysis. In this case the analysis is slightly less accurate than the forecasts which is probably due to outliers caused by local effects which can have very high errors. The bias in the direction that the GEM 48 hour forecasts show is backing  $5^\circ$  more than measurements show. The GEM analysis shows about a negative  $8^\circ$  bias at 17 m and this switches to a  $3\text{-}4^\circ$  bias at 90 and 120 m.

Some may argue that a portion of this error is a result of including estimated data in the data set being used. To address this, Figure 6.4 shows the mean absolute error and bias between the Toronto Hydro measured wind speed and the GEM forecasts and analysis for July 2010; a month with very high measured data return

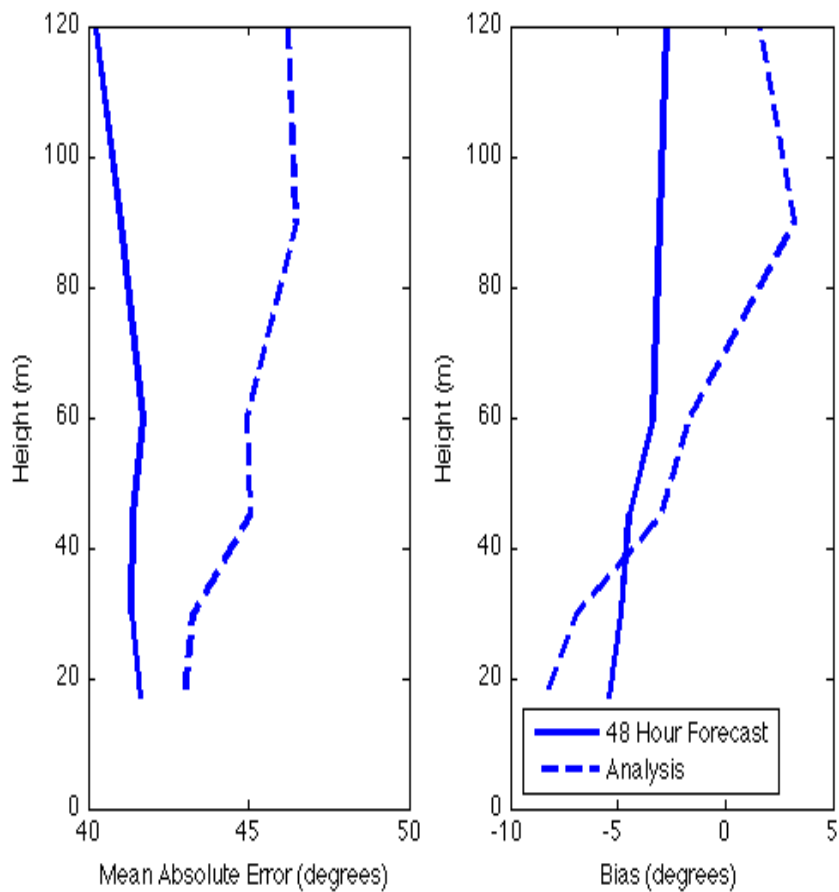


Figure 6.3: The errors in wind direction between the Toronto Hydro 6 lidar levels compared with the GEM analysis and 3 - 48 hours forecasts in solid lines and GEM analysis in broken lines for 1 year of data from June 2010 through May 2011. The left panel shows the mean absolute errors at each level while the right panel shows the bias.

therefore estimated values will have very little effect on the errors.

Comparing the errors in Figure 6.4 to the errors in Figure 6.2, the mean absolute error is about 0.5 m/s less at 17 m and almost 1 m/s less at 120 m while the bias shows similar differences. This decrease in error could be partially due to the lack of estimated data, but the more likely because July has relatively low wind speeds therefore the percentage error would be similar, but the absolute error would be much less. To test this theory of less absolute error due to low wind speeds, the calculated errors for December 2010, another month with high data return, but also relatively high wind speeds. The mean absolute errors for December 2010 are very similar to the mean absolute error for the year from June 2010 to May 2011 suggesting that the estimated data does not add much error to the forecasts. Figure 6.5 shows the mean absolute error and bias in wind direction between the Toronto Hydro lidar measurements and the GEM 48 hour forecasts and GEM analysis for data from July 2010.

Comparing the errors in Figure 6.5 to the errors in Figure 6.3, the mean absolute error actually increases showing the errors in Figure 6.2 are probably not influenced by the estimated data included in the measured data set. The bias in the wind direction for July 2010 is about 10 degrees more negative for the 48 hour forecasts than for a full year showing again that the estimated data does not add much or any error to this analysis.

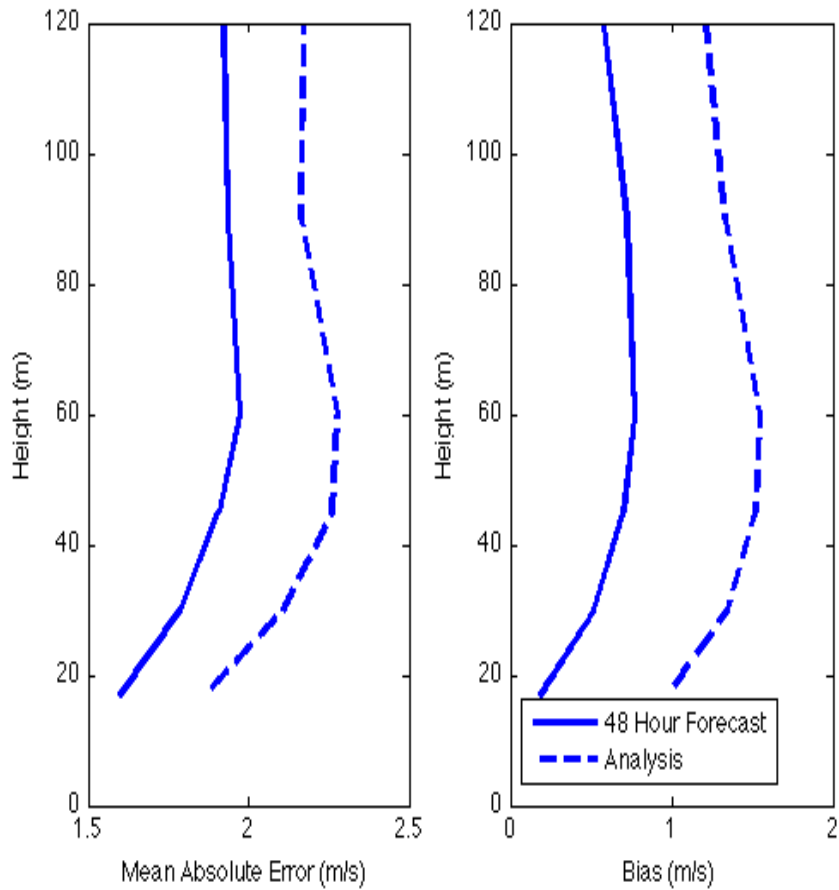


Figure 6.4: The errors in wind speed between the Toronto Hydro 6 lidar levels compared with the GEM analysis and 3 - 48 hours forecasts in solid lines and GEM analysis in broken lines for July 2010. The left panel shows the mean absolute errors at each level while the right panel shows the bias.

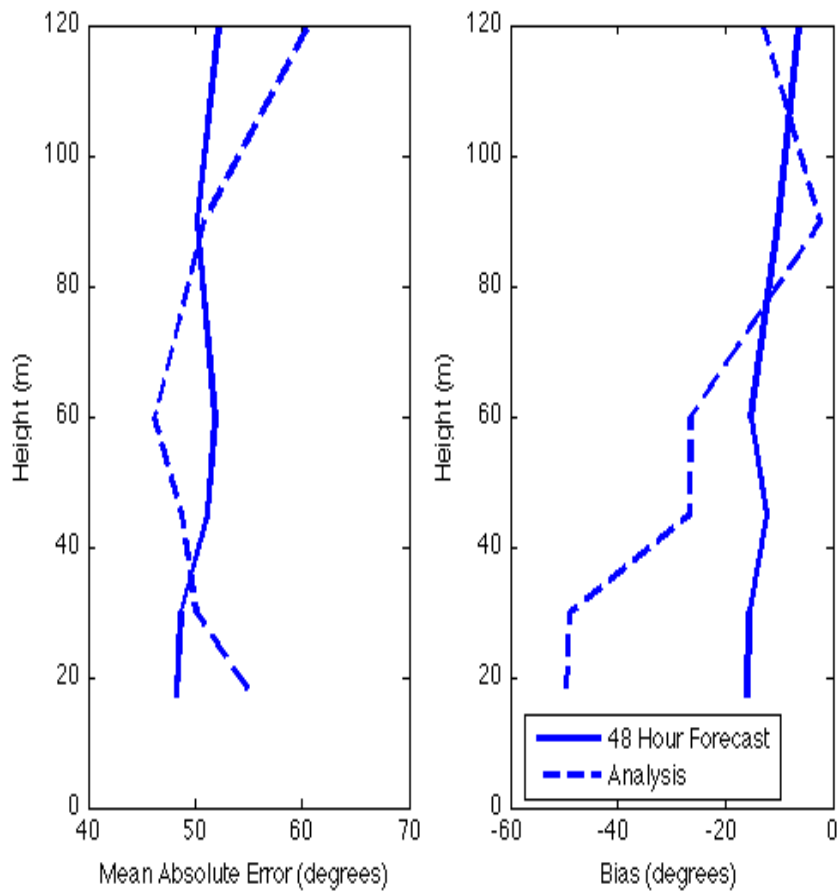


Figure 6.5: The errors in wind direction between the Toronto Hydro 6 lidar levels and the the GEM 48 hours forecasts in solid lines and GEM analysis in broken lines for July 2010. The left panel shows the mean absolute errors at each level while the right panel shows the bias.

### 6.1.2 Wind Speed and Direction Comparisons with WRF

The Weather and Research model (WRF) was first developed in the 1990's through a partnership primarily consisting of National Center for Atmospheric Research (NCAR), the National Oceanic and Atmospheric Administration (represented by the National Centers for Environmental Prediction (NCEP) and the (then) Forecast Systems Laboratory (FSL)), the Air Force Weather Agency (AFWA), the Naval Research Laboratory, the University of Oklahoma, and the Federal Aviation Administration (FAA)[14]. Since its development, WRF has grown to have a large worldwide community of users (over 20,000 in over 130 countries) and many workshops are held at NCAR. The WRF model is an open source mesoscale numerical weather prediction model that is designed to run for operational purposes as well as for research and can simulate real time situations or idealized cases for research. It has the ability to run on a single computing machine or on a large set of parallel computers [14]. The WRF model equations are nonhydrostatic and fully compressible with a vertical terrain-following hydrostatic pressure coordinate [14]. The model is set up to run at a wide range of resolutions (both vertical and horizontal) from coarse to fine and domains can be set by the user from large to small depending on the intended use. WRF has the ability have nested domains that can achieve very high resolution and boundary conditions are often obtained

from other models such as the GEM. In order to carry out these WRF computations, facilities and code owned by Dynasty Power were used. In the agreement, specific details of the WRF model settings need to be withheld which they consider commercially sensitive.

To try to improve on errors seen in the GEM model, a version of the Weather Research and Forecasting Model (WRF) model has been run at 1.5km horizontal resolution, 10 times finer resolution than the GEM regional model. This model was run for first 20 days of July 2010 using NARR data as initialization and boundary conditions every 3 hours for 24 hour forecasts. NARR data is a data set that ingested a wide range of observations that has been interpolated on a grid to be used as initial and boundary conditions for models. This period was chosen because of the very good data return of lidar data. The domain is run over most of Lake Ontario and north of the Lake shown in Figure 6.6.

This domain was chosen so to provide the largest coverage of the coastline.

Figure 6.7 shows the mean absolute error and bias between 5 levels of lidar data at the Toronto Hydro Platform and the WRF 24 hour forecasts for July 2010. This comparison analysis is done for the analysis + forecast for a 24 hour period starting at 00Z. The lowest level of lidar data has been left out of this error analysis because this particular WRF model does not calculate a wind speed at that level and since the hub height level is of most interest, the 17 m level is not that important for this

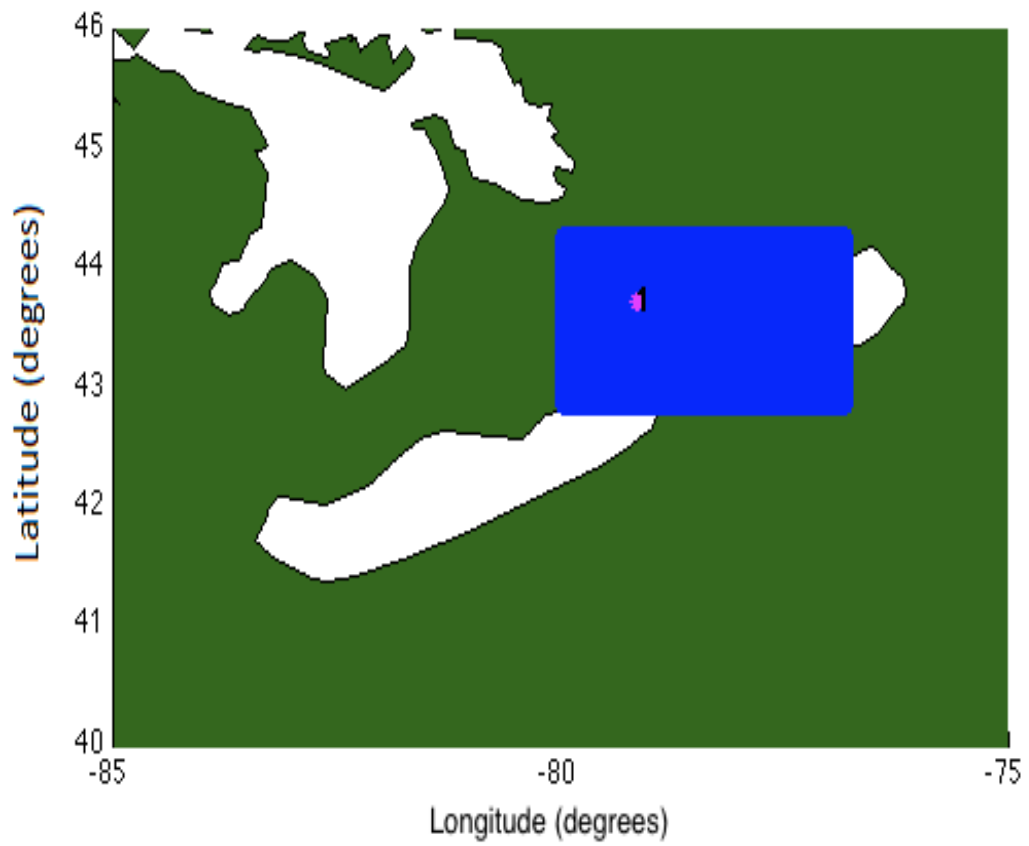


Figure 6.6: The non-nested WRF domain in blue and the Toronto Hydro platform location is marked with the pink dot and number 1.

analysis.

In Figure 6.7, the mean absolute error between the measurements and WRF model is close to 2.25 m/s at 30m and increases to about 2.5 m/s at 120m which is more than the GEM model for just the month of July, but comparable to the GEM errors for the full year of data. The bias is negative for all levels showing that the WRF model generally over predicts the wind speeds at the Toronto Hydro platform, while the GEM model shows tends to under predict these wind speeds. Figure 6.8 shows the mean absolute errors and bias in wind direction between the highest 5 lidar levels at the Toronto Hydro platform and the WRF model with 1.5 km resolution.

Figure 6.8 shows that the mean absolute error in wind direction to be between 65 and 80 degrees for the highest levels which is higher than GEM direction error for July 2010. The bias in wind direction is about about 40 degrees at the highest levels, although much lower at the 30 m level. Overall the WRF model shows more bias than the GEM model, but in the opposite direction. One cause for the large wind direction error is that fact that this site is so close to the shoreline the the high resolution model probably struggles with handling the direction with such a sharp change in surface roughness. Overall, the errors show that accuracy isn't always increased in wind forecasts by increasing the model resolution. This is studied by Clifford F. Mass et al.,[12] where they have shown that increasing horizontal resolution can increase the accuracy of certain features, but does not necessarily

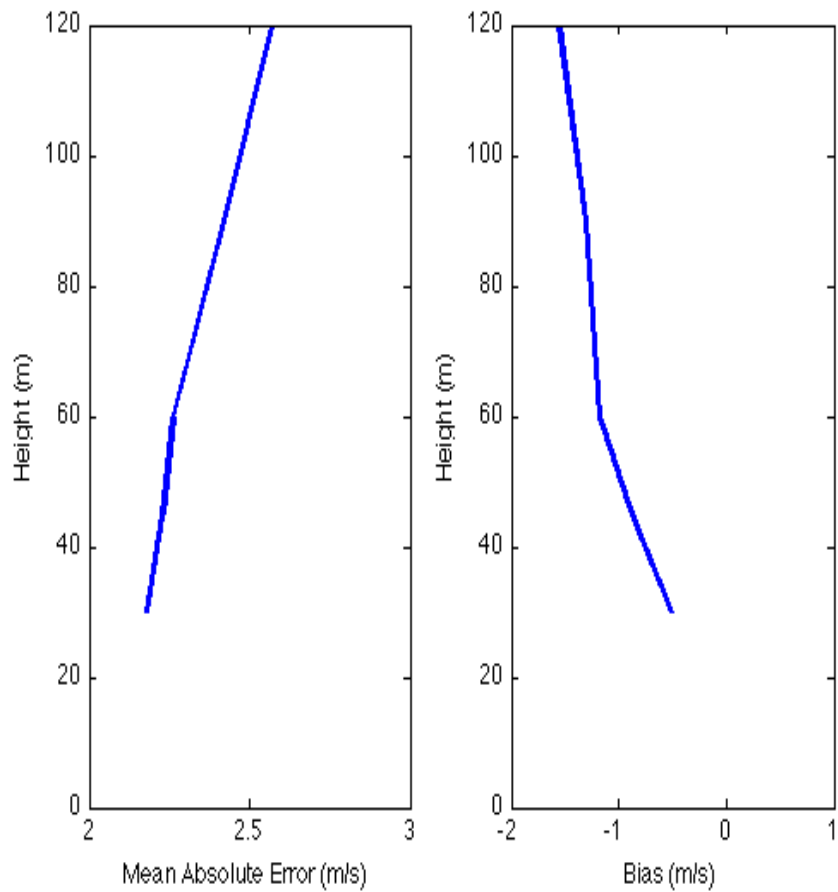


Figure 6.7: The errors (observation - model) in wind speed between the Toronto Hydro highest 5 lidar levels and the the WRF 24 hours forecasts. in solid lines for July 2010. The left panel shows the mean absolute errors at each level while the right panel shows the bias.

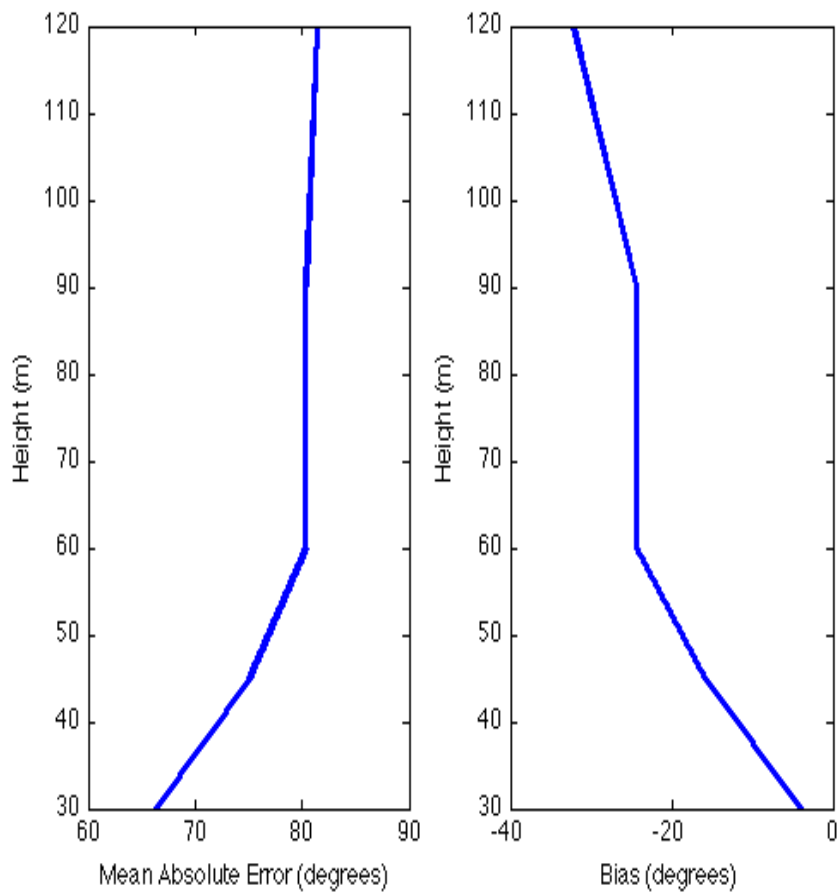


Figure 6.8: The errors in wind direction between the Toronto Hydro highest 5 lidar levels and the the WRF 24 hours forecasts in solid lines for July 2010. The left panel shows the mean absolute errors at each level while the right panel shows the bias.

increase overall forecast accuracy.

### 6.1.3 Time Series

In the previous analysis, the errors in wind speed and direction between measurements, the GEM model and the WRF model were investigated and shown to be fairly significant. To look at how these how the models compare in time, a time series of wind speed is shown in Figure 6.9.

In Figure 6.9 is a 24 hour time series on July 6, 2010 showing 90 m lidar data and model output from the WRF and GEM models. Both models match the overall trend quite well, but do not capture the ramp down at the end of the day. This is likely enhanced by the near shore location. Figure 6.10 is a time series of wind direction for July 6, 2010 showing the 90 m lidar measurements, and the WRF and GEM forecasts.

In Figure 6.10 the time series for both models show the general trend of wind direction but the GEM model shows a sharp change in direction at hour 10 and neither model captures the large direction change at the end of the day which probably helps explain the error in wind speed for the same period in Figure 6.9

This example shows how the models can get the overall trend right but often have trouble with abrupt changes, which are often very localized effects and these are effects models have a hard time forecasting

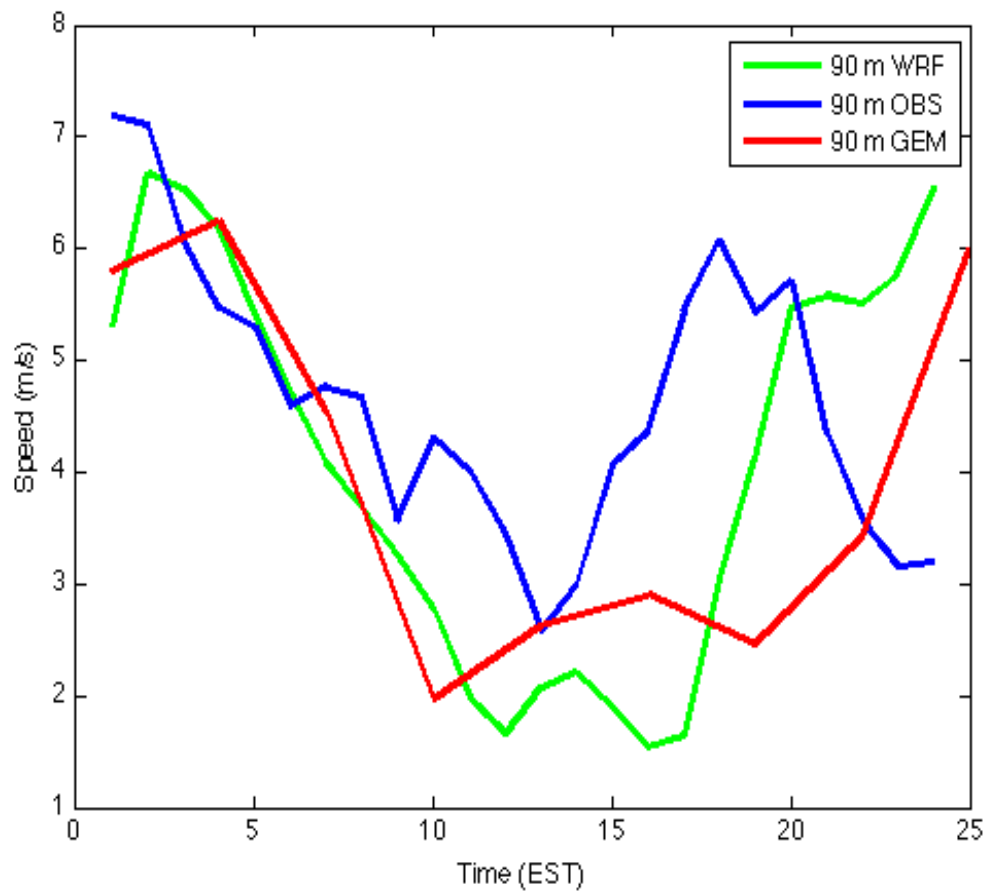


Figure 6.9: A 24 hour time series of wind speed on July 6, 2010 for the 90m lidar measurements, the WRF model and the GEM model. The measurements are made up of 6 ten minute averages, the WRF model is output every hour and the GEM model output every 3 hours. .

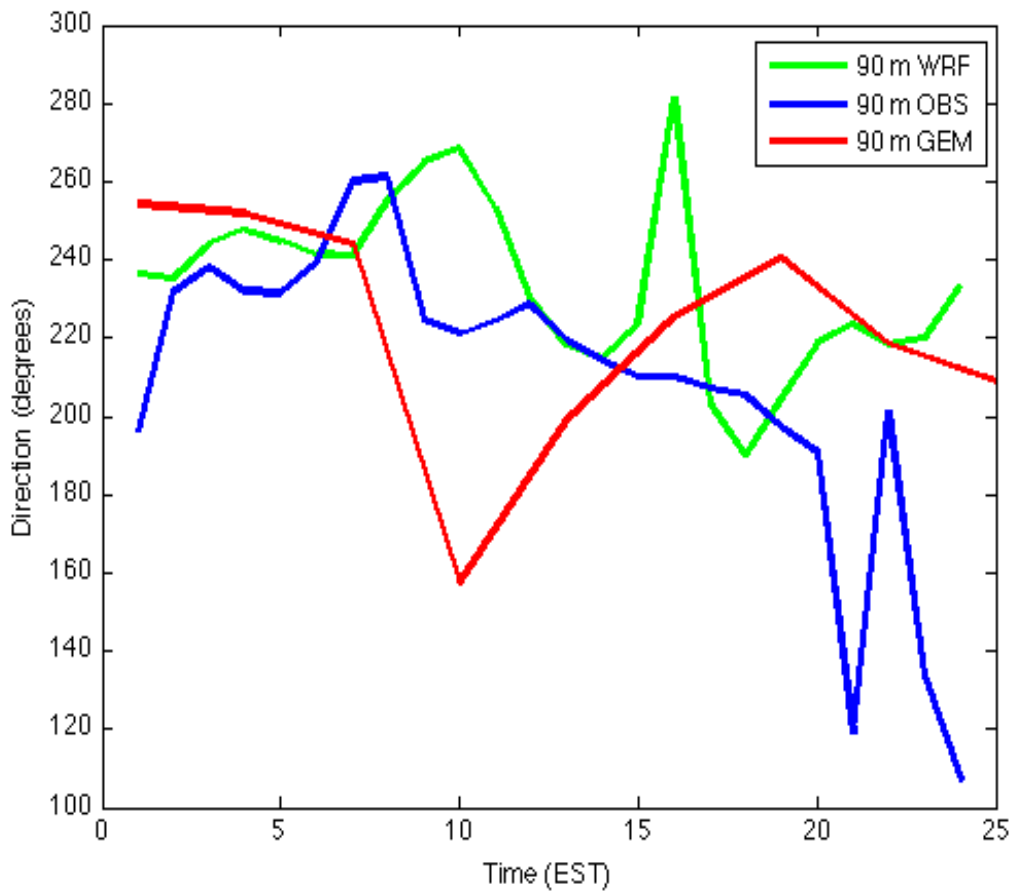


Figure 6.10: A 24 hour time series of wind direction on July 6, 2010 for the 90m lidar measurements, the WRF model and the GEM model. The measurements are made up of 6 ten minute averages, the WRF model is output every hour and the GEM model output every 3 hours. .

## 6.2 Energy Forecasting Errors

In the previous section the errors in wind forecasts were investigated for both the GEM and WRF models. But since this Chapter is focusing on wind energy applications, errors in wind speed can be converted to power output to see how errors in forecasts can affect the output of a wind turbine or wind farm.

Figure 6.11 shows a wind turbine curve for a Siemens 3.5 MW machine with a hub height typically of 90m.

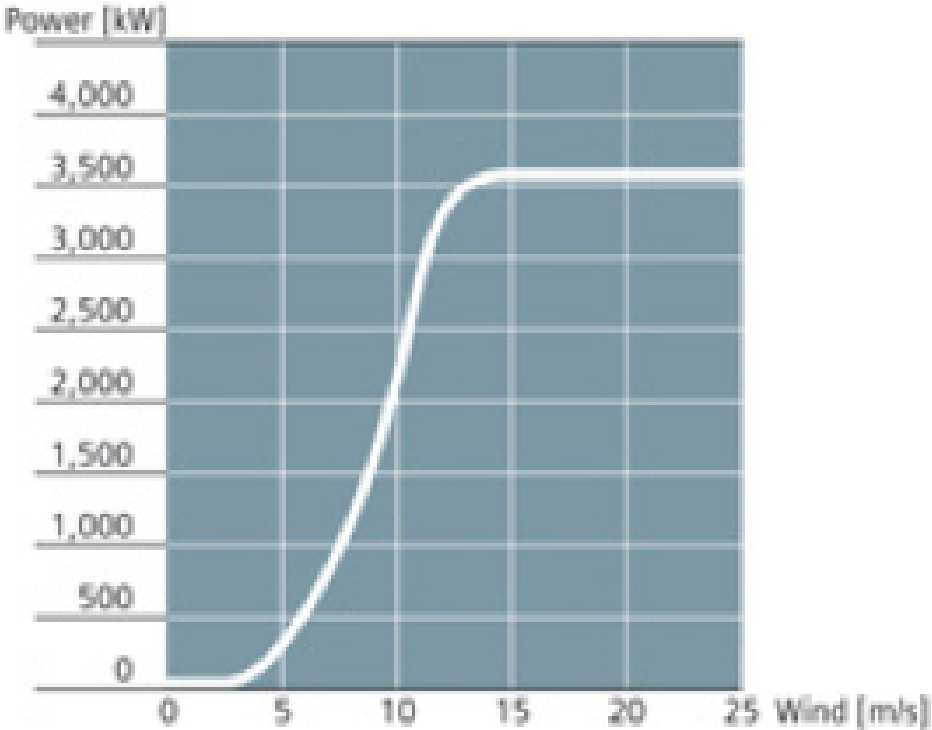


Figure 6.11: A power curve for one of the most popular wind turbines in use today; the Siemens 3.5 MW machine curves. [22]

Wind Speed	Percentage of Total Wind Power
3	1.40
4	4.30
5	10.0
6	17.1
7	28.5
8	42.8
9	57.1
10	80.0
11	91.4
12	97.1
13	100.0

Table 6.1: The approximate percentages of total wind turbine output that a Siemens 3.5 MW machine would be producing at each wind speed.

In Figure 6.11, the cut in wind speed of this turbine is 3.0 m/s and depending on the model, it reaches it's maximum output at 12 or 13 m/s.

Table 6.1 shows the approximate percentage of total output that the Siemens 3.5 MW would produce at each wind speed.

In Table 6.1 the turbine reaches about half capacity between 8 and 9 m/s and full capacity just over 12 m/s. Linking this table to the errors in wind speed forecasted by the models in the previous section, at 90 m, the GEM model had nearly 3 m/s mean absolute error (about 2.8 m/s). If the actual wind speed is assumed to be 7m/s, the wind turbine is producing about 30 % capacity however the GEM model based on 3m/s error could forecast 1.4 % output on the low side, and about 80 % on the high side. This is an error of 30 to 50 % which doesn't amount to significant

output for 1 turbine, but the 90 MW farm discussed in Chapter 3 is considered, this could be up to 45 MW of power difference between forecast and actual output. To visualize how wind speed errors correspond to energy errors for an actual wind turbine, Figure 6.12 shows the wind speed time series in Figure 6.9 converted into a energy time series using the power curve in Figure 6.11.

At hour 1 in this figure, the WRF model predicts almost 400 KW, the GEM model about 500 KW while the actual output of the turbine would be about 1200 KW which is a 200 % under estimate from the WRF model. This type of discrepancy can be troublesome for system operators to plan around when dealing with thousands of MWs.

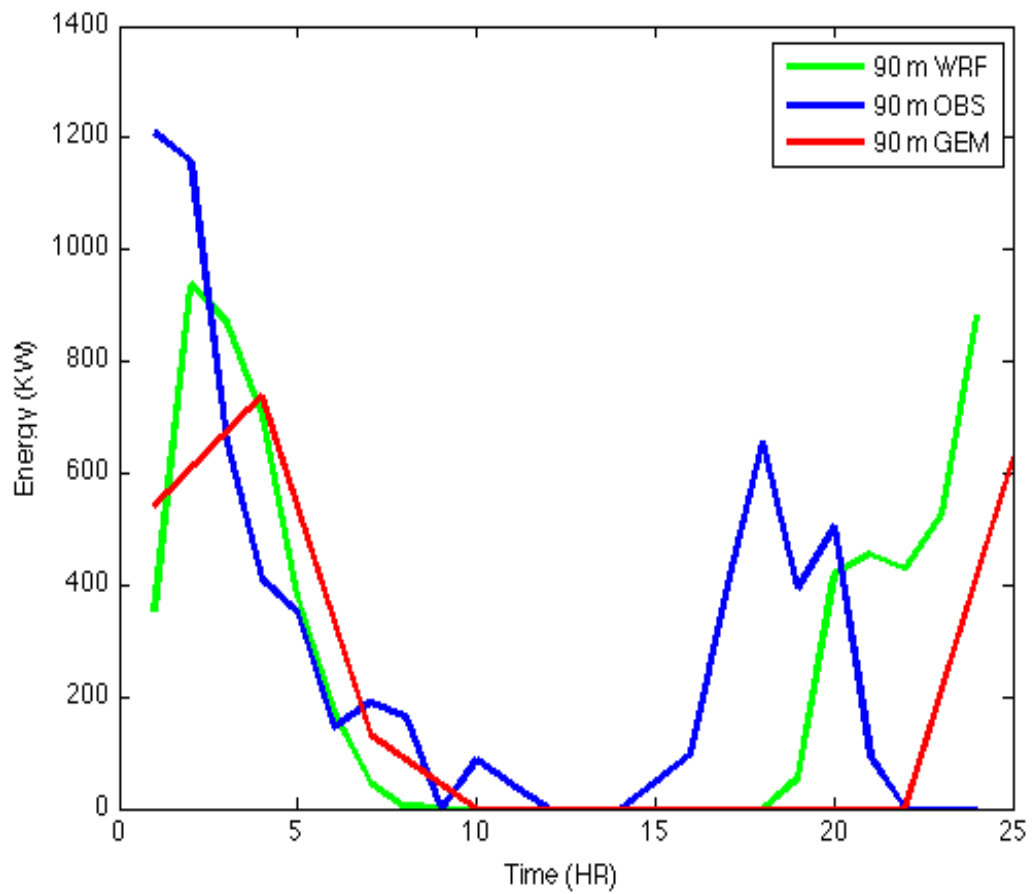


Figure 6.12: A 24 hour time series of energy output using a Siemens 3.5 MW on July 6, 2010 for the 90m lidar measurements, the WRF model and the GEM model.

## 7 Conclusions

In Chapter 2, this dissertation looked ways to quality control data from the wind profilers within the OQnet. Using probability distributions of wind direction, a problem with the algorithm to sort the different signals (wind and ground clutter) was discovered that was causing data to be missed at the 4 directions lining up with the orientation of the radio antenna. Working with the manufacturer, the algorithm was changed to fix this problem and as a result recovered significant;y more data. Also in Chapter 2, wind profiler data was found to match quite well to nearby radiosonde data that helps reinforce the accuracy of these profilers. Wind measurements from 5 of the wind profilers were compared with GEM model analysis and forecasts which uncovered large differences. A large portion of theses differences is thought to be errors in the model given the strong agreement with radiosonde. These errors help motivate the assimilation of this data into weather models.

In 2010 Toronto Hydro installed an offshore wind resource assessment platform just east of Toronto offshore of the Scarborough Bluffs in Lake Ontario. As described

in Chapter 3 of this study, Toronto Hydro used a lidar to measure winds at 6 different levels up to 120 m. In addition, wind was measured at platform level along with other important weather variables. Although there were some equipment problems with the lidar, especially in the second year of operation, two methods were developed to use platform level winds and any available lidar measurements to estimate missing upper level winds. Using these two methods, a near full set of data has been calculated and although there is no replacement for measured data this type of estimation is extremely valuable when missing data is inevitable.

Using MCP analysis with the Toronto Hydro site as a target site and Toronto Island station run by the Meteorological Service of Canada as a reference site, a long term wind speed analysis was done in Chapter 4. This analysis was based on regressions using wind speed and direction for one year, June 2010 through May 2011; the one year period where data return was highest at hub height of 90 m. The 1 year wind speed average at 90 m using measured plus estimated data is 7.19 m/s. When the MCP analysis was run for the same 1 year period as the MCP regressions were developed from; June 2010 through May 2011, the linear regression and variance mean method recalculated an annual wind speed mean very close to the actual mean wind speed. Using 21 years of data from the reference site of Toronto Island between 1989 and 2009, MCP analysis showed that the longterm 90 m mean wind speeds is slightly higher than the measured 90 m wind speed for the period of June

2010 through May 2011. Specifically the linear regression and variance mean MCP methods that produced the most accurate short term wind speed mean predict long term mean wind speeds of 7.26 m/s and 7.30 m/s respectively while the other methods (excluding those considered inaccurate) have a longterm annual mean wind speed range from 7.26 m/s to 7.38 m/s. In addition to the MCP analysis to determine how representative the wind speed during the Toronto Hydro wind resource campaign is of long term wind speeds, Chapter 4 looked at the monthly and annual wind speed averages at the reference site, Toronto Island. This analysis showed that the monthly wind speed averages during the wind resource campaign in 2010 through 2012 were overall slightly lower than the long term monthly wind speed averages found through MCP. As an alternative to using Toronto Island as the reference site in the MCP analysis, a 10 year time series of high resolution model data was obtained from VORTEX at 100m for the Toronto Hydro platform site. MCP correlations were done using these data for this same concurrent period as Toronto Island, June 2010 through May 2011. The r-squared values in these correlations showed lower values than the correlation with Toronto Island implying that in this case, MCP using VORTEX data is probably less accurate than using Toronto Island data for long term estimations. Despite lower r-squared values, short term and long term wind averages using Toronto Island and VORTEX data showed higher wind speeds than the measured wind speeds during the June 2010

to May 2011 period.

Looking at wind speed classes with respect to wind energy, a wind speed of between 7 and 7.5 m/s is generally thought of as a medium to good wind energy resource [11] which the 90 m hub height at the Toronto Hydro site falls into. This type of wind classing is one indicator of a good wind resource. Another good indicator of a good wind energy site is the capacity factor. As discussed in Chapter 5, capacity factors are around 44-46 % for 80 to 100 m hub heights which is quite high considering most sources say sites with capacity factors of 30 to 40 % are promising sites to develop. This high capacity factor is partially due to modern wind turbines having The European Wind Energy Association report a capacity factor of 25.3 % in 2010 for all EU wind farms. There are factors mentioned in Chapter 3 that can bring these capacity factors down other than wind speed, but this calculation is only to show the potential of the Scarborough Bluffs site.

Although the wind resource looks promising at the Toronto Hydro site, there are many other things to consider before saying with confidence that this project is financially viable. One of the major factors is that this location is offshore meaning it would be more costly to build wind turbines in water than on land. A related issue is the current moratorium on offshore wind which has put the project on hold. There is also talk about when or if the moratorium is lifted, there will be a 5 km buffer zone along the shore line which would greatly influence this project as the

depth of the water increases significantly past 4 km offshore, making it even more difficult to put wind turbines in the water.

A final aspect of this study looks at wind forecasting for wind energy applications. Wind energy varies as the cube of wind speed so depending on where the wind speed is on the power curve of the wind turbine of choice, the amount of wind energy output could vary significantly for a small change in wind speed. Wind energy is a non dispatchable type of energy so wind forecasts become very important for system operators seeking to run an efficient power grid. In Chapter 6, errors in hub height wind speed are on average 3 m/s from the GEM model and nearly 2.5 m/s in the WRF model, translating to up to 50 % difference in output versus forecast. This is significant in power pools with large penetration rates. There are ways of improving these model forecasts through statistics, but these method often still produce large errors. These errors can be linked back to Chapter 2 and the push for more observations to be assimilated into models to improve model wind forecasts. Along with the world, Canada needs to diversify its energy dependance on fossil fuels by expanding the amount of wind energy in the country. One way to do this is to expand wind energy to the offshore and harness the wind resource it has to offer. It will be interesting to see how private industry works with the public and government to achieve this in the coming years.

## Bibliography

- [1] Bilgili, Mehmet., Yasar, Abdulkadir., Simsek, Erdogan., *Offshore wind power development in Europe and its comparison with onshore counterpart*, *Renewable and Sustainable Energy Reviews* 15 (2011) 905 - 915
- [2] Belair, S., M. Roch, A.-M. Leduc, P. Vaillancourt, S. Laroche, and J. Mailhot, 2009: *Medium-range quantitative precipitation forecasts from Canadas new 33-km deterministic global operational system*. *Wea. Forecasting*, 24,690708
- [3] Canadian Wind Energy Association, *Canadian Wind Farms.*, [http://www.canwea.ca/farms/index\\_e.php](http://www.canwea.ca/farms/index_e.php), July 14, 2010
- [4] Environment Canada., *Canadian Wind Atlas.*, <http://www.windatlas.ca/en/maps.php>, July 28, 2013
- [5] European Wind Energy Association (2009), *Wind Energy - The Facts: A Guide to the Technology, Economics and Future of Wind Power*, First Edition, March 2009, pp. 422.
- [6] European Wind Energy Association., *The European Offshore Wind Industry key 2011 Trends and Statistics*, January 2012, 1-23
- [7] Government of Ontario - Ministry of the Environment, *Ontario Rules Out Offshore Wind Projects.*, [news.ontario.ca/ene/en/2011/02/ontario-rules-out-offshore-wind-projects.html](http://news.ontario.ca/ene/en/2011/02/ontario-rules-out-offshore-wind-projects.html), July 28, 2013
- [8] Hansen, J., Mki. Sato, R. Ruedy, K. Lo, D.W. Lea, and M. Medina-Elizade, 2006: *Global temperature change*. *Proc. Natl. Acad. Sci.*, 103, 14288-14293, doi:10.1073/pnas.0606291103.
- [9] Hocking, W., *Radar Meteorology.*, <http://quark.physics.uwo.ca/whocking/cfi/home.html>, February 2011
- [10] Holton, J. R., *An Introduction to Dynamic Meteorology*, Academic Press, p. 53, 1992.

- [11] Manwell, J.F., *Wind Energy Explained: Theory, Design and Application (Second Edition)*, Wiley, New York, 2010.
- [12] Mass, Clifford F., Ovens, David., Westrick, Ken and Colle, Brian A., *Does Increasing Model Resolution Produce More Skillful Forecasts?*, Bull. Amer. Meteor. Soc., 83, 407430., 2002 .
- [13] Melnye, Markian M.W., Anderson, Robert M., (2009) *Offshore Power Building Renewable Energy Projects in US Waters, Tulsa, Oklahoma, USA.*, PennWell Corporation
- [14] National Center for Atmospheric Research *Users Guide for Advanced Research WRF (ARW) Modeling System Version 2* , January 2009, 1-222
- [15] Ontario Power Generation., *Supply Overview.*, [www.ieso.ca/imoweb/media/md\\_supply.asp](http://www.ieso.ca/imoweb/media/md_supply.asp), June 6,2013
- [16] Ram, B., Musial, W., Butterfield, S., *Energy From Offshore Wind.*, National Renewable Energy Laboratory, Conference Paper, February 2006
- [17] Riebeek, Holli., June 3, 2010., *Global Warming.*, June 14,2013., [earthobservatory.nasa.gov/Features/GlobalWarming/page2.php](http://earthobservatory.nasa.gov/Features/GlobalWarming/page2.php)
- [18] Rogers, Anthony L., et. al., *Comparison of the performance of four measure-correlate-predict algorithms; Journal of Wind Engineering and Industrial Aerodynamics*, v 93, n 3, March, 2005, p 243-264
- [19] Salmon, James R., Walmsley, John L., *A two-site correlation model for wind speed, direction and energy estimates .*, Journal of Wind Engineering and Industrial Aerodynamics, 79 (1999), 233-268
- [20] Salmon, J. and Taylor, P. (2013), *Errors and uncertainties associated with missing wind data and short records.* *Wind Energ.* doi: 10.1002/we.1613
- [21] Savelyev, Sergiyi. A., Taylor., Peter A., *Notes on an internal Boundary-Layer Height Formula*, *Boundary-Layer Meteorology* 101: 293301, 2001.
- [22] Siemens., *Siemens Wind Turbine SWT - 3.6 - 120.*, [www.energy.s3.com/hq/pool/hq/power-generation/wind-power/E50001-W310-A169-X-4A00-WS-SWT\\_3-6\\_120\\_US.pdf](http://www.energy.s3.com/hq/pool/hq/power-generation/wind-power/E50001-W310-A169-X-4A00-WS-SWT_3-6_120_US.pdf), July 14,2013
- [23] Sucevic, Nikola., Djurisic, Zeljko., *Influence of atmospheric stability variation on uncertainties of wind farm production estimation.*, EWEA Presentation, 2012, pp.1-9.

- [24] *U.S. Department of Energy.,2011 Wind Technologies Market Report, August 2011, 1-81*
- [25] *Wang, Zheng Qi., Corkum, Matthew., Sharma, Shama., Alexander Lisa., Taylor, Peter., Hocking Wayne., Some comparisons of OQ-Net VHF radar wind profiler data with winds from radiosondes and with NWP model analyses and forecasts.,*